The Estimation of Recharge Through Unsaturated Porous Media Using the Flux of Deuterium

T.C. Hobbs

Submitted in partial fulfillment of the requirements for the degree of Master of Science in Geology

New Mexico Institute of Mining and Technology
Socorro, New Mexico
December, 1988

ABSTRACT

Twelve columns were packed with Sevilleta sand, saturated with water of known isotopic composition and allowed to gravity drain such that uniform moisture content existed throughout each column. The purpose of this study was to investigate the evaporation front phenomenon with respect to steady-state isotopic composition and the use of this front as a natural tracer in determining recharge through unsaturated material. Previous research (Barnes and Allison, 1982), has demonstrated that under equilibrium conditions, ie steady-state evaporation rate and constant ambient elements, the deuterium content at the evaporation front can be mathematically estimated. It has been demonstrated through a series of column experiments that this is indeed true, and estimations are generally within 2 ‰ of the actual measured value. However, analysis of soil samples for ^{18}O do not correlate well with estimated values. The evaporation-front isotopic composition, δef, can also be calculated as a function of depth using the relationships of Barnes and Allison (1982). It is hypothesized that the δef for any soil profile exists in quasi steady-state condition, representing the average depth of penetration of the evaporation front and average atmospheric parameters. If this is true, then the profile below this zone should reflect the rate at which water has passed through the δef zone above.

A relationship developed between the physical characteristics (i.e. moisture content, evaporation zone thickness, specific retention and precipitation) and the corresponding isotopic characteristics is provided for the parameters governing recharge into a bare soil and the isotopic profile developed in equilibrium with recharge. For the purpose of these experiments, recharge is assumed synomonous with infiltration from the surface and percolation through the soil profile. Column experiments performed demonstrate that for an initially wet profile, a clear progression of development of the isotopic profile can be observed as recharge and evaporation continue. Once the profile is in a condition of equilibrium with the recharge water and evaporation, total recharge can be estimated using the average evaporation zone D composition, the evaporation zone thickness derived from a theoretical D profile and mean D composition along a best fit line of the recharge zone below the depth directly influenced by evaporation. Analysis of the isotopic profile samples from the column experiments produced recharge estimates with a mean error of -0.14 cm of the actual recharge measured using a bromide tracer. The use of ^{18}O does not correlate well with the bromide recharge estimates, differing by as much as 200 %. This is probably because kinetic fractionation is more prevalent in oxygen than hydrogen.

Table of Contents

List of Tables and Figures

List of Figures Cont.

INTRODUCTION

Recharge through the unsaturated zone can be estimated using various techniques such as soil lysimetry, neutron probe, or chemical tracers. Natural isotopes have been used to estimate source of historical waters at the water table as well as general historical recharge values (Allison et al. ,1982, Allison et al., 1985, Hoy and Gross ,1982, Phillips et al., 1986, Vuataz and Goff ,1986, Yapp ,1985). Further, recent research has provided insight towards the use of deuterium (D) and oxygen-18 (^{18}O) in estimating evaporation and recharge flux through bare soils, (Allison et al.,1983, Barnes and Allison,1982, Walker et al.,1988). However, a direct quanitative approach is lacking, due mainly to the complexity of processes involved in the isotopic variations within the unsaturated zone, and isotopic variations of the annual precipitation. The intent of this research is to investigate the plausibility of using D in conjunction with catchment basin and soil profile characteristics in order to estimate recharge through the unsaturated zone.

THEORY

Two main areas have to be addressed in order to estimate recharge characteristics. These include the isotopic and physical characteristics of the soil profile. Each is discussed separately below.

ISOTOPIC CHARACTERISTICS

Figure 1 shows the typical isotopic variations that occur in a soil profile. D concentrations in a soil profile are typically enriched (less negative) near the top of the

profile, and become lighter (more negative) with depth towards somewhat constant value. The occurrence of the enriched values near the surface is primarily due to evaporation from the soil surface leaving behind higher isotopic concentrations (the Rayleigh process). Figure 1 shows the typical isotopic variations that occur in a soil profile. Plotting ^{18}O vs D should yield a slope of 3 to 5 or similar to that for free water evaporating under the same conditions (Allison et al.1982, Barnes and Allison, 1982).

For a homogenous soil profile with uniform water content, Barnes and Allison (1982), have provided a mathematical model that predicts the isotopic composition at the top of the soil profile where water content is at a minimum. The dry-zone is defined as the portion of the soil profile with very low water contents, which extends from the surface to the evaporation front. The evaporation front is defined as a point of maximum D concentration at the base of the dry-zone. The recharge zone is that area directly below the evaporation front. From Barnes and Allison (1982), vapor movement upwards from the evaporation front can be obtained from Fick's Law:

$$J = D_v\left(\frac{dN}{dz}\right) \qquad (1)$$

where,

J - Flux of water vapor

D_v - Effective vapor diffusivity, (L^2/T)

N - Concentration of water vapor in the soil air, (M/L^3)

z - depth, (L).

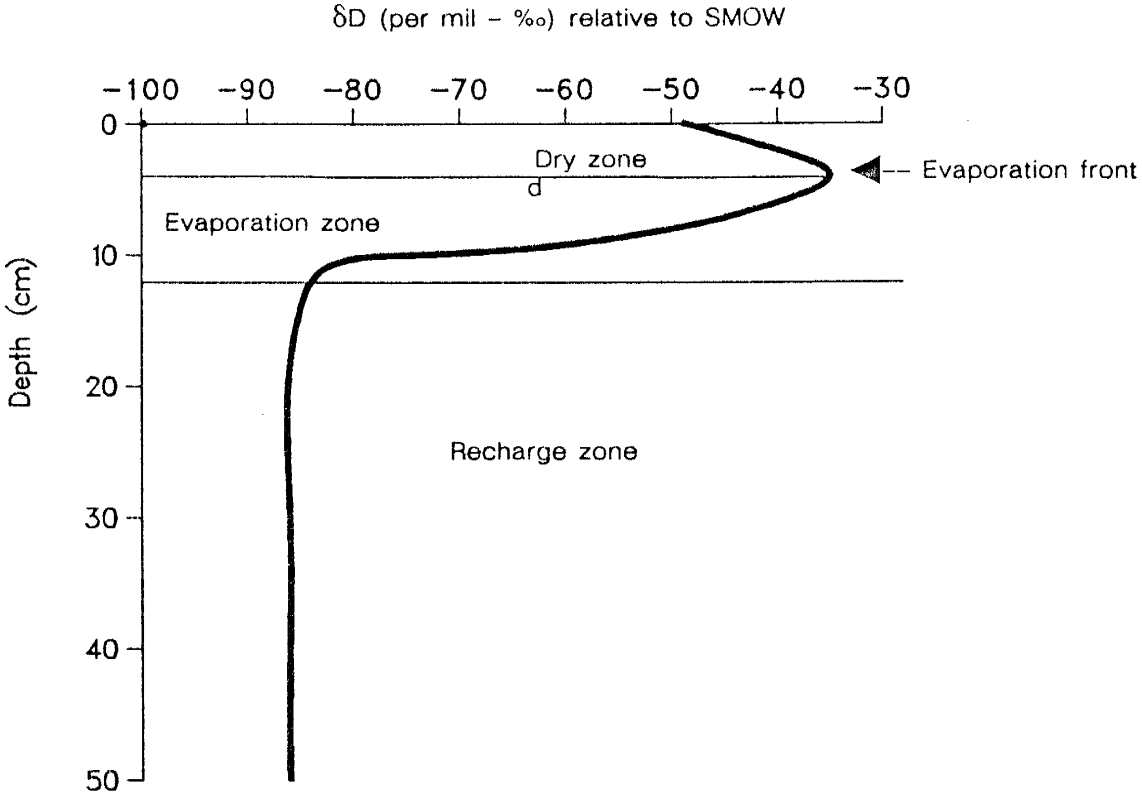

FIGURE 1. Idealized isotopic profile in soils showing evaporation zone, evaporation front, dry zone and recharge zone.

At steady state, then

$$J = \varrho_w E = D_v\left(\frac{dN}{dz}\right) = constant \qquad (2)$$

where,

ϱ_w - density of water, (M/L^3)

E - evaporation rate, (L/T).

For water moving away from the liquid-vapor boundary within a soil by evaporation under isothermal conditions, the total flux of the water vapor is proportional to the

difference in vapor concentration across the boundary divided by the resistance at the boundary. For purposes here, the subscript $_{ef}$ will denote the boundary at the evaporation front and the subscript $_a$ will represent the free atmosphere above the evaporation front. Therefore, from equation 2

$$\frac{J}{\varrho_w} = E = \frac{h_{ef} - h_a}{r_{ef}} \tag{3}$$

where,

h_a – relative humidity above the evaporation front

h_{ef} – relative humidity at the evaporation front

r_{ef} – resistance to water movement (T/L)

Assuming that the humidity at the evaporation front is unity, equation 3 becomes

$$E = \frac{1 - h_a}{r_{ef}} \tag{4}$$

The isotopic species i can be assigned to equation 4 to yield:

$$E_i = \frac{R_{ef}\alpha - h_a R_a}{r_{efi}} \tag{5}$$

where,

R_a – isotopic ratio of the heavy species compared to the light species above the evaporation front

R_{ef} – isotopic ratio of the heavy species compared to the light species at the evaporation front

α – equilibrium fractionation factor for water vapor compared to liquid water, defined here as

$$\alpha = \frac{R_v}{R_l},$$

where v and l represent vapor and liquid phase respectively

r_{efi} – resistance to isotope movement of isotope i.

At equilibrium, the isotopic composition of the water passing the evaporation front will be equal to the evaporative flux of species i divided by the evaporation rate, or;

$$\frac{E_i}{E} = R_{in} \tag{6}$$

where,

R_{in} – isotopic ratio of the input water.

Combining equations 4, 5 and 6 yields

$$R_{in} = \left[\frac{R_{ef}\alpha - h_a R_a}{r_{efi}}\right]\left[\frac{r_{ef}}{1 - h_a}\right] \tag{7}$$

$$= \frac{r_{ef}}{r_{efi}}\left[\frac{R_{ef}\alpha - h_a R_a}{1 - h_a}\right] \tag{8}$$

Rearranging equation 8 to solve for R_{ef}, the isotopic ratio of the water at the evaporation front is then:

$$R_{ef} = \left[R_{in}(1 - h_a)\left(\frac{r_{ef}}{r_{efi}}\right) + h_a R_a \right]\alpha^{-1} \qquad (9)$$

The ratio r_{ef}/r_{efi} is defined as the diffusion ratio factor (Barnes and Allison ,1982) and is related to the diffusion ratio excess (η) by:

$$\frac{r_{ef}}{r_{efi}} = 1 + \eta \qquad (10)$$

Substitution into equation 12 then yields :

$$R_{ef} = [R_{in}(1 - h_a)(1 + \eta) + h_a R_a]\alpha^{-1} \qquad (11)$$

By letting $1 + \delta/10^3 = R/R_{standard}$ and $\alpha = 1 - \epsilon_o$, where ϵ_o is the equilibrium enrichment factor:

$$1 + \frac{\delta_{ef}}{10^3} = \left[\left(1 + \frac{\delta_{in}}{10^3}\right)(1 - h_a)(1 + \eta) + h_a\left(1 + \frac{\delta_a}{10^3}\right)\right]\alpha^{-1} \qquad (12)$$

$$\frac{\delta_{ef}}{10^3} = \left[\left(1 + \frac{\delta_{in}}{10^3}\right)(1 - h_a)(1 + \eta) + h_a\left(1 + \frac{\delta_a}{10^3}\right)\right]\alpha^{-1} - 1 \qquad (13)$$

$$\delta_{ef} = \left[\frac{\left[\left(1 + \frac{\delta_{in}}{10^3}\right)(1 - h_a)(1 + \eta) + h_a\left(1 + \frac{\delta_a}{10^3}\right) - 1 + \epsilon_o\right]}{1 - \epsilon_o}\right]10^3 \qquad (14)$$

:

$$\delta_{ef} = \left[\frac{\left[\left(1 + \frac{\delta_{in}}{10^3} + \eta + \frac{\delta_{in}}{10^3}\eta \right)(1 - h_a) + h_a\left(1 + \frac{\delta_a}{10^3} \right) - 1 + \epsilon_o \right]}{1 - \epsilon_o} \right] 10^3 \quad (15)$$

$$\delta_{ef} = \left[\frac{\left[\left(1 + \frac{\delta_{in}}{10^3} + \eta\left(1 + \frac{\delta_{in}}{10^3} \right) \right)(1 - h_a) + h_a\left(1 + \frac{\delta_a}{10^3} \right) - 1 + \epsilon_o \right]}{1 - \epsilon_o} \right] 10^3 \quad (16)$$

Assuming that as time passes and the evaporation front progresses downward, the dry zone soil-air humidity will be equal to the relative humidity of the atmosphere above the soil surface, Phillip (1967). It follows then that the upper boundary δ_a will be equal to the isotopic composition of the atmospheric water vapor.

Consider a column of uniform sand which is initially saturated and allowed to gravity drain such that unsaturated conditions exist with uniform moisture content throughout the column. Under steady-state conditions, the evaporation rate is constant as the soil water equals the evaporation rate(Hillel,1971). However, it was shown by Black et al. (1969) that as the soil surface begins to dry to a negligible water content, the evaporation rate falls proportionally to the inverse square root of time. Walker et al. (1988), stated that the isotopic composition of waters at the evaporation front is a unique function of this depth / time relationship.

Following Barnes and Allison (1982), equations 4 through 16 can be solved for the region where vapor transport dominates, *i.e.* from the surface down to the evaporation front, as a function of depth. Turning back to equation 4, the evaporation front humidity (h_{ef}) can no longer be assumed to be at unity since the soil air is now dependent upon mixing from air from the surface (Zimmerman et al. 1967).

Therefore,

$$E = \frac{h_{ef} - h_a}{r_{ef}} \tag{17}$$

and

$$E_i = \frac{R_{ef} a h_{ef} - h_a R_a}{r_{efi}} \tag{18}$$

and once again using the relationship of $R_{in} = E_i / E$

$$R_{in} = \frac{\dfrac{(R_{ef} a h_{ef} - h_a R_a)}{r_{efi}}}{\dfrac{(h_{ef} - h_a)}{r_{ef}}} \tag{19}$$

$$R_{in} = \frac{r_{ef}}{r_{efi}} \left[\frac{(R_{ef} a h_{ef} - h_{ef} R_a)}{h_{ef} - h_a} \right] \tag{20}$$

Solving for R_{ef}, then yields:

$$R_{ef} = (a h_{ef})^{-1} \left[R_{in} \left(\frac{r_{efi}}{r_{ef}} \right) (h_{ef} - h_a) + h_a R_a \right] \tag{21}$$

and applying equation 10

$$R_{ef} = (a h_{ef})^{-1} [R_{in}(1 + \eta)(h_{ef} - h_a) + h_a R_a]. \tag{22}$$

The relative humidity (h_{ef}) is given by $h_{ef} = N/N_{sat}$, where N is the water vapor concentration (M/L^3) and N_{sat} is the water vapor concentration at saturation (M/L^3) at a given temperature. The penetration depth is given by Barnes and Allison, (1982) and Zimmerman et al. (1967) as

$$\bar{z} = \frac{n \tau D_{li}}{E} \tag{23}$$

where,

n – total porosity

τ – tortuosity

D_{ll} – liquid coefficient of diffusion of species i, (L^2/T)

E – evaporation rate as before.

From Zimmerman et al. (1967) the relative humidity of the soil air is a result of mixing soil water vapor and atmospheric water vapor from the surface. Barnes and Allison (1982) provides a relationship between the penetration depth and the humidity at both the soil surface and within the soil as

$$\bar{z} = \frac{z}{h_{ef} - h_a} \tag{24}$$

where,

z – depth within the soil from the surface

Equation 24 implies that as the soil air approaches unity, the total penetration depth decreases, which is in agreement with Zimmerman et al. (1967). Rearranging equation 24 and combining with equation 22 then yields

$$R_{ef} = (\alpha h_{ef})^{-1}\left[R_{in}(1+\eta)\left(\frac{z}{\bar{z}}\right) + h_a R_a\right] \tag{25}$$

$$R_{ef} = \alpha^{-1}\left[R_{in}(1+\eta)\frac{z}{\bar{z}h_{ef}} + \frac{h_a R_a}{h_{ef}}\right]. \tag{26}$$

Letting $1 + \delta/103 = R/R_{standard}$, $\alpha = 1-\epsilon_o$ and further using the relationship in equation 24 provides:

$$1+\frac{\delta_{ef}}{10^3}=\alpha^{-1}\left[\left(1+\frac{\delta_{in}}{10^3}\right)(1+\eta)\left(\frac{z}{\bar{z}h_{ef}}\right)+\left(\frac{\left(h_{ef}-\frac{z}{\bar{z}}\right)\left(1+\frac{\delta_a}{10^3}\right)}{h_{ef}}\right)\right] \tag{27}$$

$$\frac{\delta_{ef}}{10^3}=\alpha^{-1}\left[\left(\eta\left(1+\frac{\delta_{in}}{10^3}\right)+1+\frac{\delta_{in}}{10^3}\right)\frac{z}{\bar{z}h_{ef}}+\left(1-\frac{z}{\bar{z}h_{ef}}\right)\left(1+\frac{\delta_a}{10^3}\right)-1+\epsilon_o\right] \tag{28}$$

$$\frac{\delta_{ef}}{10^3}=\alpha^{-1}\left[\frac{\eta\left(1+\frac{\delta_{in}}{10^3}\right)z+z+\frac{\delta_{in}}{10^3}z}{\bar{z}h_{ef}}+1+\frac{\delta_a}{10^3}-\frac{z}{\bar{z}h_{ef}}-\frac{\delta_a}{10^3}\frac{z}{\bar{z}h_{ef}}-1+\epsilon_o\right] \tag{29}$$

$$\frac{\delta_{ef}}{10^3}=\alpha^{-1}\left[\left(\eta\left(1+\frac{\delta_{in}}{10^3}\right)+1+\frac{\delta_{in}}{10^3}\right)\frac{z}{\bar{z}h_{ef}}+\frac{\delta_a}{10^3}-\frac{z}{\bar{z}h_{ef}}-\frac{\delta_a}{10^3}\frac{z}{\bar{z}h_{ef}}+\epsilon_o\right] \tag{30}$$

$$\frac{\delta_{ef}}{10^3}=\alpha^{-1}\left[\left(\eta\left(1+\frac{\delta_{in}}{10^3}\right)+1+\frac{\delta_{in}}{10^3}-1-\frac{\delta_a}{10^3}\right)\frac{z}{\bar{z}h_{ef}}+\epsilon_o+\frac{\delta_a}{10^3}\right] \tag{31}$$

$$\delta_{ef}=\alpha^{-1}\left[\left(\eta\left(1+\frac{\delta_{in}}{10^3}\right)+\frac{\delta_{in}}{10^3}-\frac{\delta_a}{10^3}\right)\frac{z}{\bar{z}h_{ef}}+\epsilon_o+\frac{\delta_a}{10^3}\right]10^3 \tag{32}$$

$$\delta_{ef}=\alpha^{-1}\left[\left(\eta\left(1+\frac{\delta_{in}}{10^3}\right)+\frac{\delta_{in}}{10^3}-\frac{\delta_a}{10^3}\right)\left(\frac{z}{(z+h_a\bar{z})}\right)+\epsilon_o+\frac{\delta_a}{10^3}\right]10^3 \tag{33}$$

$$\delta_{ef}=\left[\frac{\left(\frac{z}{z+h_a\bar{z}}\right)\left(\eta\left(1+\frac{\delta_{in}}{10^3}\right)+\frac{\delta_{in}}{10^3}-\frac{\delta_a}{10^3}\right)+\epsilon_o+\frac{\delta_a}{10^3}}{1-\epsilon_o}\right]10^3 \tag{34}$$

which is identical to equation 18 of Barnes and Allison (1982).

This implies that equation 34 can be used to estimate the isotopic progression of an initially wet soil profile under steady-state isothermal conditions. Further, subsequent recharge events of identical isotopic composition will progress in an identical manner, with δ_{ef} significantly enriched as a result of evaporation. Given the time / depth relationship, a evaporation front should take on a steady-state isotopic composition with depth.

PHYSICAL CHARACTERISTICS

A soil profile at evaporative equilibrium can be broken up into three distinct regimes. The first is the dry zone where evaporation reduces moisture contents to a negligible amount. Immediately at the base of the dry zone is the static evaporation front. Here, as previously stated, the isotopic composition is at its maximum for the soil profile and moisture contents are low. The zone below the evaporation front is defined here as the evaporation zone, meaning the zone where the soil water is under the influence of evaporation from the surface. Below the evaporation zone is the recharge zone, defined here as that zone within the soil profile which contains water percolated down from the surface, but is below the influence of direct evaporation. Figure 2 shows the orientation of each of these zones. During a precipitation event, water which is not caught up by interception or does not run off, will infiltrate into the ground. In order for percolation of the infiltrated water to occur, the specific retention (Sr) of the soil must be fulfilled, Davis and DeWiest (1966). Additionally, upward movement of percolated water will take place in the evaporation zone and dry zone until such time soil moisture no longer meets the evaporation demand. Therefore, at any given time the mass balance for the total water from the surface to the recharge zone is given by :

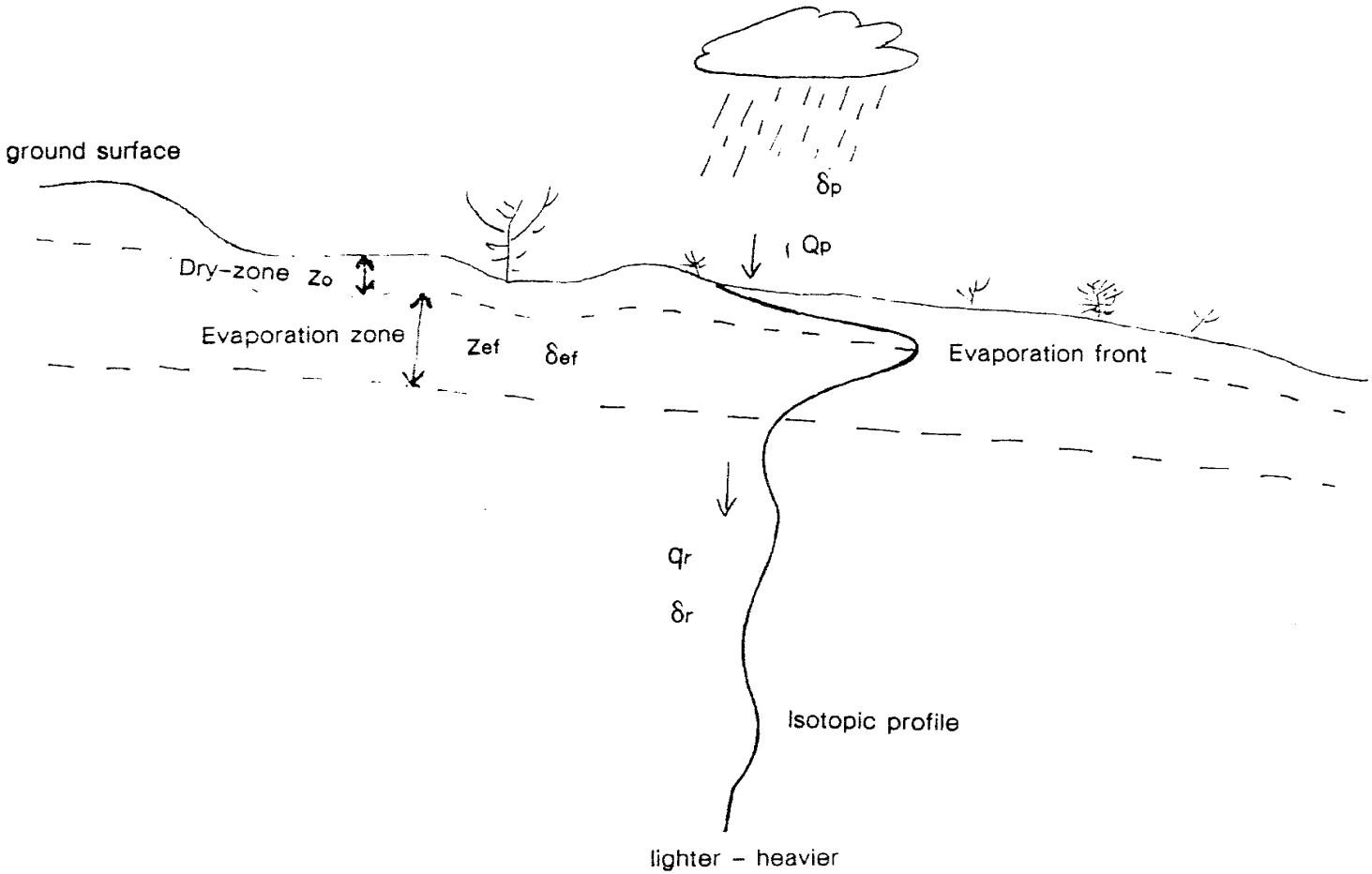

FIGURE 2. Illustration showing configuation of infiltration water (Q_p), isotopic composition of the infiltration water (δ_p), thickness of the dry-zone (z_o), thickness of the evaporation zone (z_{ef}), recharge zone (q_r) and the isotopic composition of the recharge zone (δ_r).

$$Q_p - z_o S_r + z_{ef}\theta_{ef} = q_r + z_{ef}S_r \qquad (35)$$

where,

q_r – recharge through the soil that would eventually be part of the water table (L)

Q_p – water infiltrated from surface (L), (p=precipitation)

z_o – dry zone depth (L)

S_r – specific retention of soil

z_{ef} – thickness of zone of depletion by evaporation (L)

θ_{ef} – average water content of the evaporation zone.

As previously stated , the isotopic composition at the evaporation front (δ_{ef}) should approach a steady state composition with depth as it moves deeper with time. Therefore a mass balance based upon equation 35 can be applied using the input water of variable isotopic composition and the average isotopic composition of the evaporation zone.

$$\delta_p Q_p - z_o S_r \delta_p + z_{ef}\theta_{ef}\delta_{ef} = q_r\delta_r + z_{ef}\delta_r S_r. \qquad (36)$$

Rearranging equation 36 to solve for q_r then yields

$$q_r = \frac{\delta_p(Q_p - z_o S_r) + z_{ef}(\theta_{ef}(\delta_{ef} - \delta_r) - \delta_r S_r)}{\delta_r} \qquad (37)$$

where,

δ_p = isotopic composition of the infiltrate, (precipitation)

δ_r = isotopic composition of the water in the recharge zone

δ_{ef} = average isotopic composition of the evaporation zone.

EXPERIMENT

In an effort to test the validity of the method described above, a column experiment was conducted. The procedures outlined below were performed in an attempt to duplicate those of Allison et al. (1982).

COLUMNS

The experimental set up consisted of 12 clear schedule-40 PVC columns. Each was 10.2 cm in diameter and 36 cm in length, capped on the bottom with a 10.2 cm PVC coupling cemented and sealed with silicon to prevent leakage. A valved drainage outlet was attached to the base of each column. Figure 3 provides a schematic of the column construction. Each column was manually packed in 1-cm lifts with 30 cm of Sevilleta sand. The Sevilleta is a well sorted, fine to medium grained, clean dune sand occurring approximately 20 miles north of Socorro, New Mexico. Figure 4 shows a grain size distribution of the Sevilleta. The packed porosity was measured to be about 40 percent.

Once all twelve columns were packed, they were simultaneously saturated with deionized water of known isotopic composition, capped with plastic wrap and allowed to gravity drain for 24 hours. This procedure was performed three times to help ensure that uniform saturation was obtained and that three pore volumes of water

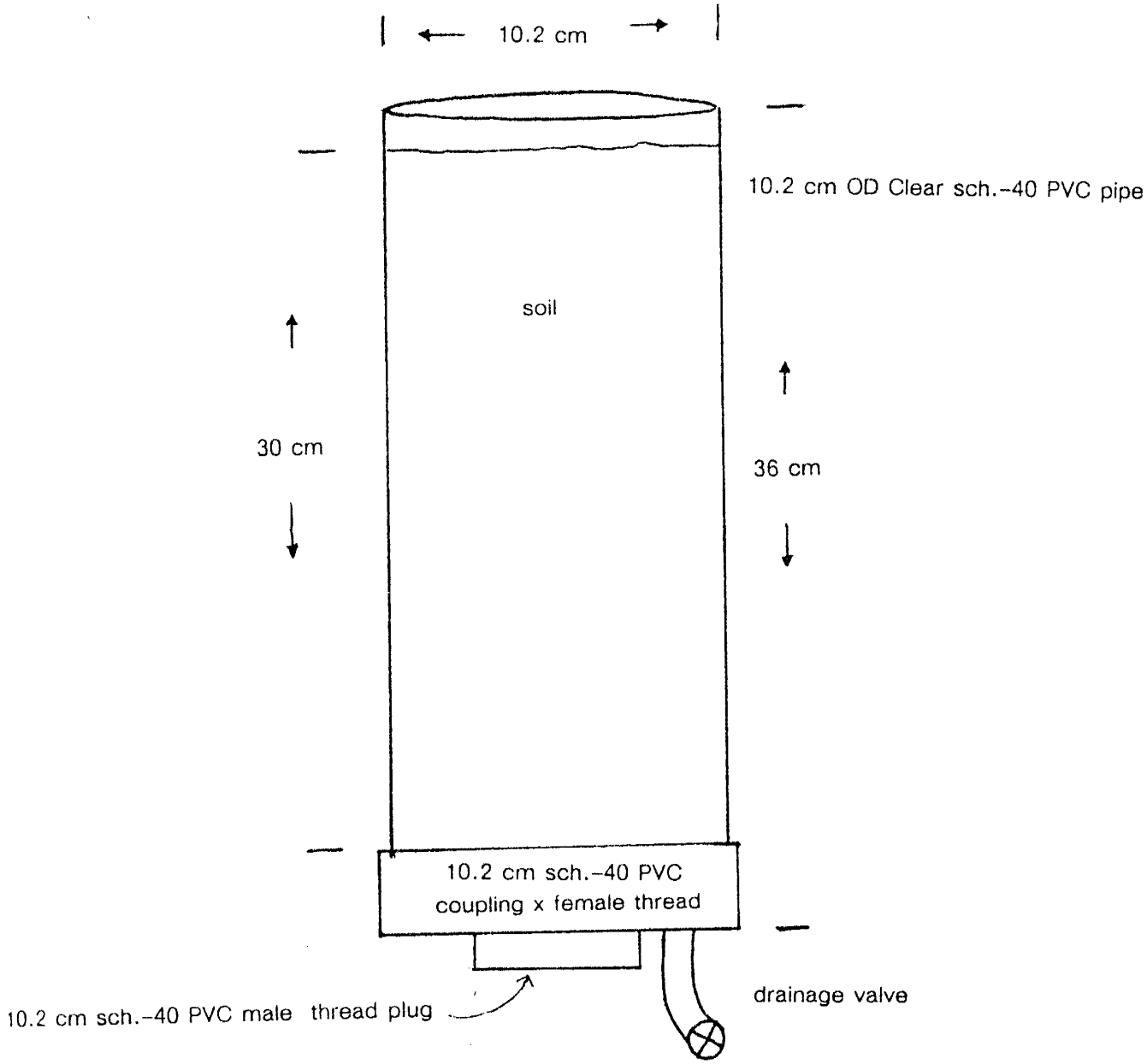

FIGURE 3. Typical column construction.

had passed through each column in accordance with the procedures of Allison et al. (1982). Following the final drainage of the columns, the top caps of each column was removed so that evaporation could proceed. A dry bromide tracer was added to the top of each column. Bromide was chosen due to its high solubility and its excellent tracer properties. The advance of the dry front was visually recorded daily, as well as the relative humidity and temperature. Appendix A provides temperature and humidity data of the laboratory during the experiment. Once the dry-front depth averaged 2 cm for all 12 columns, an aliquot of de-ionized water of known isotopic composition was added to each of the columns. The volume of aliquot was computed individually as one pore volume over the entire dry-front depth.Once again, the progression of the dry-front was visually noted until an average depth of 2 cm was observed, and another aliquot of water was added to the columns. This procedure was repeated throughout the remainder of the column experiment.

There are two distinct evaporation regimes evident which correspond to the abovementioned relationship of Black et al. (1969). The first-stage evaporation occurs almost linearly, as water within the soil fully compensates for the water lost by evaporation, and no surface drying is evident. As evaporation proceeds and the soil no longer compensates for evaporation, the soil surface begins to dry and second-stage evaporation takes over and progresses downward at a rate equal to the inverse square root of time. This second-stage evaporation relationship was found to be somewhat constant between additions of water to the top of the columns. The only major exception to this was the first episode of evaporation following uncapping of the columns. It is believed that initially the columns were not at equilibrium and higher moisture conditions existed than originally thought. Initially,

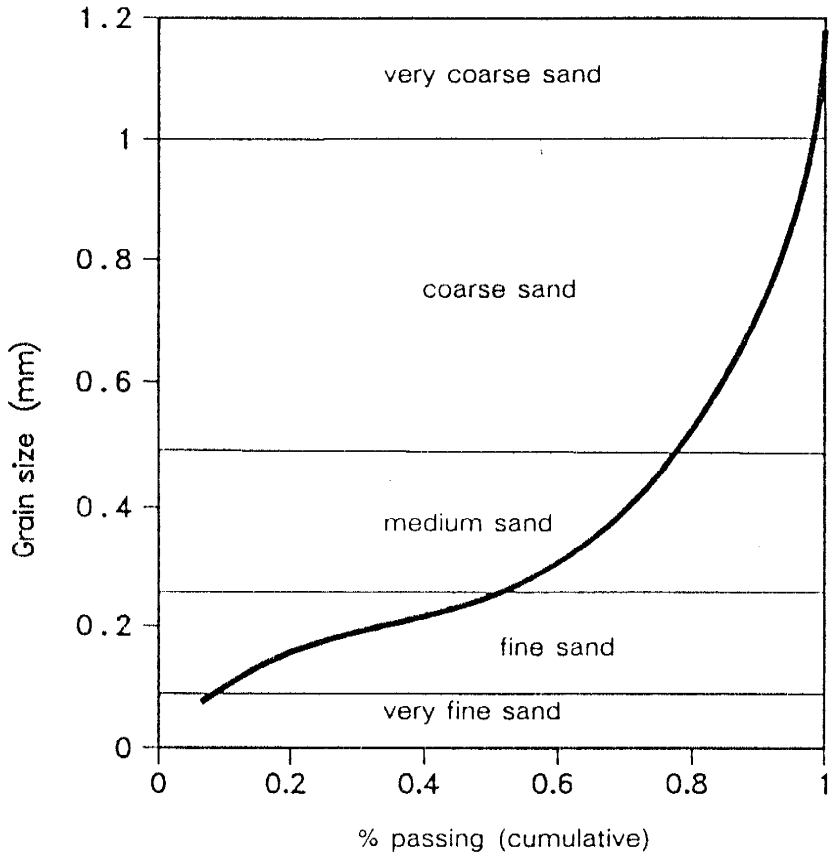

FIGURE 4. Typical grain size distribution for the Sevilleta sand, (Kirkman, 1987).

the second-stage evaporation did not occur until 384 hours following the uncapping of the columns. From then on, and throughout subsequent additions of water to the top of the columns, second-stage evaporation was observed to occur after roughly 30 hrs.

SAMPLING

The first column was destructively sampled by extrusion after 4 aliquots of water had been added. Column 2 was likewise sampled following 8 additions of aliquots

of water to the top of each column. The remainder of the columns were then sampled following the end of each evaporation episode, *e.g.* just prior to the addition of an aliquot of water. Sampling consisted of removing the bottom plug and extruding the soil from the column with a wooded piston. The soil from the column was sampled at 2 cm intervals. Each sample was thoroughly mixed and then divided for water content measurement, bromide analyses and isotopic analyses.

LABORATORY ANALYSES

Soil-column samples were analyzed for water content, bromide concentration and isotopic composition. Water content was determined gravimetrically. The bromide analyses were performed by adding 80 ml of deionized water to the oven-dried soil sample and mechanically agitating for 8 hrs. Approximately 40 mls were then decanted, centrifuged and the bromide concentration measured using an Orion standard pH meter and bromide electrode. Results were then converted to moles of bromide per kilogram of soil, (mol/kg).

SOIL-WATER EXTRACTION

In order to perform the required D and ^{18}O analyses, the soil water in each sample must be removed without causing fractionation of oxygen or hydrogen or without causing any chemical contamination. This turned out to be a very serious problem. Previous studies (Allison et al. 1983), used distillations of moist soil mixed with various hydrocarbon liquids which, when heated in the presence of water, form a vapor azeotrope at a temperature below the boiling point of water. The azeotrope was then condensed and the water separated from the azeotropic mixture. The

water sample was then further purified by gentle heating with parafin to remove any traces of contamination by organic liquid. Theoretically, the benefit of this process is that it is not necessary to reclaim all soil-water since the water itself enters vapor phase only as an azeotrope, and thus the potential fractionation is negligible. However, several azeotropic distillations of this type, using toluene as the azeotropic medium, showed severe contamination problems. Of 20 test samples, only 8 were sufficiently contaminant-free to allow mass spectrometer analysis. The D composition of the analyzed samples ranged from -99 ‰ to -126 ‰ with an average of -108 ‰ and a standard deviation of 11.3 ‰. It is believed that the final purification process is ineffective, and the presence of the toluene, even in minute concentrations, results in either total contamination or erroneous results. Unfortunately, this phenomenon while having been noted at other laboratories, has not been documented to date. Nonetheless, this implies that isotopic analyses which are performed with waters distilled in this manner need to be evaluated cautiously.

As an alternative to the azeotropic distillation method, a new technique was developed which appears at this time to provide a relatively simple means of extracting soil-water without contaminating the sample or causing fractionation. The apparatus involved consists of a soil-sample flask, cold trap container and transfer tube with a valved vacuum nipple attached, (Figure 5). The entire apparatus is flooded with nitrogen gas to displace as much atmosphere as possible. The soil sample is then added to the soil flask and is frozen with liquid nitrogen. Experience with this method show that a freezing time of 1 min per 15 g of soil with an average moisture content of 10 % is adequate. Once the sample is completely frozen, the entire apparatus is evacuated under a vacuum to 100 milli-torr. The vacuum line is then shut off. A liquid nitrogen cold trap is placed on the cold trap container and gentle

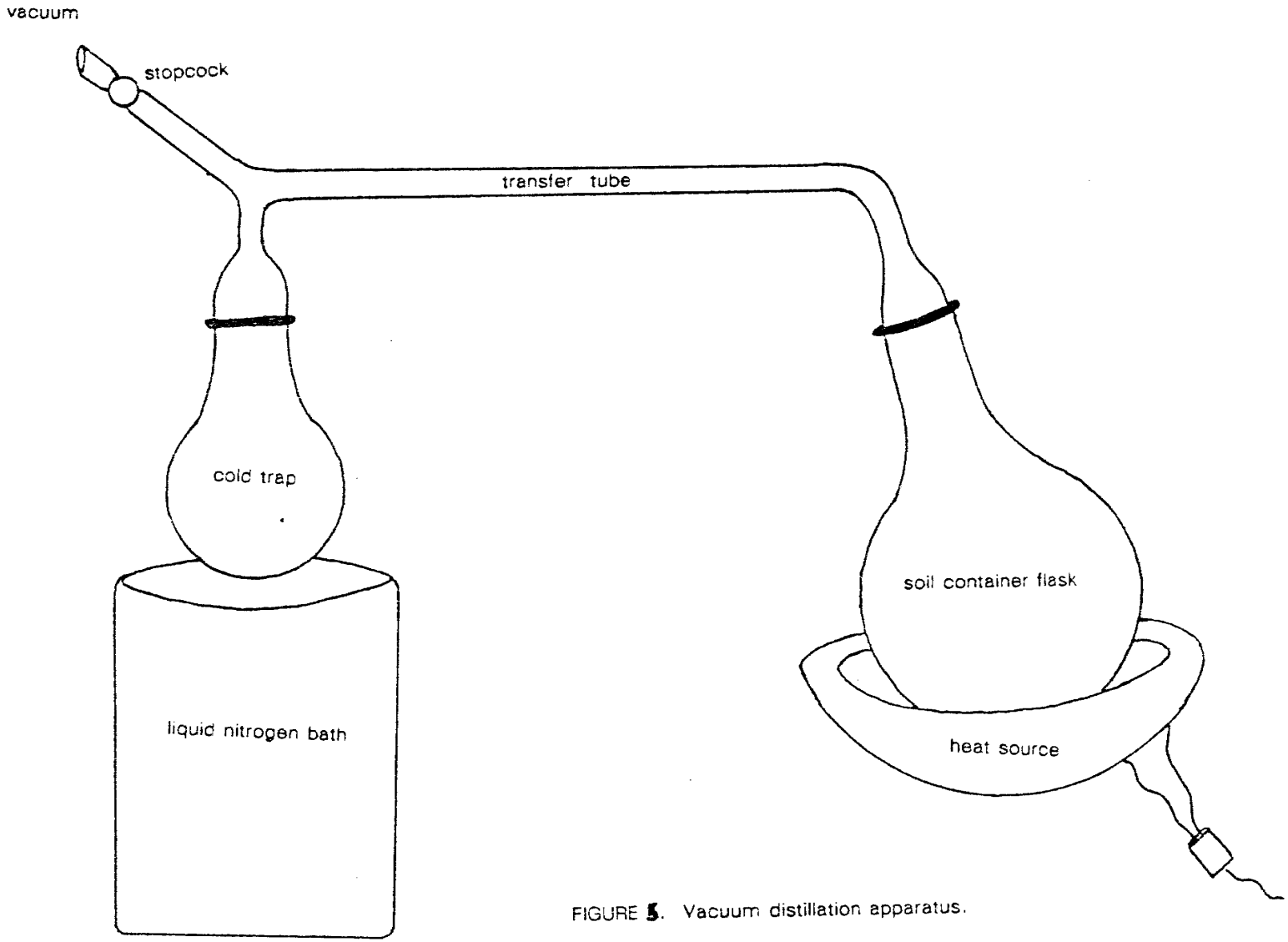

FIGURE 5. Vacuum distillation apparatus.

heating is applied to the soil-sample flask. As a result, water from the soil sample is transferred to the cold trap through diffusion under high temperature gradient without condendensing in the transfer tube. This high vacuum distillation proceeds by normal Rayleigh distillation and can be numerically simulated by the relationship of Merlivat and Jouzel (1979):

$$\delta_v = \left(\alpha^{-1} \left[\frac{1-k}{1-kh} \right] \delta_l + 1 \right) - 1 \qquad (38)$$

where,

δv – isotope value of species in vapor phase, ‰

δl – isotope value of species in liquid phase, ‰

α – frationation factor

k – profile coefficient, (D, k=0.0168 ‰, ^{18}O, k=0.0189 ‰)

h – relative humidity.

The estimation of the isotopic value of the water in the cold trap can be modeled as a simple Rayleigh Distillation process by:

$$\delta = \delta i + \epsilon \ln f \qquad (39)$$

where,

δ – isotopic composition of remaining soil water

δi – isotopic composition of the initial soil water

ϵ – isotopic enrichment factor in the vapor-liquid (v,l) phase, given by:

$$\epsilon = -\left[\frac{\left(\frac{\delta_l - \delta_v}{1+\delta_v} \right)}{\frac{1+(\delta_l - \delta_v)}{(1+\delta_v)}} \right] \qquad (40)$$

f - mass fraction of water remaining in the soil.

Solving by mass balance, the isotopic composition of the water retrieved in the cold trap can be obtained:

$$\delta_r = \frac{\delta_i - f(\delta)}{1 - f} \qquad (41)$$

where,

δr - isotopic composition of the water retrieved in the cold trap.

For example, assuming a humidity inside the distillation apparatus of 85%, and further assuming a net yield from the soil of 90%, at room temperature equations 38 through 41 estimate fractionation of D and ^{18}O of -21‰ and -3.1 ‰, respectively.

If no heat were applied to the soil, and transfer was allowed to proceed where the soil was kept at room temperature, (eg. 20 ^{o}C), even at 99 % yields of extraction of water from the soil will produce a fractionation of D and ^{18}O of 4 ‰ and 0.57 ‰ , respectively. Since the fractionation factor is temperature dependent, generally decreasing with increasing temperature, it was believed that increasing the temperature would not only speed up the extraction process, but reduce the potential fractionation. In an effort to evaluate this, the above equations were applied using varying fractionation factors for D and ^{18}O from 20 ^{o}C to 100 ^{o} C. Fractionation factors for liquid-vapor H_2O were taken from Majoube (1971), as:

$$10^3 ln\alpha_{lv} = 24.844\left(\frac{10^6}{T^2}\right) - 76.248\left(\frac{10^3}{T}\right) + 52.612 \qquad \textit{for Deuterium} \qquad (42)$$

$$10^3 ln\alpha_{lv} = 1.137\left(\frac{10^6}{T^2}\right) - 0.4156\left(\frac{10^3}{T}\right) - 2.0667 \qquad \textit{for Oxygen-18} \qquad (43)$$

where,

T - Degrees Kelvin.

Figure 6 shows a plot of ΔD and Δ18O against percent yield for a range of temperatures. As can be seen, the effect of increasing temperature is most pronounced at lower yields, decreasing to insignificant fractionation as yields approach 100%. At 90% yield for example, 100° C results in a potential fractionation of -7.4‰ for D and -3.13‰ for 18O, while at 99% yield, potential fractionations for D and 18O at 100° C are 1.35‰ and 0.35‰ respectively. This indicates that while total yield dominates the potential fractionation during a distillation process of this type, increasing the temperature can significantly reduce the potential for fractionation.

In testing this procedure, water of known isotopic composition was added to 200 g of oven dried Sevilleta sand. Both water and sand were introduced to the sample container in the presence of nitrogen gas to reduce potential contamination of atmospheric water vapor. The water and sand mixture were then placed onto the distillation transfer tube, which likewise had been flooded with nitrogen gas, and placed in a liquid nitrogen bath for 10 minutes. A vacuum of 100 milli-torr was then applied and the vacuum line was then closed leaving the entire soil water and trans-

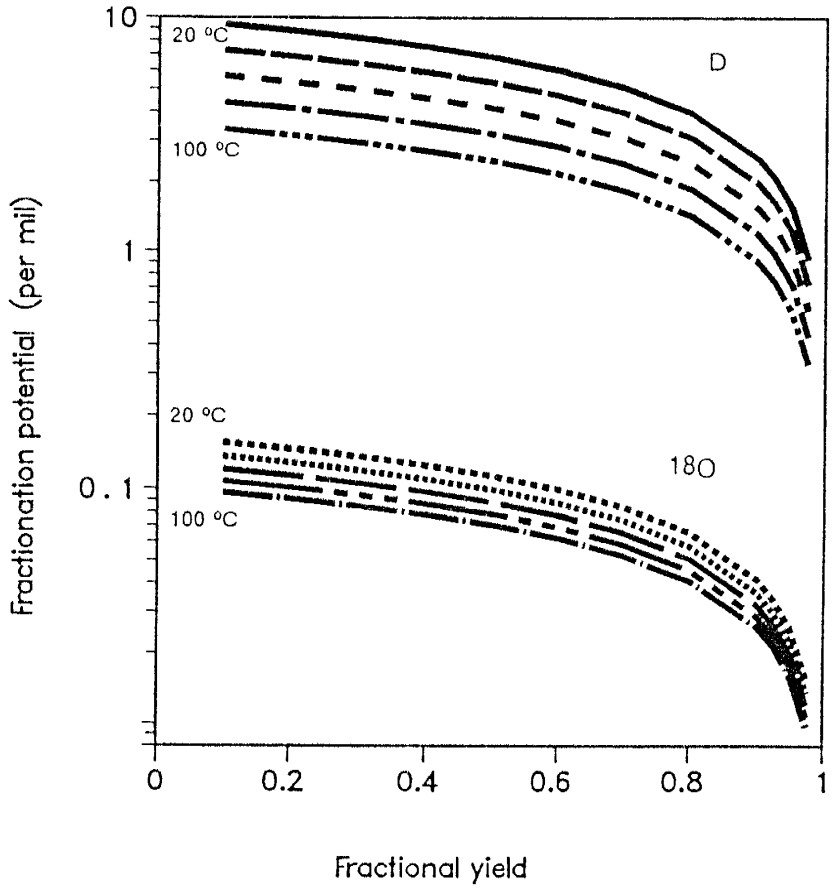

FIGURE 6. Fractionation as a result of changing temperature and yield for the vacuum distillation method. Lines between temperatures indicate 40°, 60° and 80° C.

fer tube under vacuum. A liquid nitrogen bath was placed on the cold trap container side and the soil-water mixture was heated to an estimated 100 °C. The transfer of water to the cold trap was visually noted during the entire process. Additionally, the soil flask was periodically shaken to aid in freeing any trapped waters. After 1.5 hrs had passed and it was believed certain that all water had been distilled from the soil, gentle heating of the entire apparatus was applied with a heat gun. Finally, nitrogen gas was re-introduced and the frozen water was transferred to a sample container.

Altogether 14 test-distillation samples were run in this manner, however varying the heating and freezing times of the soil-water mixture. Table 1 provides a listing of the test results. The D content of undistilled test waters reduced to hydrogen using the zinc reduction method (discussed later), range from -99.85 ‰ to -102.62 ‰, with a mean of -100.743 ‰. Using this mean as an actual value, a standard error of estimate is computed at 1.67 ‰. Distillation test sample 2 was believed to be erroneous and was excluded from further analysis. The 13 distillation-test samples average -100.748 ‰ with a standard deviation of 1.56 ‰, in good agreement with the undistilled test waters discussed above. ^{18}O analyses of distillation test samples varied between -12.9 ‰ to -13.5 ‰, with a mean of -13.0 ‰ and a standard deviation of 0.63 ‰.

Table 1. Vacuum distillation test results.

Sample	Dist. Time (hrs)	Freeze Time (min)	%w	δD ‰	$\delta 18O$ ‰
Test 1	1.5	10	10	-100.2	-13.2
Test 2	1.5	10	10	- 96.1	-11.1
Test 3	1.5	10	10	-101.8	-13.0
Test 4	1.5	10	10	-102.6	-13.0
Test 5	1.5	10	10	-100.6	-13.1
Test 6	1.5	10	10	- 99.0	-13.5
Test 7	1.5	10	10	-102.6	-13.4
Test 8	1.5	10	10	-102.6	-12.9
Test 9	1.5	10	10	- 99.7	-13.3
Test 10	1.5	10	10	-102.6	-13.1
Test 11	1.5	10	10	-102.4	-13.2
Test 12	2.0	15	20	-100.5	-13.3
Test 13	2.0	15	20	-101.2	-13.2
Test 14	2.0	15	20	-102.4	-13.5

REDUCTION OF SOIL-WATER TO HYDROGEN

Once the soil-water has been obtained it is then necessary to reduce the water to H_2, for analysis on a mass spectrometer. The zinc method was used for this purpose, following the procedures of Coleman et al. (1982). Specially treated zinc shot (Hayes and Baker, 1986) is placed in a 12.5 mm OD reaction vessel with a high vacuum stopcock. Approximately 0.05 g of zinc shot per µl of water is used. After placing the zinc shot into the reaction vessel, the atmosphere in the reaction vessel is pumped away and the zinc is gently heated to remove any trace of residual water vapor. A liquid nitrogen bath is placed on the reaction vessel and the water sample is introduced via a septum situated on the vacuum line. The reaction vessel and septum area are then gently heated so that all water is transferred to zinc shot which is now at a temperature of -195 °C. The reaction vessel is then heated at 500 °C for 30 min. Hydrogen is separated from water, by the following reaction :

$$Zn + H_2O \text{ ---> } (500\,\mathrm{deg}\,C) \text{ ---> } ZnO + H_2$$

The reaction vessels are then removed and the samples were analyzed on a Finnigan ratio mass spectrometer.

RESULTS

Moisture, bromide, evaporation and recharge results are summarized in Table 2. Temperature and relative humidity during the period of experiment is provided in Appendix A. Other basic column-test data are given in Appendix B.

Table 2. Summary of column-test results

Column	1	2	3	4	5	6	7	8	9	10	11	12
Total Days of Operation	30	63	72	80	89	98	107	116	126	134	143	159
Number Aliquots Addded	4	8	9	10	11	12	13	14	15	16	17	18
Total Water Added (cm)	3.3	6.3	7.6	7.8	10.7	11.7	10.9	13.4	12.4	13.9	14.4	14.9
Water Added per Day (cm/d)	.11	.10	.10	.09	.12	.11	.10	.12	.09	.10	.10	.09
Water Added per Aliquot (cm)	.82	.79	.84	.78	.98	.98	.84	.96	.83	.87	.85	.83
Ave. Water Content (θ)	9.4	7.4	7.5	9.3	12.2	11.5	9.4	10.9	9.6	8.7	8.5	8.0
W.C. at Evap.-Zone (θ_{ef})	5.8	6.2	6.0	6.2	7.0	3)	2)	3)	6.5	6.6	6.4	5.5
Ave. Dry-Zone Thick., z_o (cm)	2.04	1.93	2.06	1.87	2.33	2.55	2.01	2.31	2.00	2.08	2.03	1.89
Evap.-Zone Thick., z_{ef} (cm)	5.0	7.0	9.0	7.0	9.0	3)	2)	9.0	7.0	9.0	9.0	9.0
Ctr. of Br Front, z_{br} (cm)	1)	11.0	12.0	12.5	14.5	14.9	16.0	15.5	16.0	16.5	24.0	13.5
Ave. θ above z_{br}	1)	6.6	7.2	7.4	8.8	8.2	7.2	6.8	6.6	7.1	7.9	6.0
D at Evap Front (‰)	(-44)	(-45)	-44	-50	-41	(-38)	(-43)	(-40)	-39	-45	-39	-51
Ave. D for z_{ef}, δ_{ef} (‰)	-59	-61	-64	-59	-63	3)	2)	3)	-61	-62	-62	-63
Ave. D Recharge, δ_r (‰)	-89	-89	-89	-88	-89	3)	2)	3)	-84	-88	-87	-89
Evap. Rate (cm/s x 10^{-6})	3.36	3.11	3.17	2.86	3.51	3.71	2.91	3.25	2.94	2.91	2.88	2.76
Recharge Using z_{br} (cm)	1)	0.72	0.86	0.92	1.28	1.22	1.15	1.05	1.06	1.18	1.86	0.82
Recharge Using Fig. 21 (cm)	0.63	0.56	0.64	0.65	0.22	3)	2)	3)	2.00	0.81	1.59	1.04
Recharge Using Eqn. 37 (cm)	1.27	0.88	1.62	1.10	1.09	3)	2)	3)	3.12	0.38	0.39	0.27

1) Bromide analysis contaminated
2) Not analyzed due to redistribution
3) Probable evaporation of samples
( ) Calculated using equation 34

MOISTURE CONTENT

Moisture content profiles are shown in Figures 7 through 18. Moisture content provided in the figures is given as a percentage of dry-soil weight. Volumetric water contents can be calculated using an average bulk density of 1.59. The volumetric water contents were used in estimating recharge through equation 37.

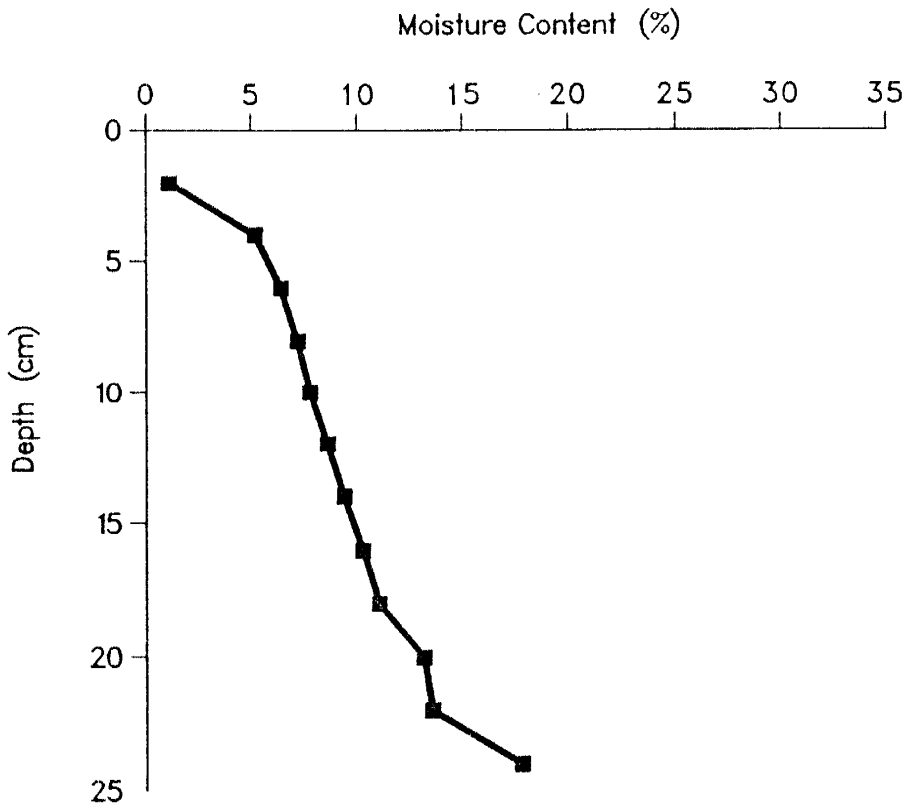

FIGURE 7. Moisture content versus depth for column 1.

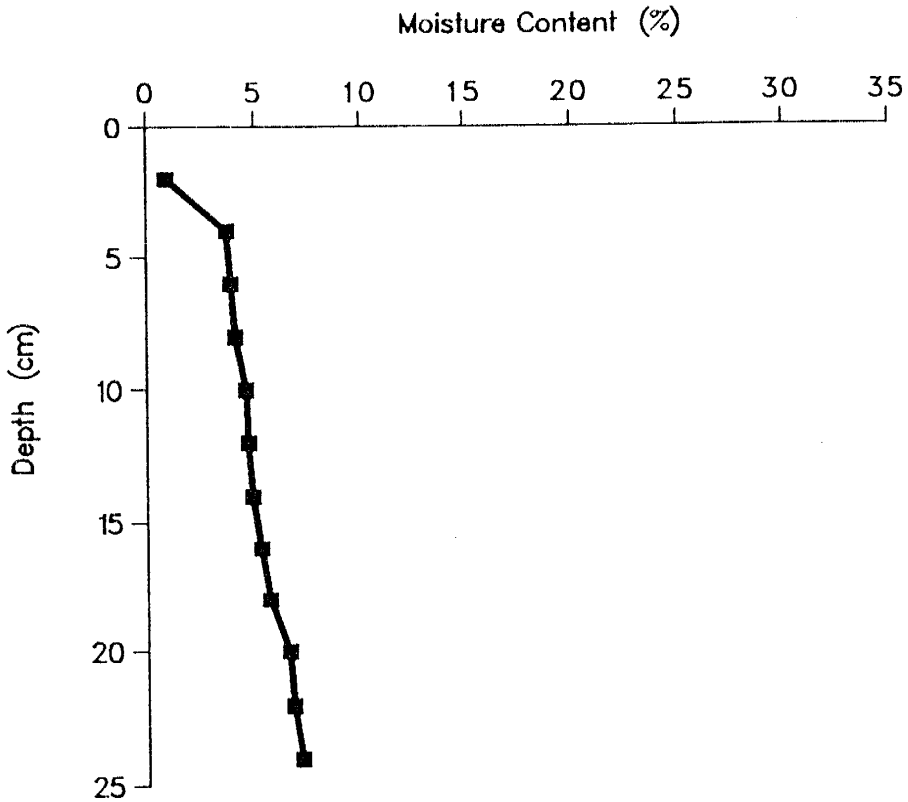

FIGURE 8. Moisture content versus depth for column 2.

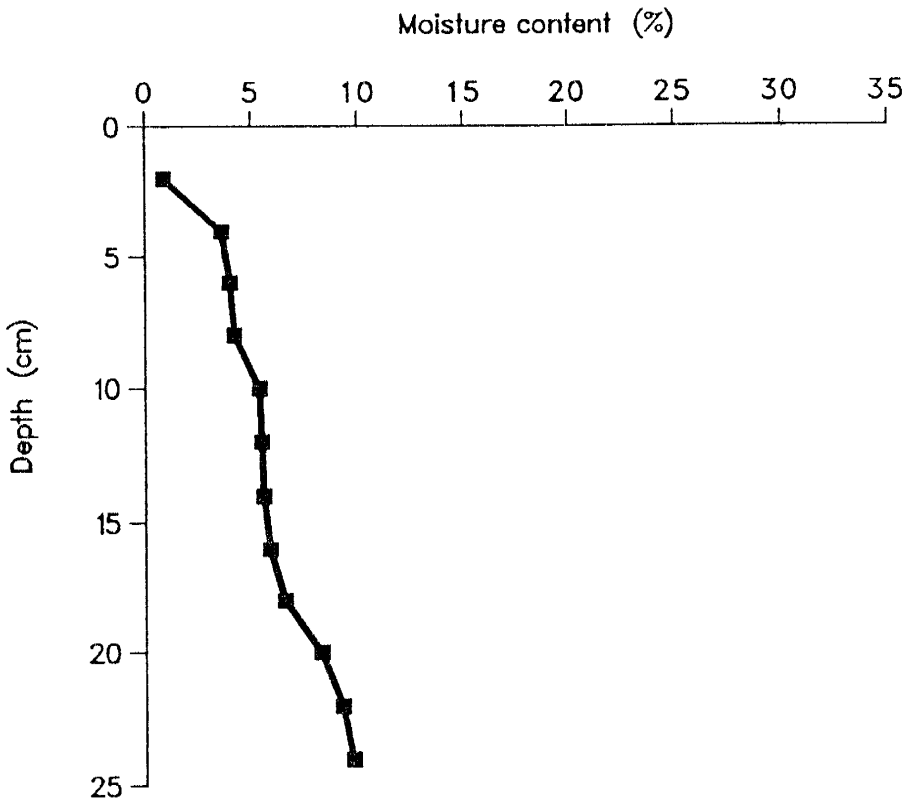

FIGURE 9. Moisture content versus depth for column 3.

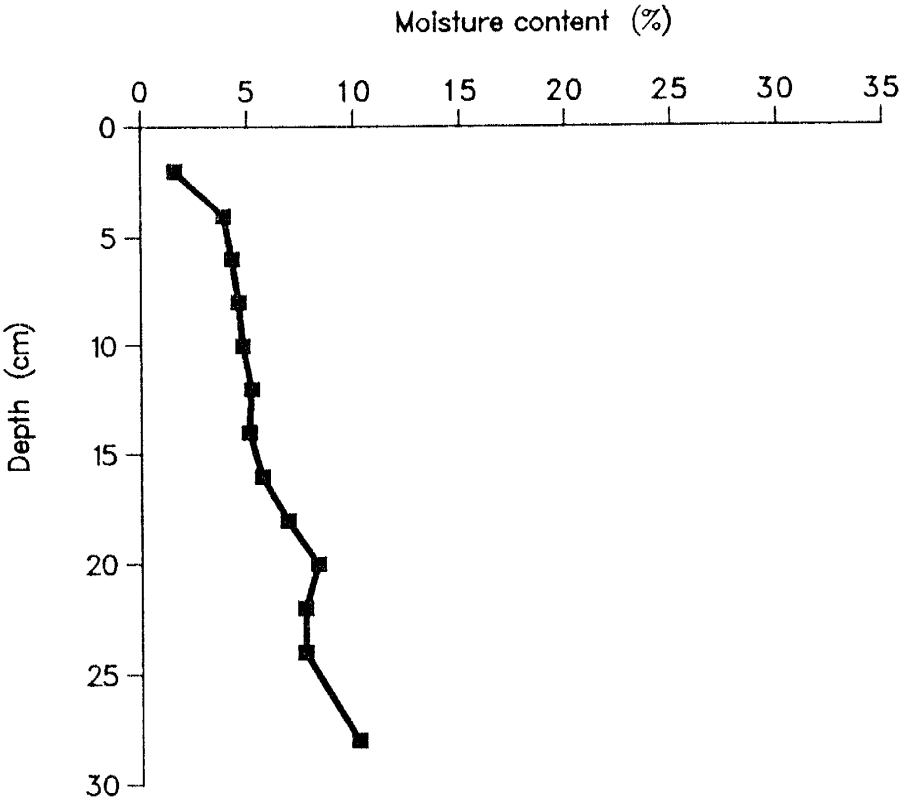

FIGURE 10. Moisture content versus depth for column 4.

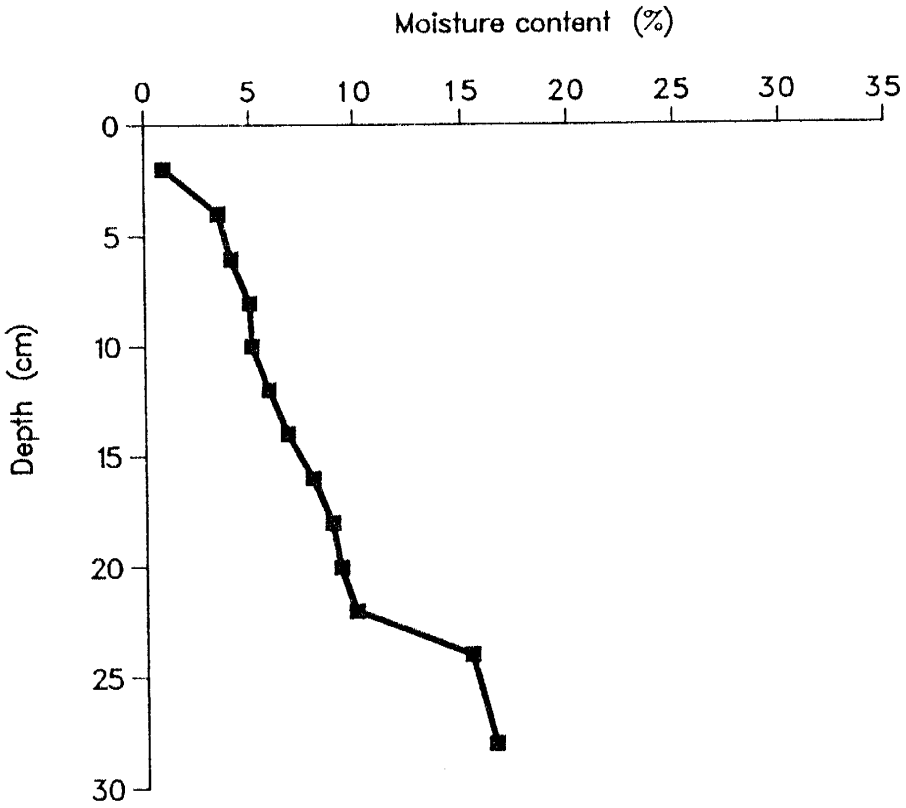

FIGURE 11. Moisture content versus depth for column 5.

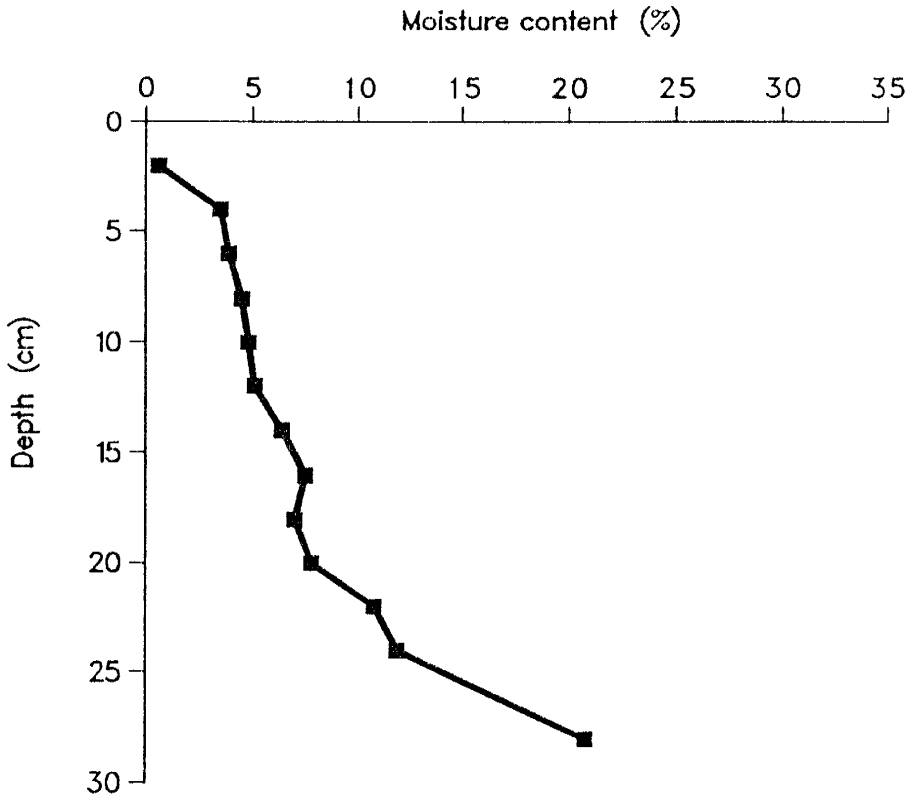

FIGURE 12. Moisture content versus depth for column 6.

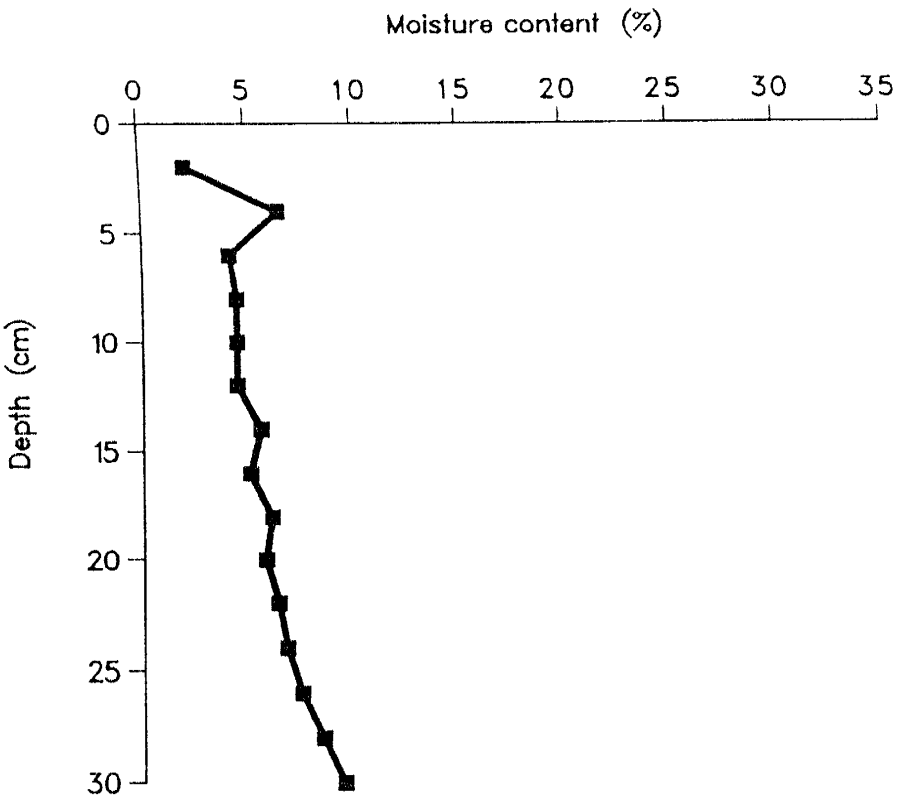

FIGURE 13. Moisture content versus depth for column 7.

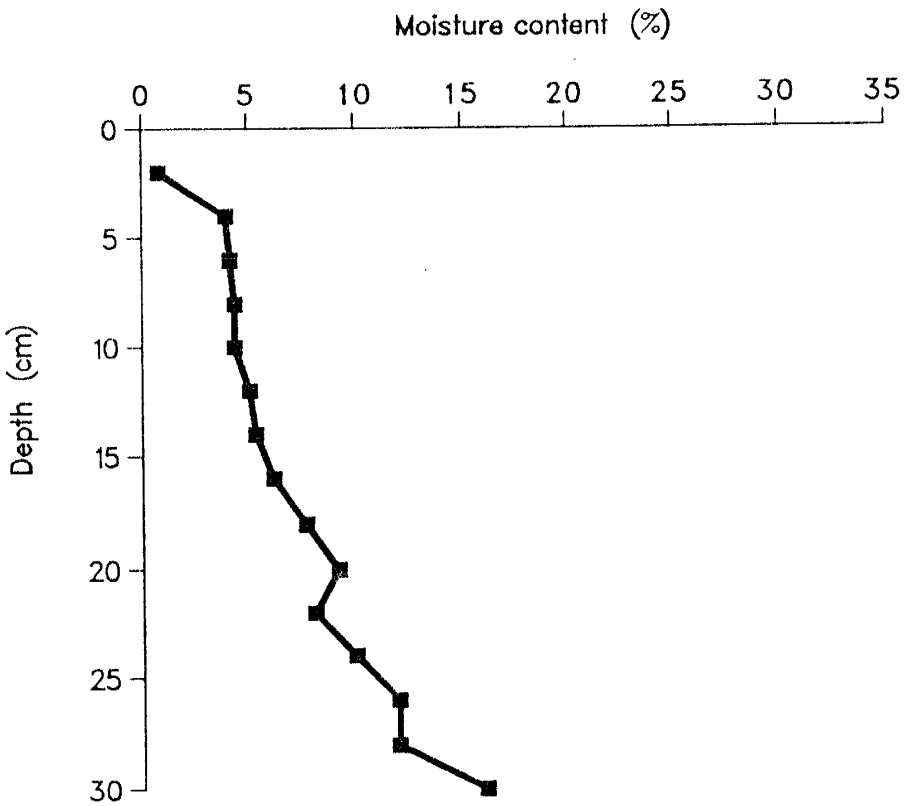

FIGURE 14. Moisture content versus depth for column 8.

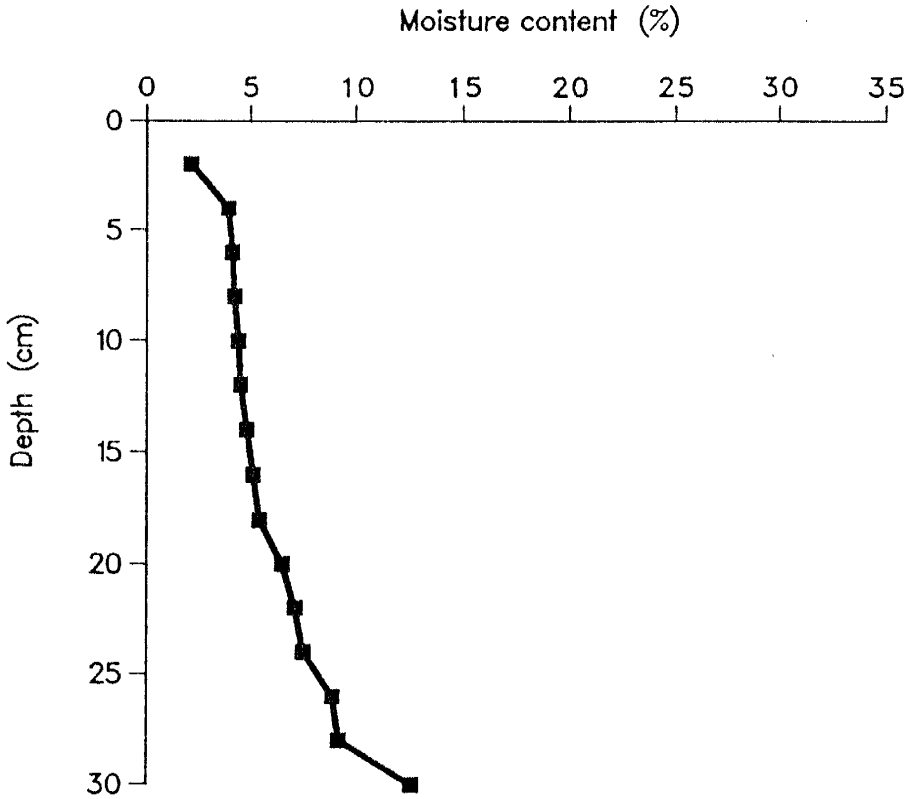

FIGURE 15. Moisture content versus depth for column 9.

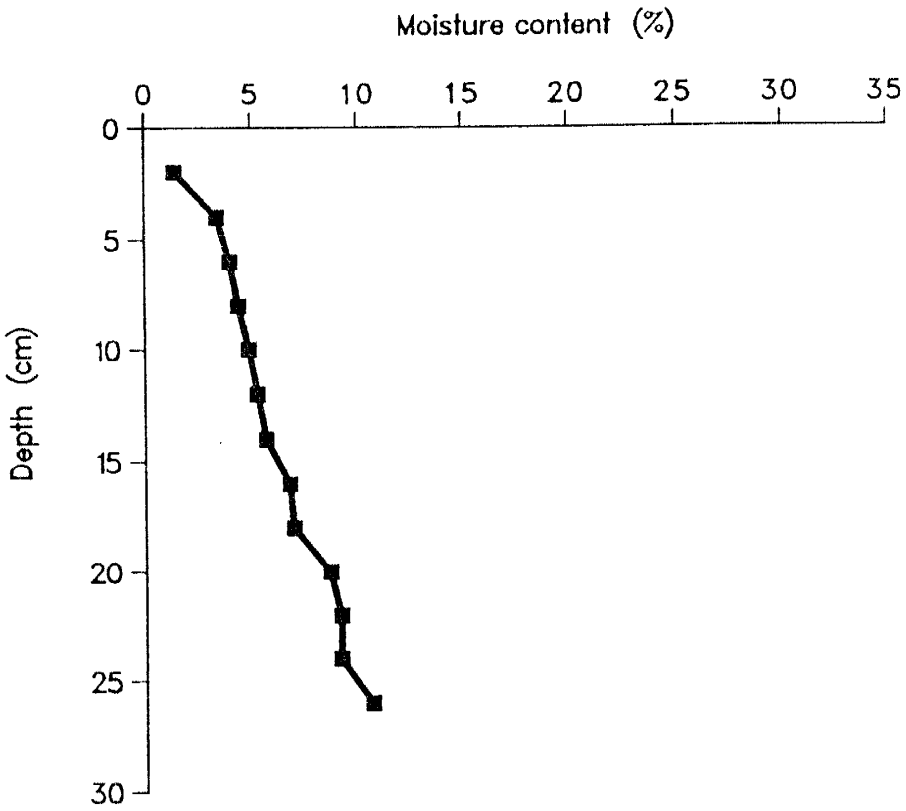

FIGURE 16. Moisture content versus depth for column 10.

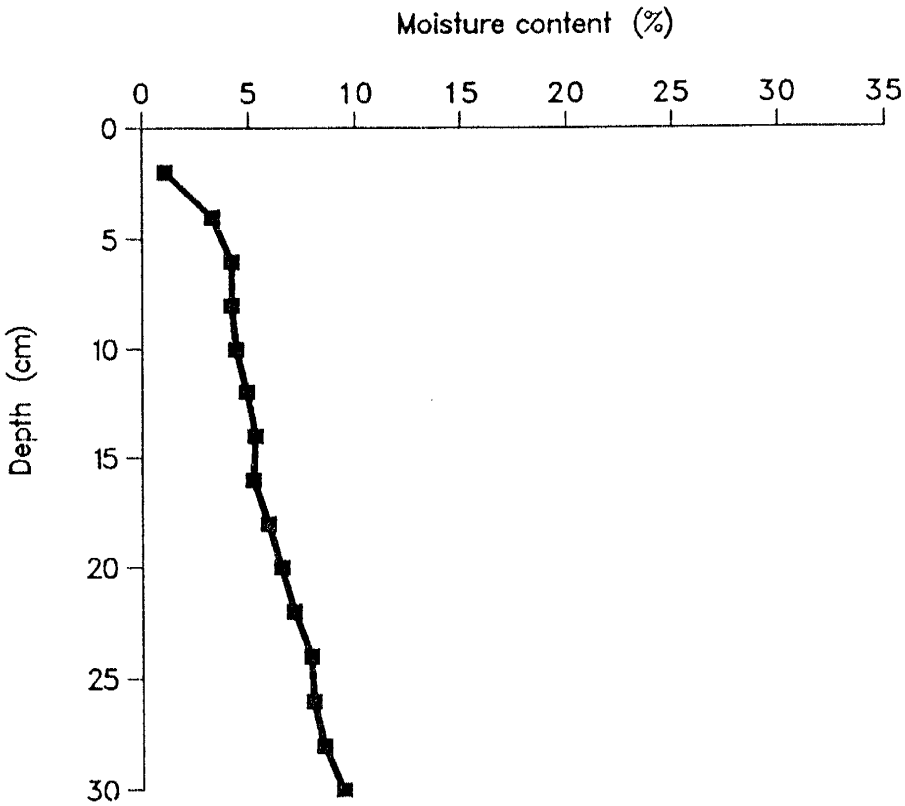

FIGURE 17. Moisture content versus depth for column 11.

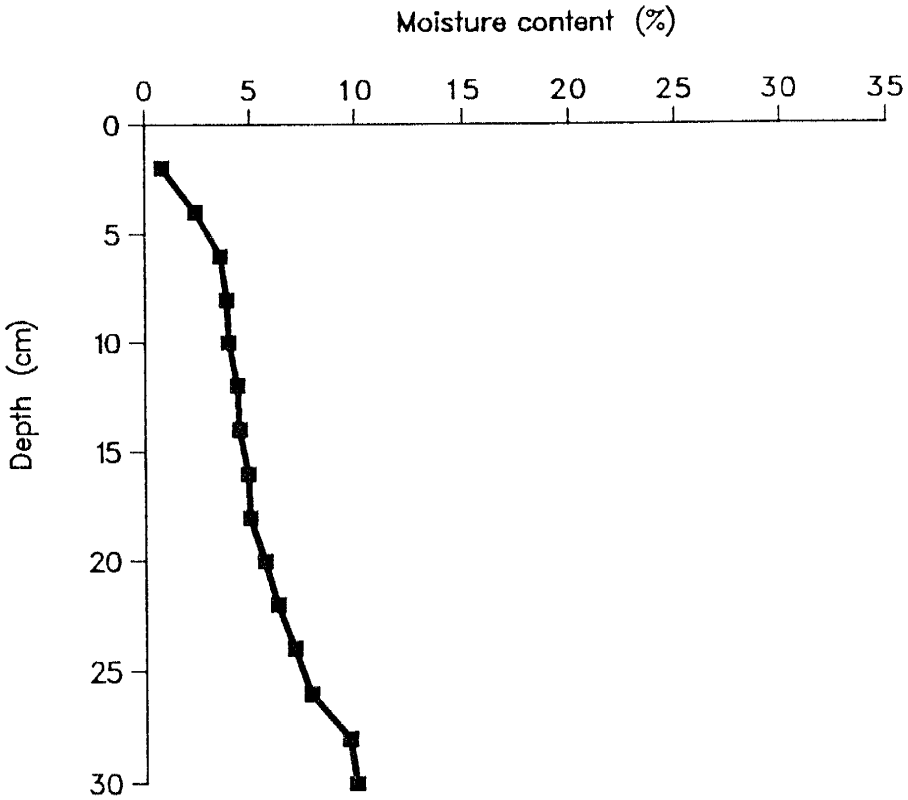

FIGURE 18. Moisture content versus depth for column 12.

BROMIDE ANALYSIS, EVAPORATION AND ISOTOPES

Due to the problems experienced with column evaporation during the initial phase of the project as discussed above (i.e. second-stage evaporation), estimates of recharge and evaporation rates were computed from the time when the first aliquot of water was added to the top of each column. Total recharge is given in cm and computed using the average volumetric water content for the entire interval above the depth of the center of mass of the bromide front, multiplied by the depth of the center of mass of the bromide front. The depth to the center of mass of the bromide front was taken as the center of the dispersed zone for each column, i.e. $c/c' = 0.5$, where c' is the concentration occurring at interval 02-04 cm (Appendix C). The 02-04 cm interval was chosen due to the high concentrations that developed in the dry zone as a result of the bromide being carried upward via the evaporative flux of water. Recharge rate is taken as total recharge divided by the number of days prior to the time the column was sampled. The second-stage evaporation rate was computed as the average time required for the dry-front to progress to an average depth of 2 cm.

Results of the isotope study are summarized in Table 2 and Appendix B. Figures 22 through 45 (following this section, starting page 57) show isotopic and bromide concentration profiles of columns 1 through 12, except column 7. Due to a power outage that occurred at the time of sampling, column 7 was mistakenly capped in efforts to prevent further evaporation. As a result, the entire column redistributed as is evident by the moisture content profile (Figure 13 and Appendix B) and isotopic analysis was not performed. Figure 33 however provides the bromide concentration versus depth profile for column 7. Figure 41 shows a ^{18}O vs D plot for column 11.

Through inspection of the sample analyses it became evident that sample preservation technique is critical to reliable results. Although all samples were placed in sealed containers with silicon vacuum grease added around the threads of the caps to prevent leakage, several samples displayed enrichment, brought about most likely by evaporation of the sample. Interestingly enough, this phenomenon appeared in a series of samples, primarily in columns 6 and 8. This would indicate that the sample containers were probably flawed in some manner. Additionally, from time to time, during the vacuum distillation process, leaking in the transfer tube as a result of either a bad stopcock or a poor seal between the transfer tube and either the soil container or cold trap. In nearly every instance where this was noted, waters analyzed were enriched with respect to the surrounding samples. In cases where either of the two abovementioned problems were noted, the results were excluded from the isotopic profile and analysis of recharge through equation 18. Further, in those cases where the top of the profile, *i.e.* interval 00–02, was believed to be erroneous as a result of either of the above two sources, the evaporation front δD was calculated using equation 34 and was used in the profile analysis. In computing the δef at the evaporation front, the average dry-zone depth was taken as z, a value of −100.75 ‰ was used for the D composition of the input water (measured value), tortuosity (τ) was assumed to be 1.52 for clean sand (Penman, 1940), porosity (n) was 40%, D_{li} was taken as 2.2×10^{-5} cm^2/s (Walker et al., 1988), the equilibrium-fractionation factor for D_{lv} was assumed to 1.0768, the diffusion ratio excess (η) was taken from Merlivat (1978), as 0.0249 and the evaporation rate was taken as the second-stage evaporation rate for each column.

The estimation of the parameters used in equation 37 was taken from Appendix B and the isotopic profiles in the manner outlined below. Figure 19 provides a typical isotopic profile showing the location of each of the isotopic parameters evaluated in equation 37.

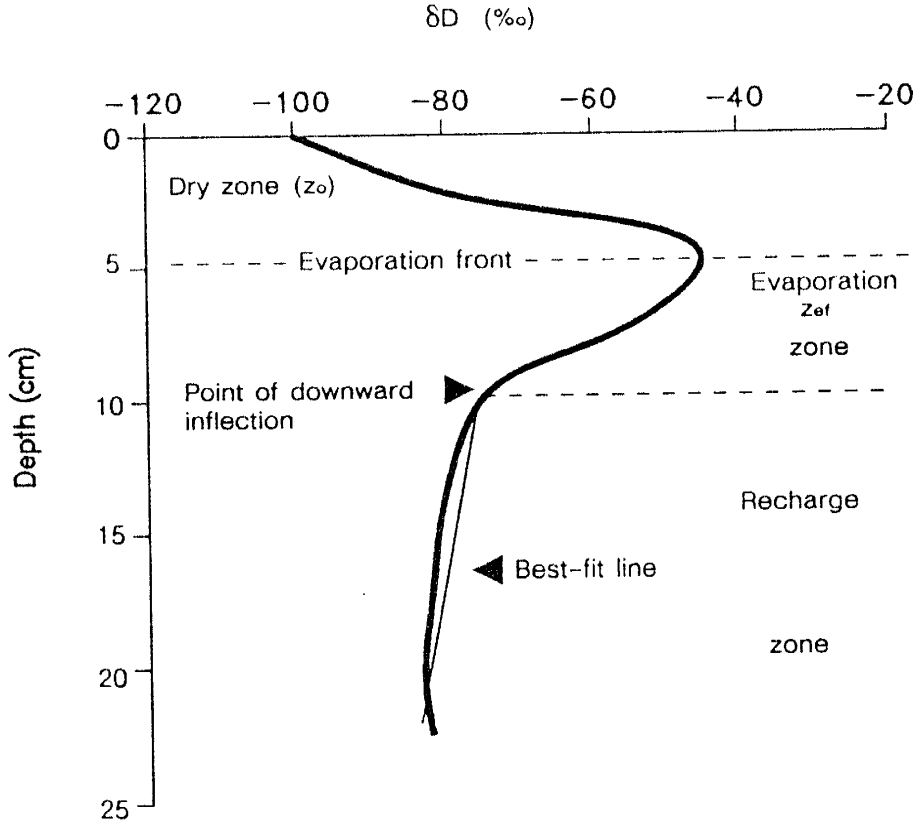

FIGURE 19. Idealized isotopic profile showing location of the evaporation front, evaporation zone, recharge zone, best-fit line of recharge zone and point of downward inflection marking the base of the evaporation zone. Note that the best-fit line should include the portion of the recharge zone that is in equilibrium with the recharge waters.

1. The water infiltrating from the surface (Q_p) is the total amount of water added divided by the total number of times water was added, *i.e.* total water / number of recharge events.

2. The dry zone thickness (z_o) was taken as the average of the dry-front progressions for each column.

3. The specific retention (Sr) for the Sevilleta sand was taken as a volumetric water content of 7%, (J.T. McCord, oral communication,1988).

4. The location of base of the evaporation zone is one of the most critical parameters in equation 37, since the value of $z_{ef} + z_o$ (z_o usually being small), represents the total depth at which water is removed from the soil by evaporation. The evaporation zone thickness (z_{ef}) is taken from the δD profile as the crest of the downward inflection of slope of the profile from the evaporation front. In validating this approach, a D profile was computed using the methods of Barnes and Allison (1984) by incorporating the evaporation data, evaporation front isotopic composition and recharge zone isotopic composition of column 11. Column 11 was chosen because it was believed that this profile best represents an equilibrium state between the profile and recharge water, as discussed later. Figure 20 provides a plot of the computed isotopic composition versus depth and the observed isotopic profile versus depth for column 11. As can be seen, there is good agreement between the computed and observed profiles. From equation 35, the evaporation zone thickness (z_{ef}) is dependent upon the amount of water passing through the soil and evaporation, and recharge (q_r) is dependent upon z_{ef} and the amount of water infiltrating into the soil (Q_p). Arriving at the appropriate z_{ef} value which balances these three parameters was accomplished by taking the computed profile of Figure 20 and solving equation 37 repeatedly for z_{ef} over a range of Q_p and q_r values. This relationship is shown on Figure 21. Entering into the y and x axis of Figure 21 with a value of Qp and q_r respectively, (the value of q_r being taken from the bromide recharge analysis), a z_{ef} value is intersected. From the isotopic profiles and the Qp and q_r of each column, it is observed that z_{ef} does fall within the general interval, $z_{ef} + z_o$, visually noted as the point of downward inflection. Since the point of inflection is a sample point which covers the entire sample interval above it, (i.e. 2 cm), the median value of this interval is used as z_{ef}.

5. The average isotopic composition of the evaporation zone (δ_{ef}) was taken as the arithmatic mean of the isotopic composition of the samples from z_{ef} upward.

6. The average volumetric moisture content of the evaporation zone (θ_{ef}) was taken as the average moisture content over the z_{ef} range.

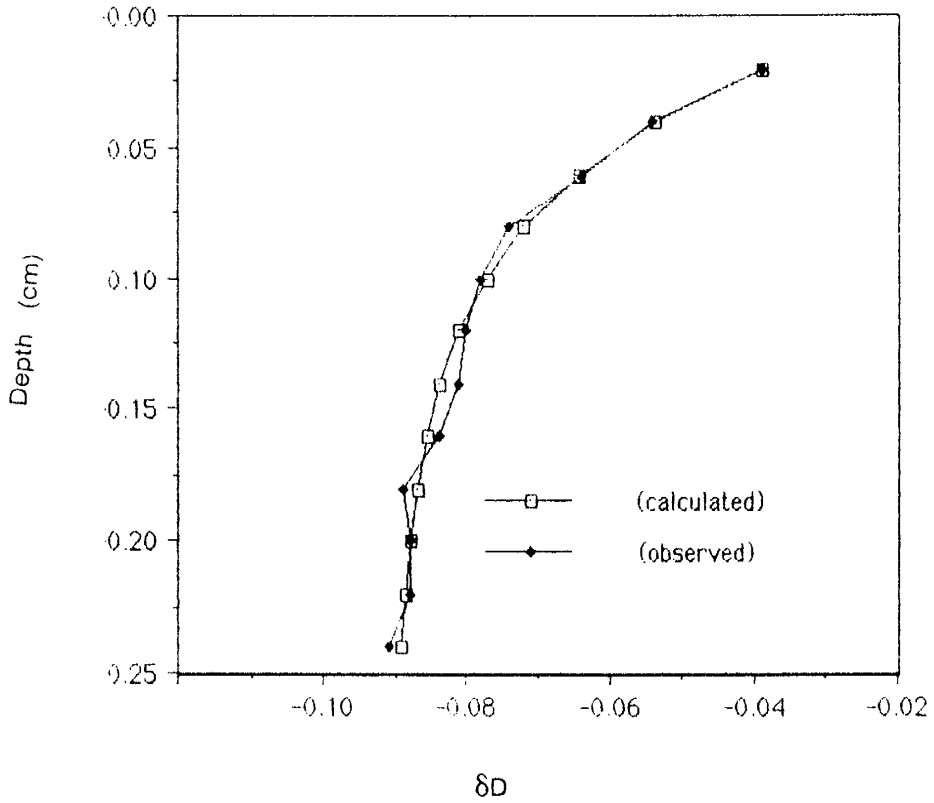

FIGURE 20. Observed D profile versus depth and computed D profile versus depth.

7. The average δD of the recharge zone (δr) was arrived at by placing a best fit line through the isotopic profile from the base of the evaporation zone downward and then taking the mean isotopic composition of this line. The value of δr should plot asymptonically to the δD axis, but be enriched compared to the Qp water, proportional to the amount of recharge. Generally, as time passes and recharge continues, the recharge

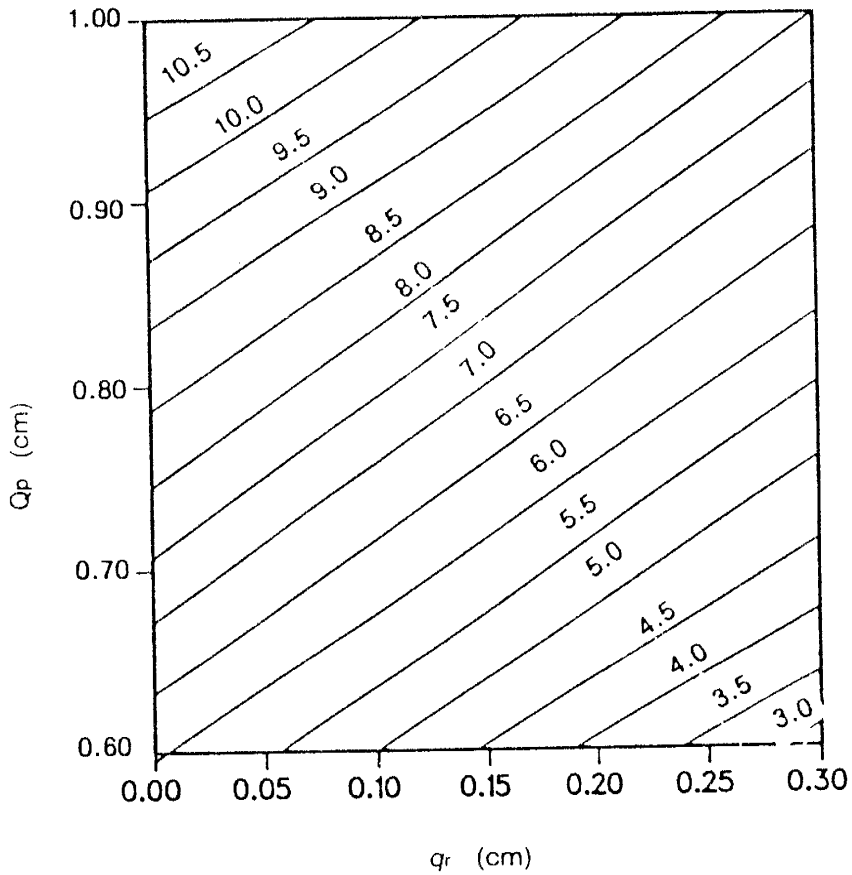

FIGURE 21. Qp versus qr for computed profile showing z_{af} (along diagonal) obtained through equation 37.

zone should approach an equilibrium condition. The δr should represent this equilibrium. In some instances, the base of the recharge zone for the columns was chosen as the point where incomplete mixing of recharge water with initial flush water was evident. For exam-

ple, the recharge zone in column 3 was observed to extend down to 18 cm. Below 18 cm the profile displayed concentrations that approach the isotopic composition of the initial flush water, (-100‰). This exclusion would not be appropriate in the natural setting.

The following discussion provides basic column isotopic and recharge information derived as previously outlined. There are three recharge estimates for each column: bromide recharge, designated as Br recharge which was computed through the center of mass of the bromide front; theoretical profile δD recharge using the z_{ef} from Figure 21 and applying equation 37, and; the inflection point δD recharge method computed using the z_{ef} from the isotopic profiles and applying equation 37.

Column 1

No sample was taken at interval 00-02 where the evaporation front is located. However, using equation 34, a value for D of -44‰ was calculated. Column 1 exhibited profile characteristics displaying an evaporation zone extending down to about the 6-8 cm interval with an average D composition of this zone of -59‰. Below this point the profile over an interval of only 2 cm, a δDr is observed to be -89‰. Below 10 cm, the profile exhibited isotopic characteristics approximate to that of the initial flush water, *e.g.* -100 ‰. The average dry-zone thickness was 2.04 cm and the average moisture content of the evaporation zone was 5.8 %. The total water added to column 1 was 3.29 cm over 4 aliquots, or 0.823 cm of water per event. Due to sampling problems, the bromide analysis was erroneous and therefore the Br recharge estimate is not possible. However, upon inspection of

Figure 22, the depth at which the initial flush water is observed is 16 cm. Assuming that this depth represents the actual amount of recharge into column 1, then by applying the volumetric water contents above this interval, recharge was found to be 0.726 cm. Using Figure 21, with Q_p=0.82 cm and q_r = (0.726/4) = 0.182 cm, z_{ef} was found to be 6.8 cm and the corresponding theoretical profile δD recharge was 0.158 cm/event or 0.63 cm total recharge. Taking the median from the 6–8 cm interval, and subtracting the 2 cm dry-zone, (i.e. z_{ef} = 5 cm), an inflection point δD recharge of 0.319 cm/event or 1.27 cm total recharge is computed.

Column 2

Using equation 34, a δD_{ef} was computed to be -45 ‰. Column 2 displays an isotopic profile in early stages of development, however significantly more developed than column 1. In comparison to column 1, enrichment of the lower portion of the profile was observed. The exact location of the extent of the evaporation zone is not clear from the profile in that the downward inflection appears to occur at a depth of 10 cm. Using this depth, an average D composition of the evaporation zone was observed to be -61 ‰. From 10 cm to 18 cm the isotopic profile averaged -89 ‰ (δr), and below 18 cm approached that of the initial flush water. The total water added to column 2 was 6.29 cm or an average of 0.786 cm per event. The average dry zone depth was 1.93 cm and the average moisture content of the evaporation zone was 6.2 %. Br recharge is computed to be 0.72 cm. The theoretical profile δD recharge using Figure 21 and equation 37 is 0.07 cm/event or 0.56 cm total

recharge. The inflection point δD recharge using the isotopic profile is 0.110 cm/event or 0.88 cm total recharge.

Column 3

Column 3 displays a profile similar to column 2, however slightly more enriched in the evaporation zone. 7.6 cm of water was added to column 3 over a period of 72 days, averaging 0.84 cm/event. The average dry zone thickness was 2.06 cm. The point of downward inflection was observed at the 10–12 cm interval with an average D and moisture content of –64 ‰ and 6.0 %, respectively of the evaporation zone. A poorly developed recharge zone extends down to only 18 cm and was observed to be –89‰. The reason for this anomaly is not clear since column 3 not only had more total water added during the 72 day period, but had more water added per aliquot, (0.84 cm) than either columns 1 or 2. Intuitively, it would be expected that the recharge zone would be more developed than either of the previous columns, yet possible packing heterogeneities or sampling and analytical errors could explain this discrepancy. Using equation 34, a δ_{ef} is computed as –43 ‰. This compares well with the measured value of –44 ‰. A Br recharge was found to be 0.86 cm. The theoretical profile δD recharge using Figure 21 was found to be 0.071 cm/event or 0.639 cm total recharge. The inflection point δD recharge using the observed median of the interval at the point of downward inflection (e.g. 11 cm, z_{ef} = 9 cm) was found to be 0.180 cm/event or 1.62 cm total recharge.

Column 4

Column 4 exhibited one of the lowest second stage evaporation rates and consequently, had one of the lowest volumes of water per unit time added over 80 days prior to sampling. 7.77 cm of water was added over 10 aliquots, averaging 0.78 cm per event. An average dry zone thickness was observed to be 1.87 cm. The profile was poorly developed as a result of lack of recharge, displaying an isotopic composition similar to the initial flush water at depth interval 14-16 cm. The evaporation zone was observed to extend down to 8-10 cm interval with an average D composition of this zone of -59 ‰. The recharge zone is, as to be expected, poorly defined and is interpreted to exist over 8 cm to 14 cm with an average δDr of -88 ‰. Br recharge was observed to be 0.92 cm. The theoretical profile δD recharge was found to be 0.065 cm/event or 0.65 cm total recharge. The inflection point δD recharge estimated using equation 37 and the observed profile was found to be 0.11 cm/event or 1.10 cm total recharge. A computed δef was found to be -46 ‰. The measured value for interval 00-02 in column 4 was -50‰.

Column 5

10.7 cm of water was added to column 5 over 11 aliquots, during the 89 days prior to sampling. The average dry zone depth was 2.33 cm and the average moisture content of the evaporation zone was 7%. Column 5 exhibited an evaporation front δef of -41 ‰ which compares well with the computed value using equation 34 of -40 ‰. Column 5 displayed

an overall enrichment in comparison to the previous columns, however the recharge zone was observed to be poorly developed showing variations near the top of the zone. Taking the crest of the downward inflection as the base of the evaporation zone to be 6-8 cm interval with an average D composition of -58 ‰, recharge was computed to be 0.526 cm per event, 5.79 cm total recharge. This however does not seem reasonable since column 5 exhibited one of the highest second stage evaporation rates and consequently one of the highest volumes of water added per alliquot *i.e.* 0.975 cm per event. This would indicate that both the evaporation zone and the recharge zone would be more developed with depth than was observed at 6 cm and 10 cm respectively.

From Figure 21, a z_{ef} is noted at 10.0 cm, (Q_p = 0.98 cm, q_r = 0.116 cm). Using this value as the base of the evaporation, ie 10-12 cm interval, the evaporation zone composition was -63‰. The recharge zone was then observed to extend from 12 cm to 20 cm with an δr of -89‰. Br recharge is computed as 1.28 cm. A theoretical profile δD recharge using Figure 21 results in 0.02 cm/event or 0.22 cm total recharge. The inflection point δD recharge is estimated as the median of the 10-12 cm interval, i.e. z_{ef} = 9 cm, and was computed to be 0.11 cm/event or 1.09 cm total recharge.

Columns 6,7,8

All samples from columns 6 and 8 displayed significant enrichment due to evaporation as previously discussed. Therefore, no further discussion on their profiles will occur. Column 7 was not sampled for isotopic analysis.

Column 9

Column 9 received 12.39 cm of water over a 126 day period with an average of 0.826 cm per event, similar in magnitude to columns 4 and 12. The average dry zone depth was 2.0 cm and the average moisture content of the evaporation zone was 6.5 %. Column 9 exhibited a δef of -39 ‰, in fair comparison with a δef of -43 ‰ computed using equation 34. Column 9 displayed a point of downward inflection at about the 4-6 cm interval, and applying this value with the average D composition for this zone of -57‰, a δD recharge is computed to be 5.8 cm. This is somewhat higher than would be expected given the length of time and amount of water added to column 9 in comparison to the previous columns. Therefore, using Figure 21, a z_{ef} was found to be 7.9 cm or at interval 8-10 cm. Using this as the base of the evaporation zone, an average D composition of this zone was found to be -61‰. The recharge zone was then from 12 cm to 24 cm with a δr of -84‰. A Br recharge was found to be 1.06 cm. A theoretical profile δD recharge using 7.9 cm from above, was 0.13 cm/event or 2.00 cm total recharge. The inflection point δD recharge using the median of the 8-10 cm interval, (i.e. 9 cm, z_{ef} of 7 cm) was found to be 0.21 cm/event or 3.12 total recharge.

Column 10

Using equation 34, the δD of the evaporation front is computed to be -43 ‰, which compares well with the measured value of -45 ‰. From inspection of the δD profile, the

evaporation zone was observed to extend down to 10-12 cm interval, with an average D composition and moisture content of -62 ‰ and 6.6 %, respectively. The recharge zone is taken as the best fit line through interval 12 cm to 18 cm and results in a δr of -88 ‰. The total water added to column 10 was 13.87 cm over 16 aliquots of 0.867 cm per event. The average dry zone thickness was 2.08 cm. Br recharge was 1.18 cm. The theoretical profile δD recharge using Figure 21 and a z_{ef} of 8.7 cm was 0.05 cm/event or 0.81 cm total recharge. The inflection point δD recharge using a z_{ef} of 9 cm observed from the profile was 0.02 cm/event or 0.38 cm total recharge.

Column 11

The computed δef using equation 34 was -43 ‰ in good agreement with the measured value of -39 ‰. The crest of the downward inflection of the isotopic profile was at the 10-12 cm interval, resulting in an average D composition at the evaporation zone of -62 ‰ and an average moisture content of the evaporation zone of 6.4 %. The recharge zone extends down to 24 cm and a δr was computed from the best fit line to be -87 ‰. The total water added to column 11 was 14.43 cm or 0.849 cm per event. The average dry front depth was 2.03 cm. Br recharge was 1.86 cm. The theoretical profile δD recharge using Figure 21, (z_{ef} = 8.2 cm) was 0.09 cm/event or 1.59 cm total recharge. The inflection point δD recharge using the observed z_{ef} of 9 cm, was 0.02 cm/event or 0.39 cm total recharge.

Figure 41 shows the ^{18}O profile for column 11. Figure 43 provides the ^{18}O versus D plot for column 11. As can be seen from figure 43, column 11 data plots to the right of the meteoric water line with a slope of approximately 3. This slope was computed excluding

interval 8-10 cm and using the calculated $\delta^{18}O$ value at the evaporation front of +7.8 ‰ This is in good agreement with slopes for waters evaporating from soils, (Allison et al. 1983). Using equation 34, a $\delta^{18}O_{ef}$ is computed to be +7.8 ‰, significantly heavier than measured at interval 00-02 cm of -0.7 ‰. The ^{18}O profile displayed large variations throughout the entire profile. However, using the z_{ef} from Figure 21, a ^{18}O composition of the evaporation zone was computed as -2.2‰, and assuming that the recharge zone extends down to 24 cm as was the D profile, (e.g. 12-24 cm), a δr of -9.52‰ observed. Using these parameters a theoretical profile $\delta^{18}O$ recharge and inflection point $\delta^{18}O$ recharge was found to be negative, (-0.106 cm/event).

Column 12

14.9 cm of water over 159 days was added to column 12 averaging 0.83 cm/event. The average dry front thickness was 1.89 cm. Column 12 was similar to columns 4 and 9 with respect to the amount of water added per unit time, second stage evaporation rate and over all isotopic profile. Column 12 exhibited a poorly defined profile reaching original flush water D composition at about 28 cm. Choosing the δ parameters necessary for equation 37 was difficult, however using Figure 21, a z_{ef} was found to be 8.5, corresponding to a profile depth of 10-12 cm, an average D composition of the evaporation zone was found to be -63 ‰. The recharge zone was observed to extend from 12 cm to 26 cm with a δr of -89‰. Br recharge was 0.82 cm. The theoretical profile δD recharge using the z_{ef} from Figure 21 was 0.058 cm/event or 1.04 cm total recharge. The corresponding inflection point δD recharge was then 0.015 cm/event of 0.27 cm total recharge.

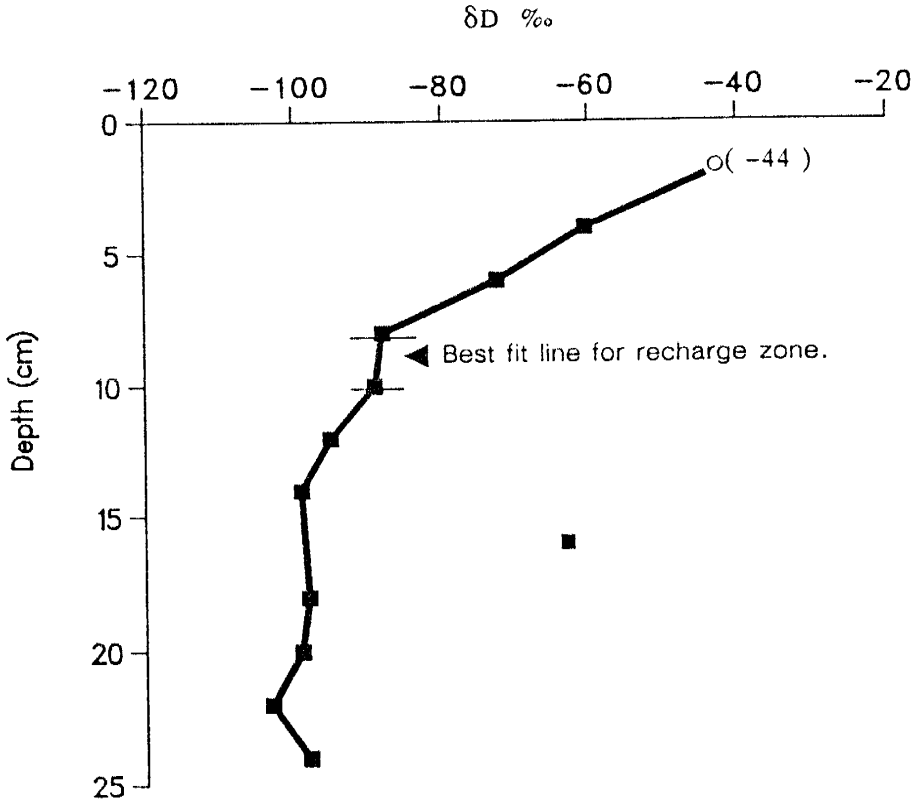

FIGURE 22. δD versus depth profile for column 1. Light line shows best-fit of data within the recharge zone interval used equation 37. Number in parenthesis is the isotopic composition computed through equation 34. Open circle indicates the computed value is used in the isotopic profile.

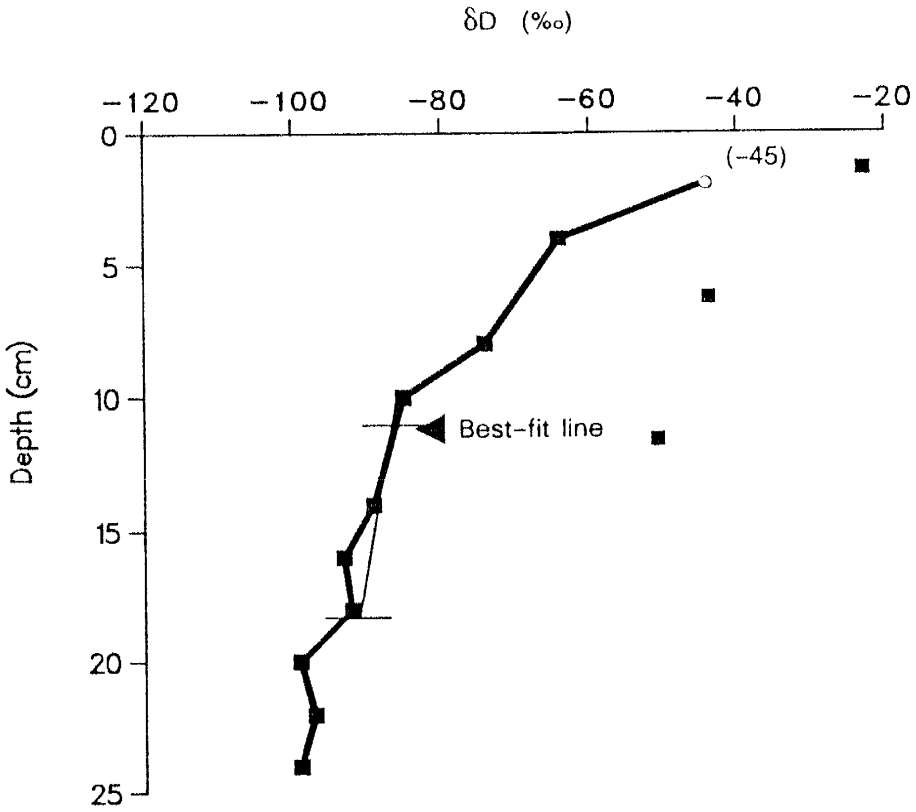

FIGURE 23. δD versus depth profile for column 2. Light line shows best-fit of data within the recharge zone interval used in equation 37. Number in parenthesis is the isotopic composition at the evaporation front computed through equation 34. Open circle indicates computed value used in profile analysis.

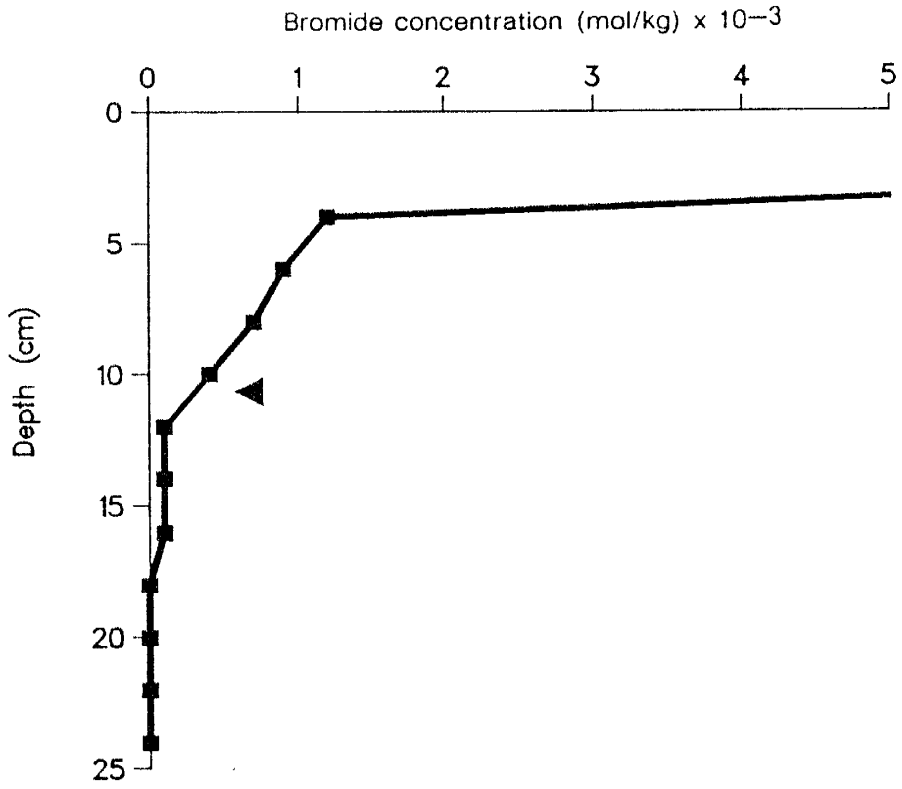

FIGURE 24. Bromide concentration versus depth for column 2. (◀) indicates the center of mass of the bromide front.

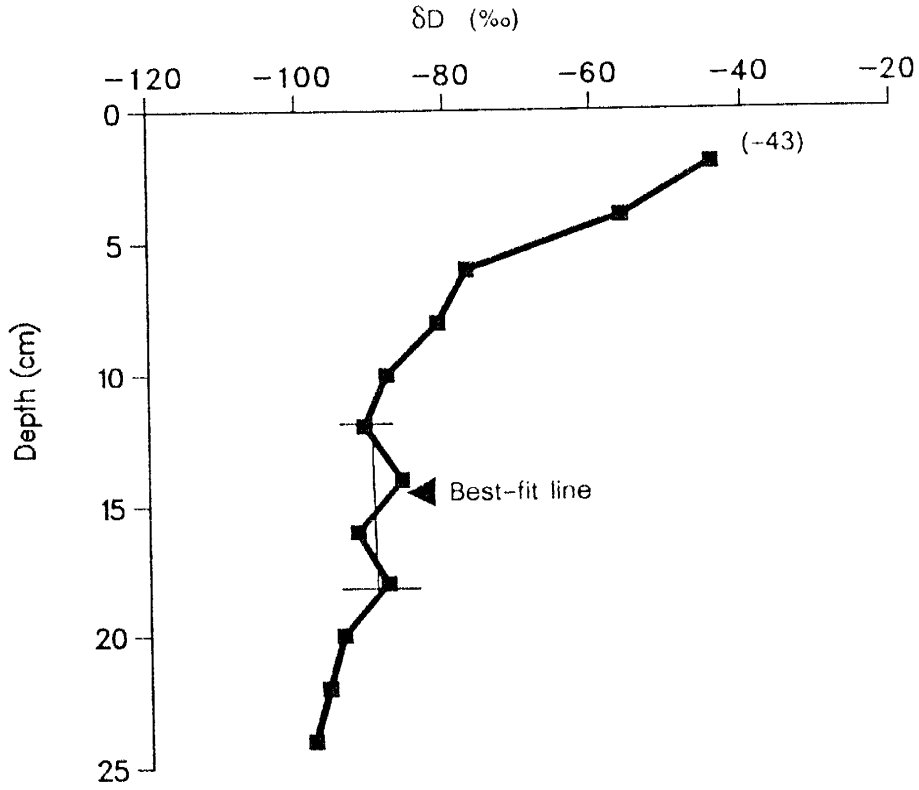

FIGURE 25. δD versus depth profile for column 3. Light line shows best fit of data within the recharge zone used in equation 37. Number in parenthesis is the isotopic composition at the evaporation front computed through equation 34.

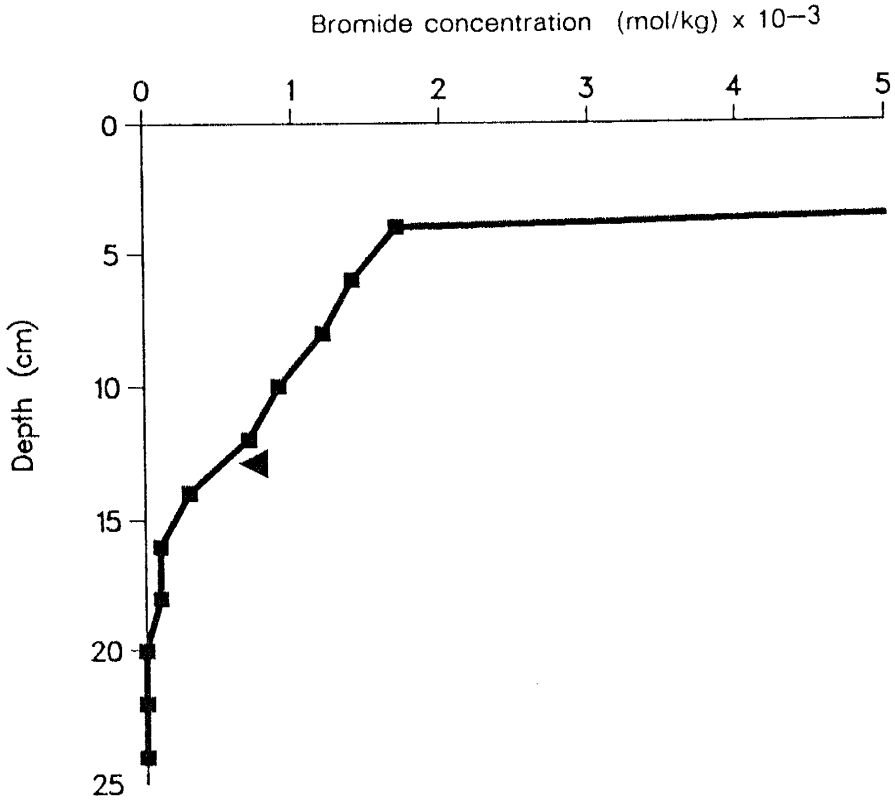

FIGURE 26. Bromide concentration versus depth for column 3. (◀) indicates center of mass of bromide front.

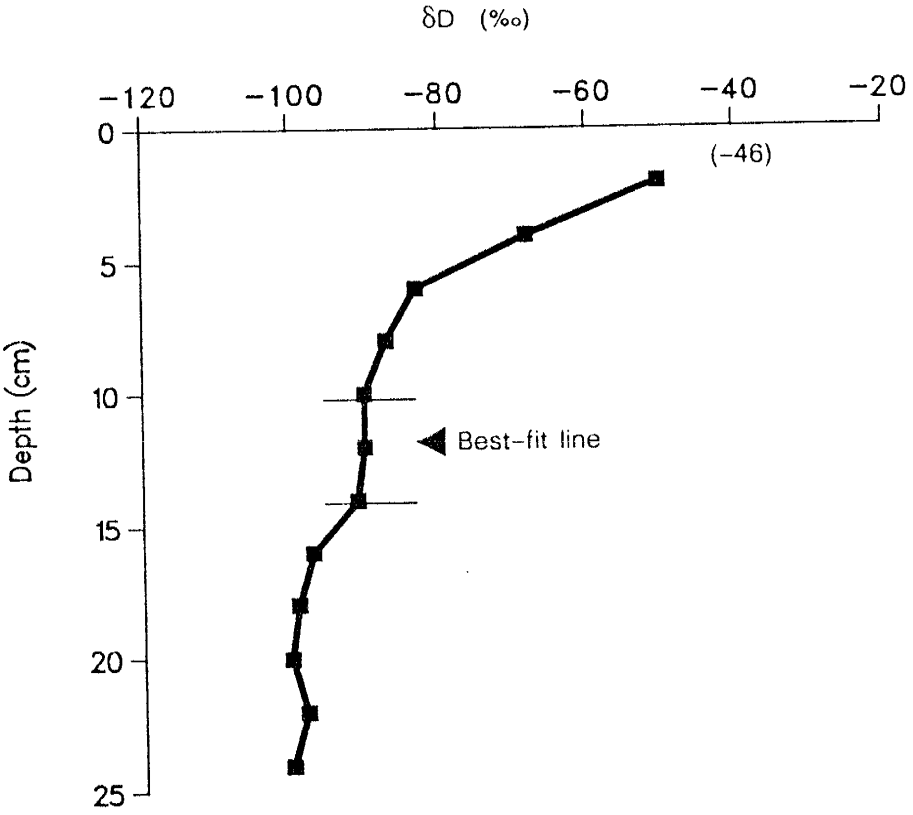

FIGURE 27. δD versus depth profile for column 4. Light line shows best-fit of data with the recharge zone interval used in equation 37. Number in parenthesis is the isotopic composition at the evaporation front computed through equation 34.

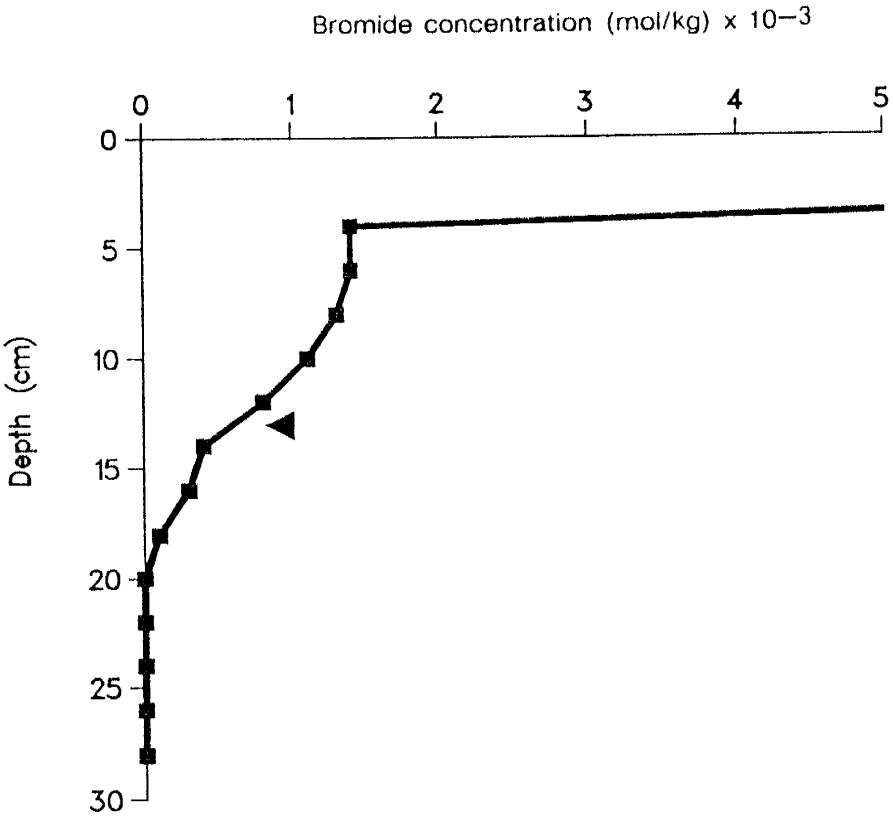

FIGURE 27. Bromide concentration versus depth for column 4. (◀) indicates center of mass of the bromide front.

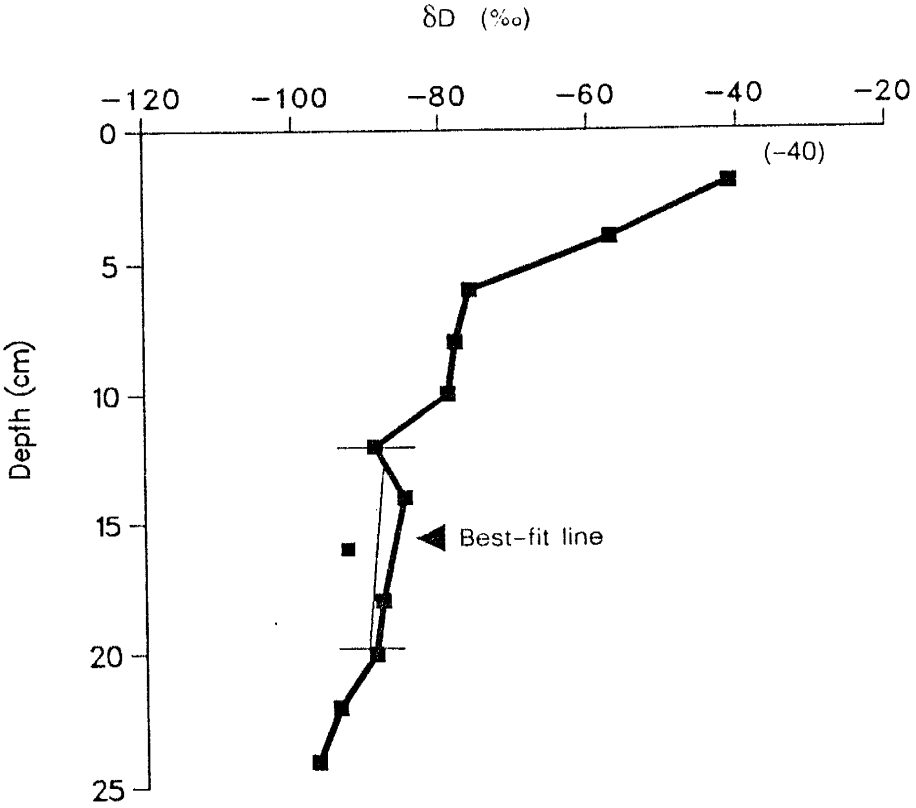

FIGURE 29. δD versus depth profile for column 5. Light line shows best-fit of data within the recharge zone; however, as stated in the text, this line is placed as a best guess for use in equation 37. Number in parenthesis is the isotopic composition at the evaporation front computed through equation 34.

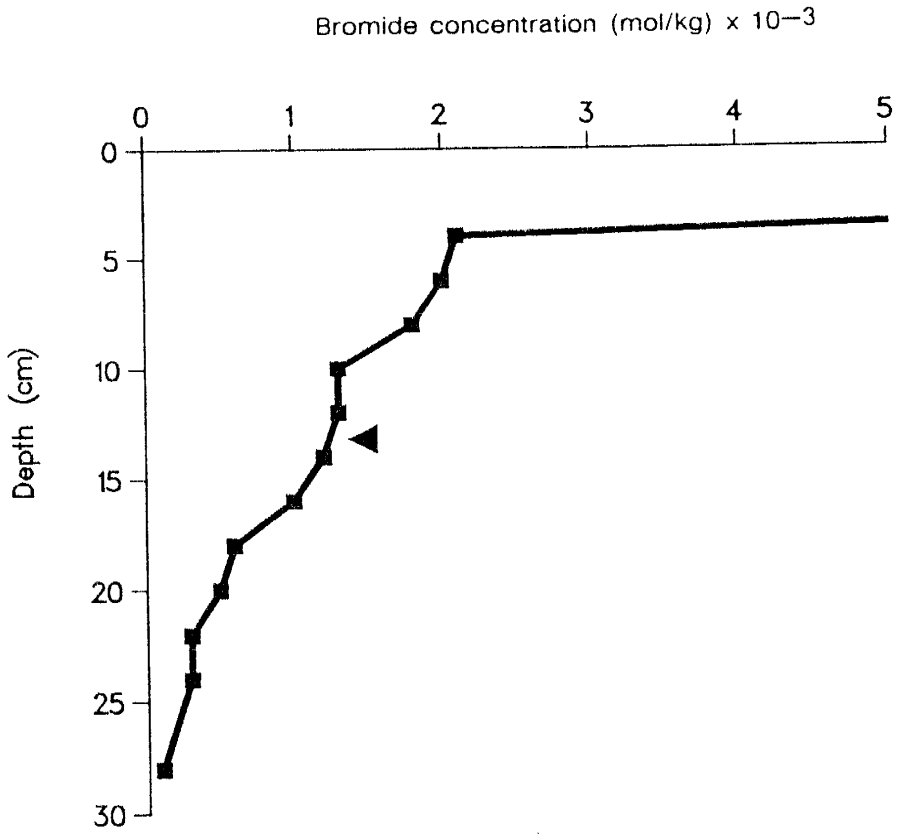

FIGURE 30. Bromide concentration versus depth for column 5. (◀) indicates center of mass of the bromide front.

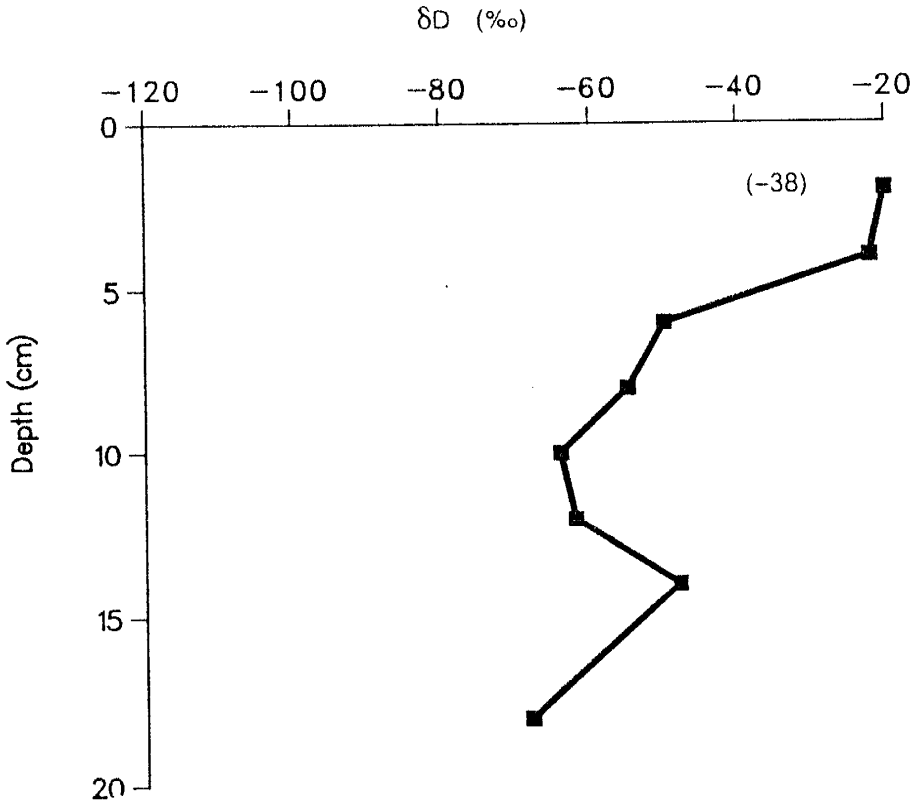

FIGURE 31. δD versus depth profile for column 6. Note significant enrichment believed to be a result of evaporation from the sample container. Number in parenthesis is the isotopic composition at the evaporation front computed through equation 34. Recharge was not computed for column 6.

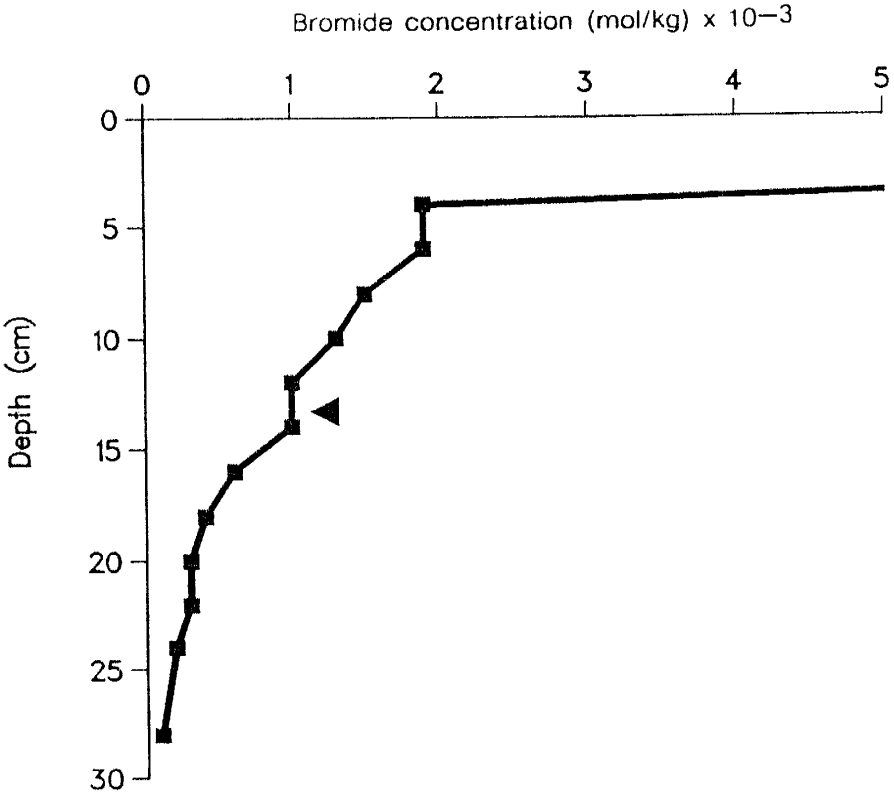

FIGURE 32. Bromide concentration versus depth for column 6. (◀) indicates center of mass of the bromide front.

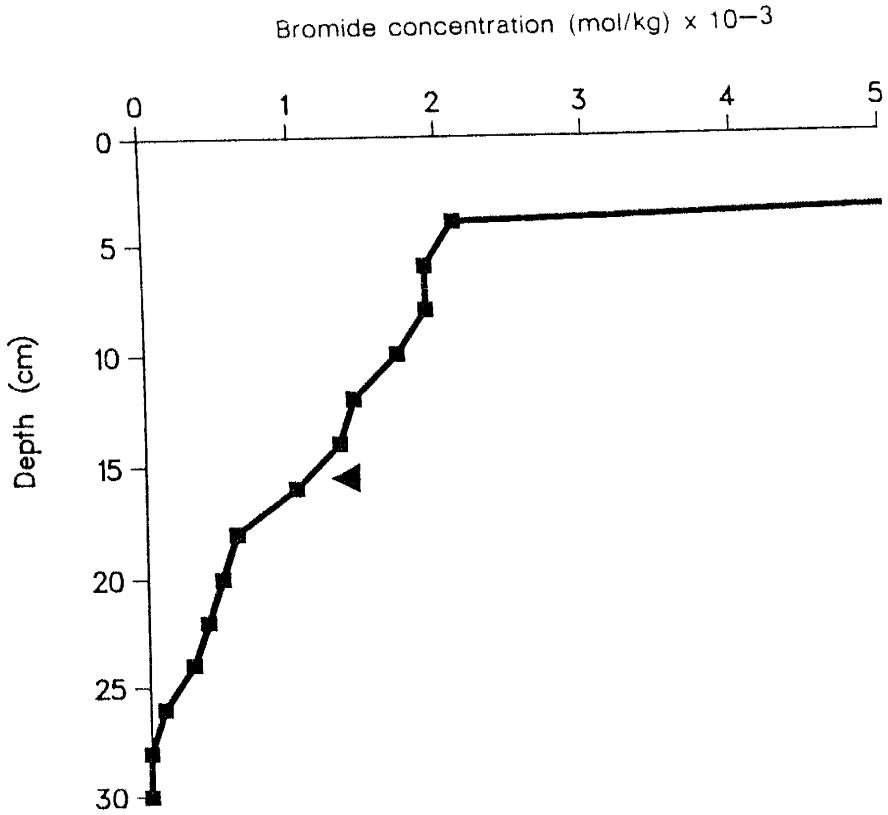

FIGURE 33. Bromide concentration versus depth for column 7. (◀) indicates center of mass of the bromide front.

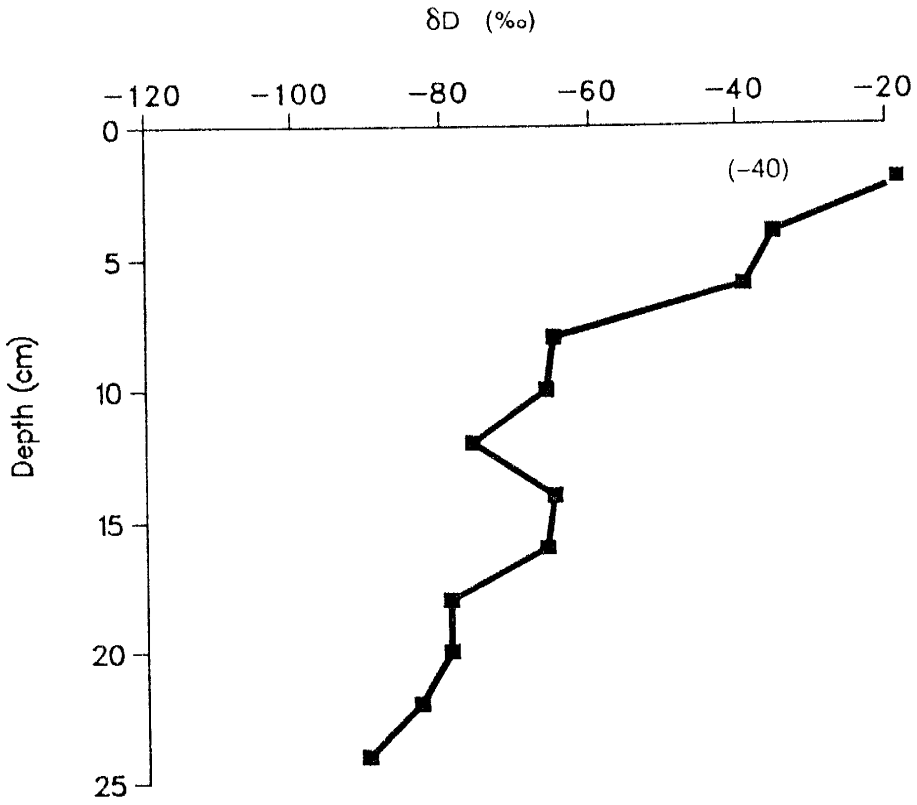

FIGURE 34. δD versus depth profile for column 8. Note significant enrichment believed to be a result of evaporation of the sample. Number in parenthesis is the isotopic composition at the evaporation front computed through equation 34. Recharge was not computed for column 8.

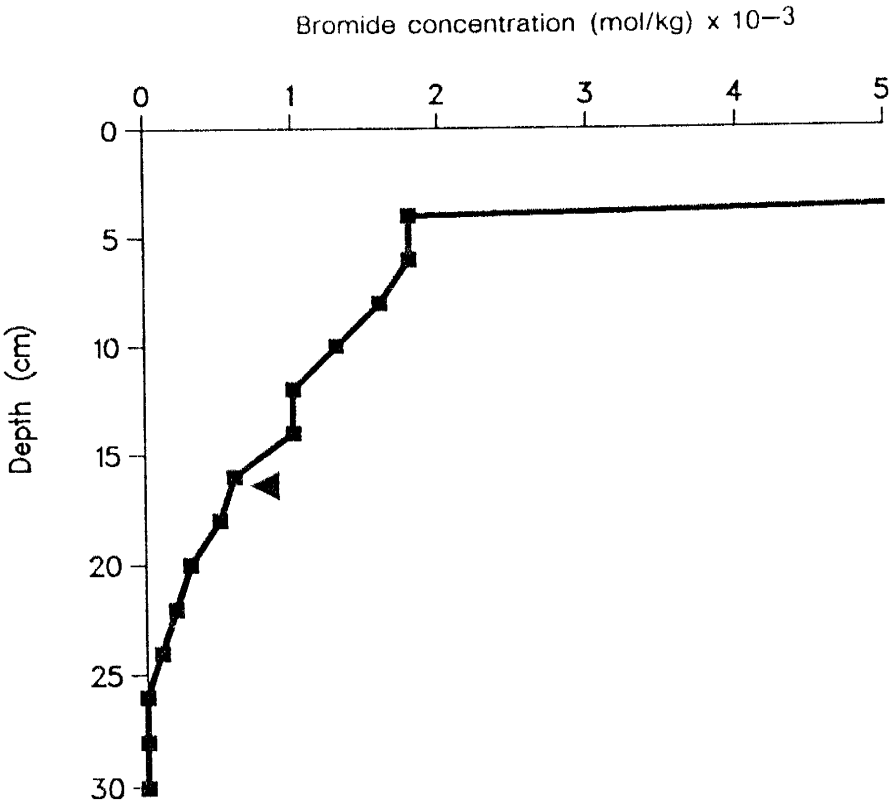

FIGURE 35. Bromide concentration versus depth for column 8. (◀) indicates center of mass of the bromide front.

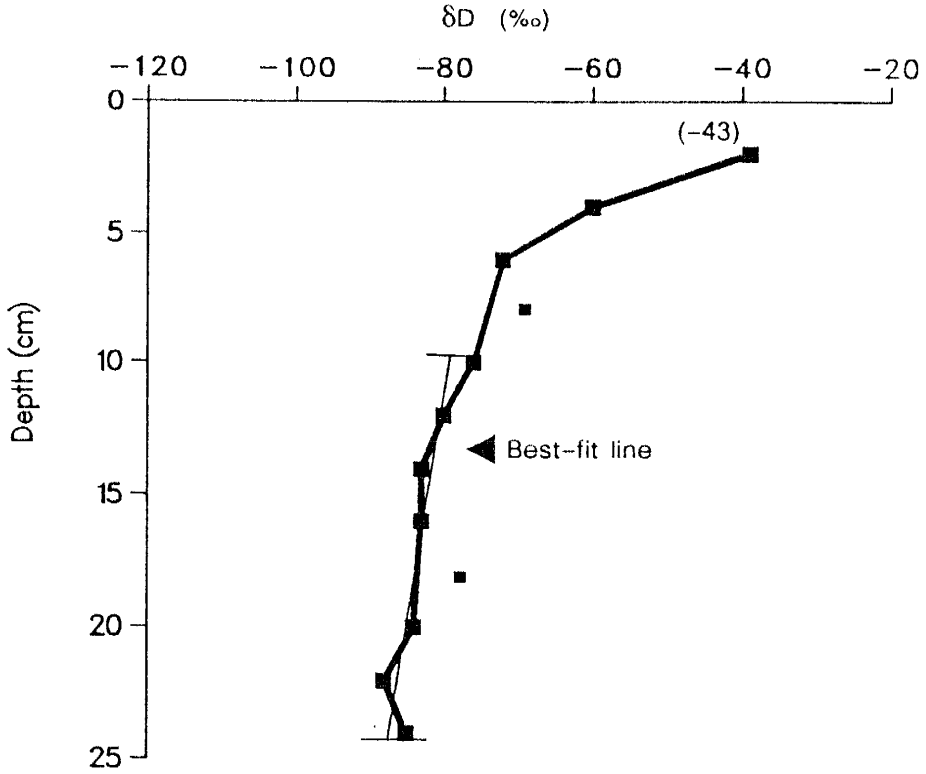

FIGURE 36. δD versus depth profile for column 9. Light line represents the best fit of data within the recharge zone interval used in equation 37. Number in parenthesis is the isotopic composition at the evaporation front computed through equation 34.

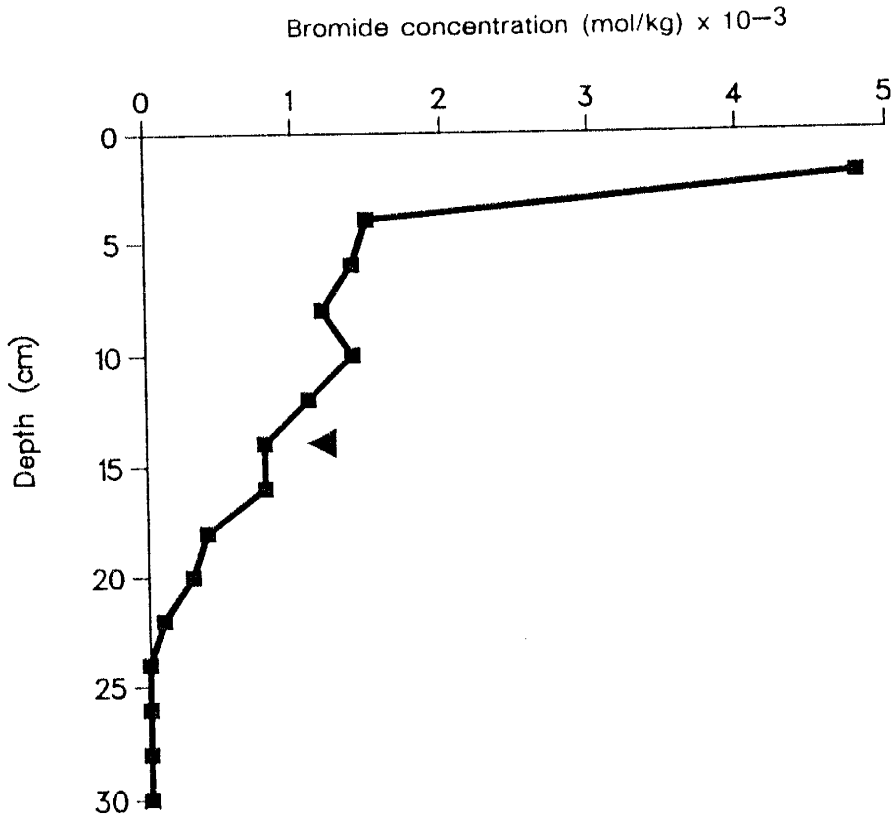

FIGURE 37. Bromide concentration versus depth for column 9. (◀) indicates center of mass of the bromide front.

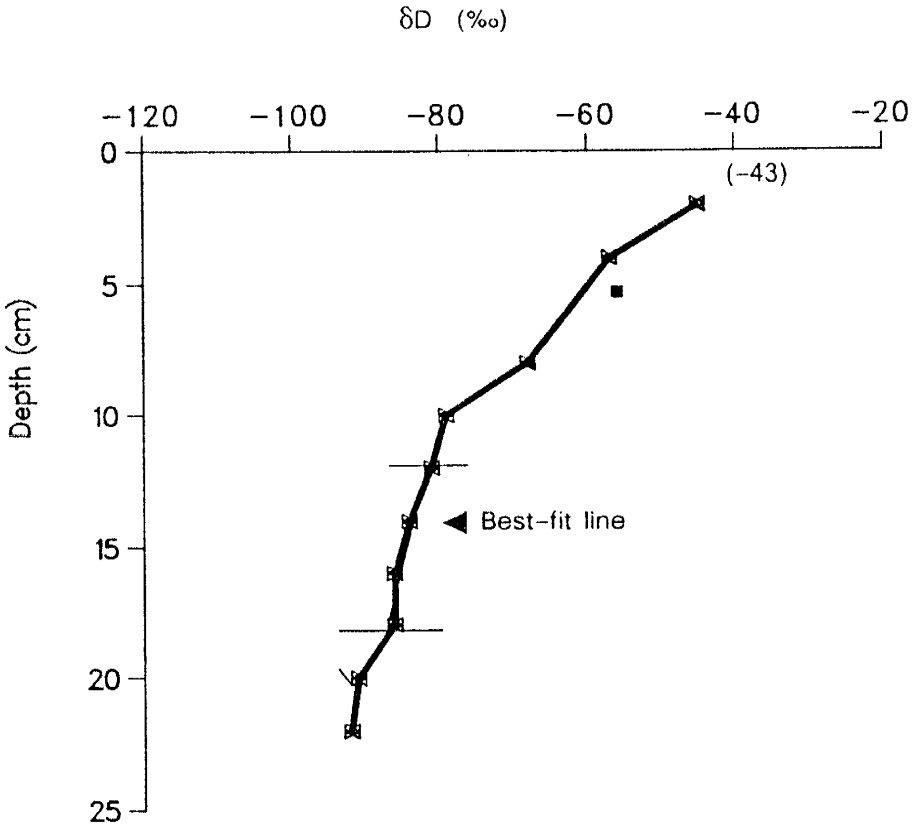

FIGURE 38. δD versus depth profile for column 10. Light line shows best fit of data within the recharge zone interval used in equation 37. Number in parenthesis is the isotopic composition at the evaporation front computed through equation 34.

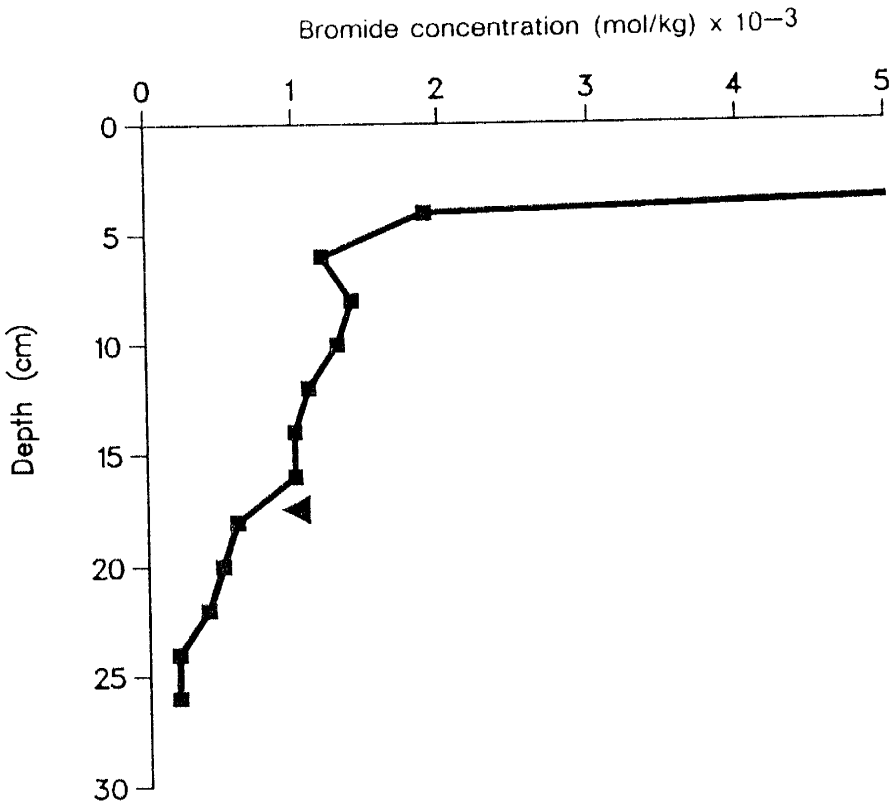

FIGURE 39. Bromide concentration versus depth for column 10. (◀) indicates center of mass of the bromide front.

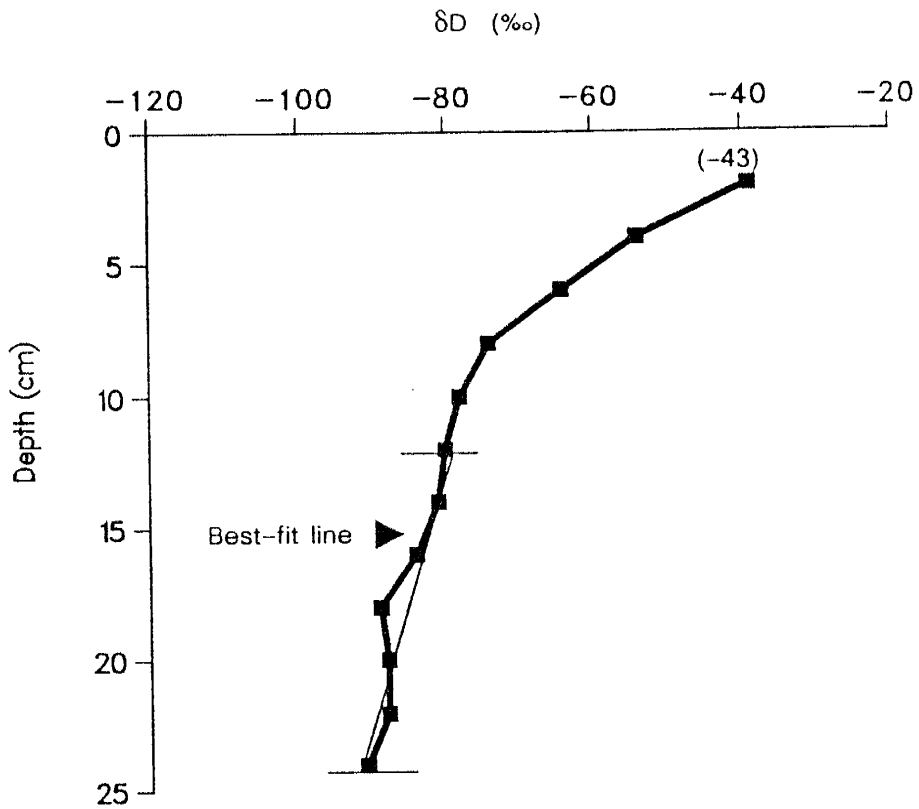

FIGURE 40. δD versus depth profile for column 11. Light line shows best-fit of data with in the recharge zone interval used in equation 37. Number in parenthesis is the isotopic composition at the evaporation front computed through equation 34.

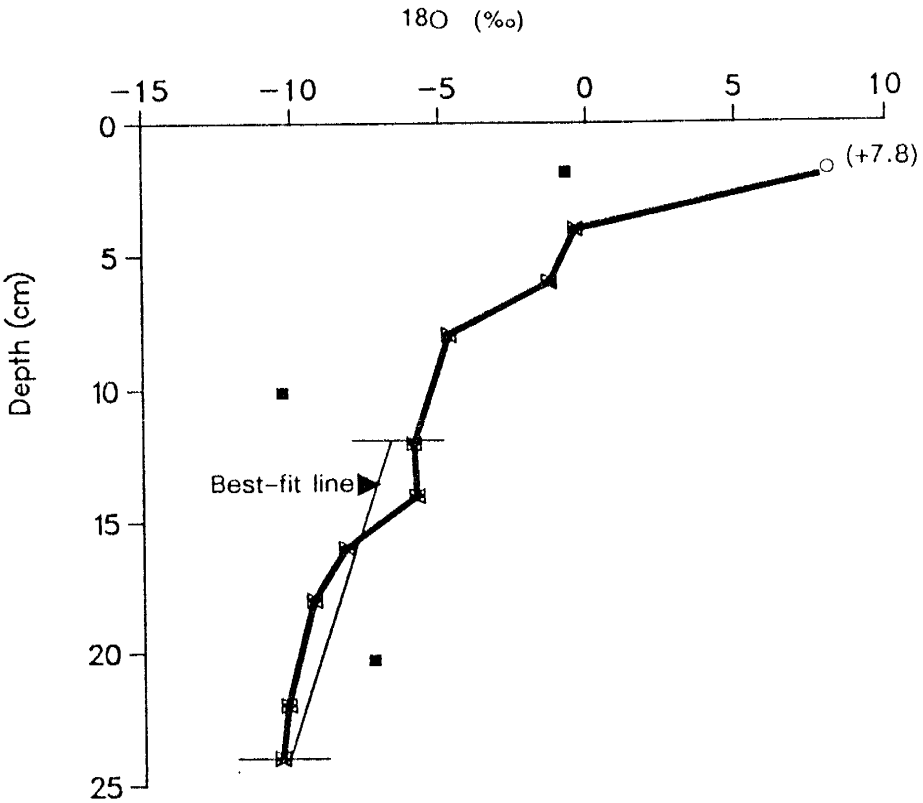

FIGURE 41. 18O versus depth for column 11. Light line represents best-fit of data within the recharge zone, however excluding the value at depth 14 and 20 cm. Number in parenthesis is the isotopic composition at the evaporation front computed through equation 34. Recharge estimates using equation 37 in text were performed excluding data points 6 cm, 10 cm, 14 cm and 20 cm. Open circle indicates computed value used in profile analysis.

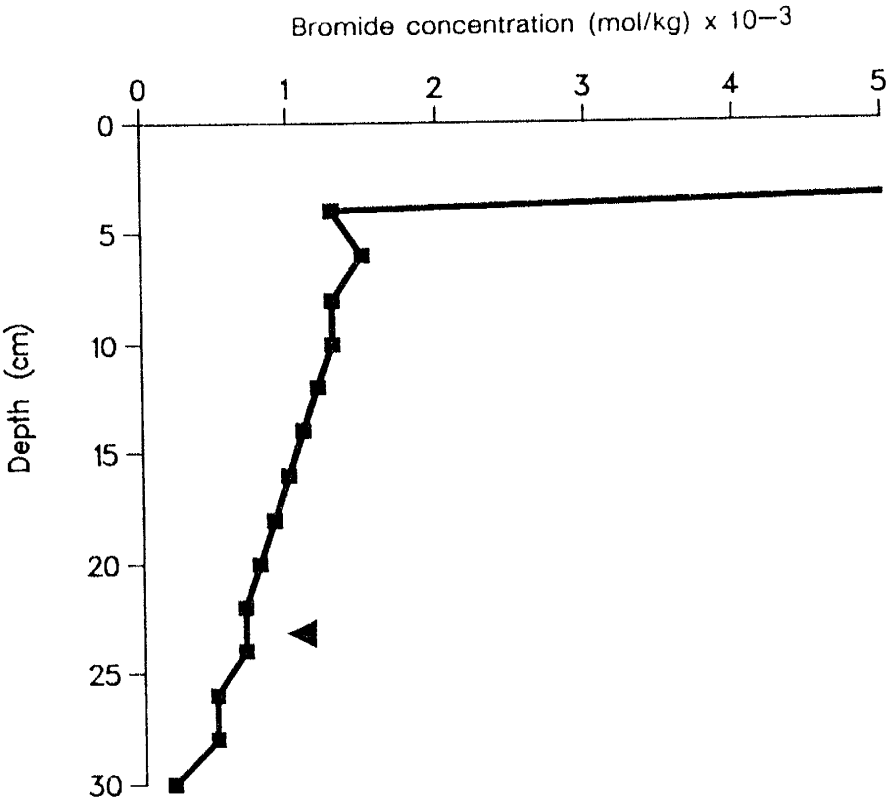

FIGURE 42. Bromide concentration versus depth for column 11. (◀) indicates center of mass of the bromide front.

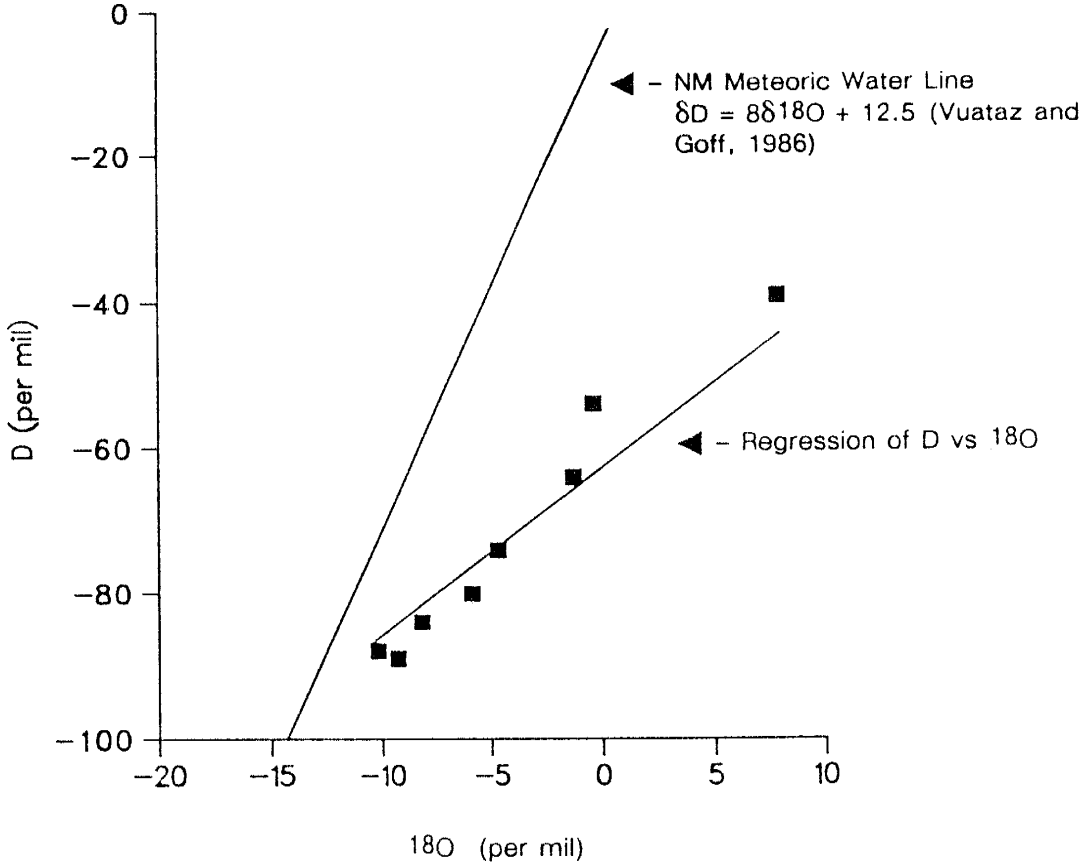

FIGURE 43. ^{18}O versus D plot for column 11. Slope of data for column 11 is observed as 3.02 using a computed value of +7.8‰ for interval 00-02 cm.

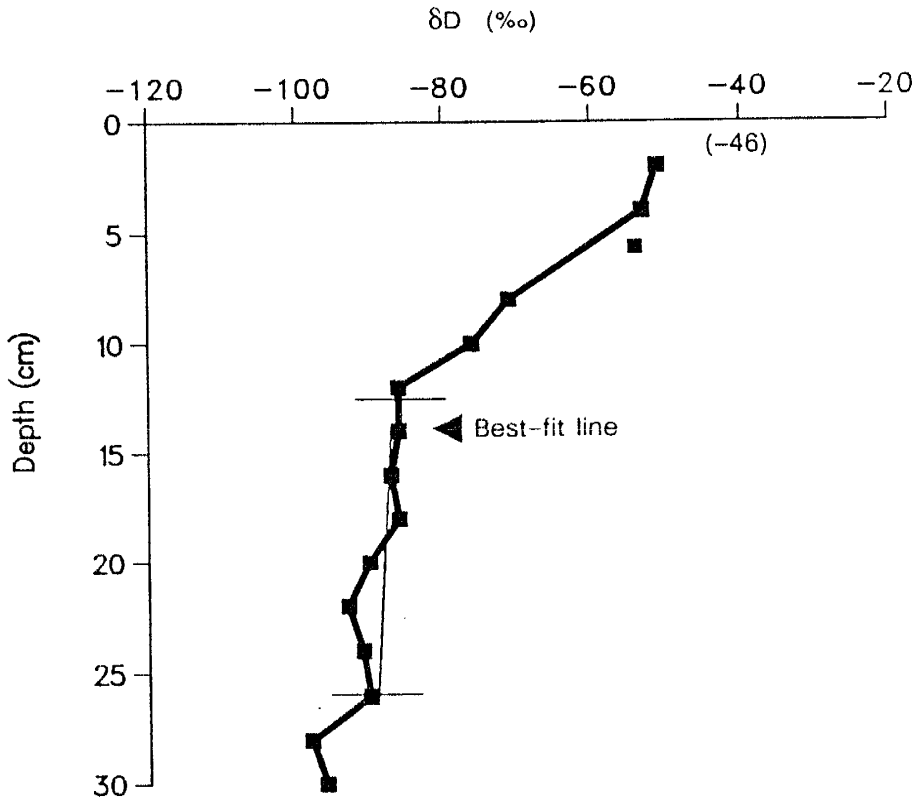

FIGURE 44. δD versus depth profile for column 12. Light line shows best-fit of data within the recharge zone interval used in equation 37. Note the poorly developed evaporation zone. The downward inflection observed here at 12 cm results in a negative net recharge value. Number in parenthesis is the isotopic composition at the evaporation front computed through equation 34.

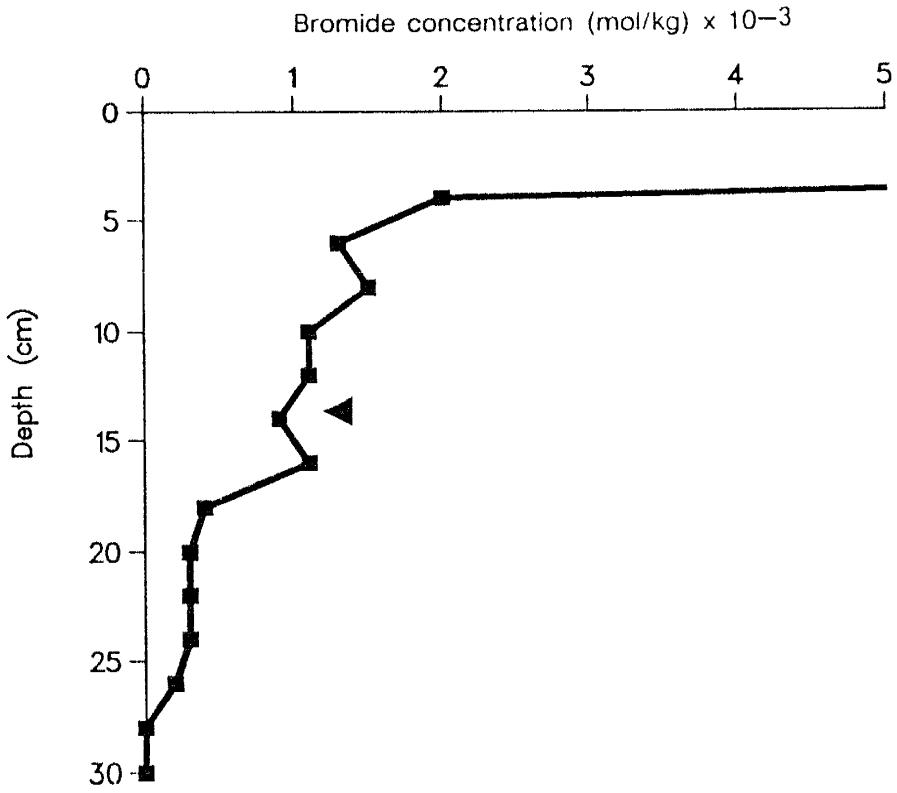

FIGURE 45. Bromide concentration versus depth for column 12. (◀) indicates center of mass of the bromide front.

DISCUSSION AND CONCLUSIONS

Table 2 provides a summary of the column experiment with all variables used in equation 37. Recharge computed using equation 37 is compared to recharge computed using the center of the bromide front as well as recharge computed using Figure 21. Due to contamination of samples, Br recharge comparison cannot be performed for column 1. Instead, recharge computed by using the depth where the initial flush water was observed was used as comparison to the computed and δD recharge estimates.

VALIDITY OF EXPERIMENT / RESULTS

Column 1 displayed recharge estimated at the depth where the initial flush water was observed of 0.736 cm, a theoretical profile δD recharge of 0.63 cm and an inflection point δD recharge of 1.27 cm, representing 0.63 cm difference between methods. For column 2, a Br recharge was 0.72 cm, a theoretical profile δD recharge of 0.56 cm and an inflection point δD recharge gave 0.88 cm representing 0.32 cm difference in results between the three methods. Column 3 gave Br, theoretical profile and inflection point δD recharge values of 0.86 cm, 0.64 cm and 1.62 cm respectively, resulting in 0.98 cm difference in the three methods. These values for bromide seem reasonable since column 3 did receive more recharge per event as well as a higher rate of water added on a daily basis. Total evaporation for columns 2 and 3 was estimated to be 5.6 cm and 6.7 cm respectively, or 0.7 cm/d and 0.74 cm/d respectively. However, the δD recharge values differ by an order

of magnitude, which does not seem appropriate since neither rate of water input nor evaporation rate varied as much as 10 %. This is probably a result of the poorly developed isotopic profile and the δ parameters used in the δD recharge computation. Column 4 exhibited a Br recharge, theoretical profile and inflection point δD recharge values of 0.92 cm, 0.65 cm and 1.10 cm respectively. The difference between the Br, theoritical and inflection point δD recharge estimates was 0.45 cm. Total evaporation was estimated for column 4 to be 6.8 cm or 0.69 cm/d. Column 5 on the other hand, displayed a significantly more enriched profile with large variations in the recharge zone. The Br recharge was computed to be 1.28 cm, the theoretical profile δD recharge 0.22 cm and the inflection point δD recharge was estimated to be 1.09 cm, resulting in a 1.04 cm difference in methods. The total evaporation was found to be 9.5 cm or 0.85 cm/d. Due to sampling problems, columns 6, 7 and 8 were not evaluated for recharge as previously discussed. Column 9 displayed recharge and evaporation rate characteristics similar to column 4 with Br, theoretical profile and inflection point δD recharge estimated at 1.06 cm and 2.00 cm and 3.12 cm respectively, for a 2.06 cm difference. The total evaporation was 11.3 cm or 0.76 cm/d. Br, theoretical profile δD recharge and inflection point δD recharge were estimated for column 10 to be 1.18 cm, 0.81 cm and 0.38 cm respectively, resulting in a difference of 0.80 cm. Total evaporation was found to be 12.7 cm or 0.79 cm/d. Column 11 had an estimated Br recharge of 1.86 cm, a theoretical profile δD recharge of 1.59 cm and an inflection point δD recharge of 0.39 cm resulting in a difference of 1.45 cm between the methods. Column 11 displayed the most developed D profile of all of the columns. Total evaporation for column 11 was estimated to be 12.57 cm or 0.74 cm/d. Recharge computed using the ^{18}O profile was performed using $\delta p = -13‰$, $Qp = 0.85$ cm, $z_o = 2.03$ cm, $\delta_{ef} = -2.2‰$ and $\delta r = -9.52‰$, was found to be negative. Column 12 displayed isotopic profile characteristics and recharge characteristics similar to those of columns 4 and 9.

The Br, theoretical profile and inflection point δD recharge was found to be 0.82 cm, 1.04 cm and 0.27 cm respectively, resulting in 0.77 cm difference between the three methods. Total evaporation was estimated to be 14.04 cm or 0.78 cm/d.

For D, equation 34 results in estimates at the evaporation front in good agreement with measured values. Using equation 34 to predict ^{18}O at the evaporation front however, appears not to produce compatible estimates compared to measured ^{18}O data. This is probably due to kinetic fractionation, which is more prominent in ^{18}O than D. Zimmerman et al. (1967) determined that the kinetic contribution to fractionation can raise the equilibrium enrichment (ϵ_o) by a factor of 4 ‰ in ^{18}O. Zimmerman stated that this is most importantly true for situations where humidity is low, in this case at the evaporation front. Zimmerman further noted that in order to use equilibrium fractionation data, kinetics would need to be ignored, which is not possible for ^{18}O. Adjusting ϵ_o by a factor of 4 still produces an ^{18}O estimate at the evaporation front for column 11 of +3.6 ‰, in comparison to -0.7 ‰ measured value. Using this value, an average δef is computed to be -2.88‰ for ^{18}O. Applying equation 37 with the z_{ef} found in the D profile yields 0.106 cm/event or 1.81 cm total recharge, which is in good agreement with the bromide recharge estimate. This implies that using ^{18}O in estimating recharge equation 37 may be valid however, interpretation of the downward inflection point in the evaporation zone may prove difficult. Clearly the ^{18}O data in comparison to the D profile, show more variation, possibly attributable to the sources of error discussed later.

Figure 46 provides a plot of δD versus bromide recharge and δD versus computed recharge for each of the columns. From Table 2, it can be seen that the rate at which the water was added, the dry zone depth, second-stage evaporation rate, and water content all varied inconsistently. Heterogeneities within the columns would effect movement of both the bromide and isotopes. Allison et al. (1983) stated that the environmental factors, eg evaporation and humidity, play a more significant role in the development of isotopic profile than do hydraulic characteristics of the soil. If this true then the bromide profile development may reflect different conditions than the isotopic profile. Assuming

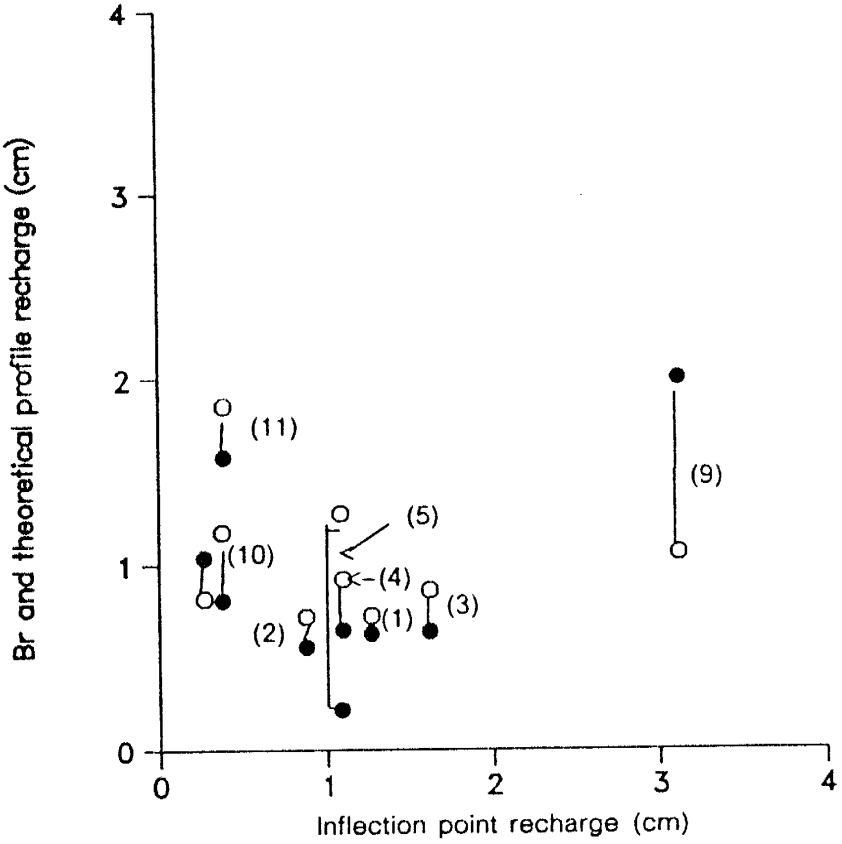

FIGURE 46. Plot showing Br versus inflection point recharge (open circles) and theoretical profile versus inflection point recharge (solid circles). Column nos. are represented in parenthesis.

that the bromide and deuterium movement are identical, then the only other variables would be those used in the computation of δD recharge. From Figure 46, it can be observed that the Br recharge and computed recharge correlate much better than does the δD recharge and either Br or computed recharge. This relationship is primarily controlled by the interpretation of the isotope profile, in particular the z_{ef} parameter. In nearly all cases, the computed z_{ef} was less than the z_{ef} observed from the profiles. Even though the z_{ef} for both methods exists within the same sampling interval, (i.e. 10–12 cm) as previously stated, relatively small fluctuations in z_{ef} results in large variations in recharge estimates computed through equation 37. Figure 47 shows a plot of Br recharge versus the theoretical profile δD recharge for the columns. The mean deviation from a true 1:1 relationship with Br recharge was –0.143 cm, (i.e. the theoretical recharge averaged 0.143 cm less than the Br recharge) and a standard deviation of 0.53 cm. This would imply that in order to arrive at a reasonable recharge estimate, a known curve would need to be developed for each sample profile from the corresponding δr and δef measured values and then z_{ef} determined graphically as was done using Figure 21.

There are several sources of error that influence the comparison of the two recharge estimates. The first source, and that most likely in all columns, is the calculation of recharge through the center of mass of the bromide front. As previously stated, the center of mass of the bromide front was computed as the depth where c/c'=0.5, where c' is the bromide concentration at the 02–04 cm interval. This relationship is only intended as an approximation in evaluating the dispersed bromide zone. Further, analytical errors can alter the evaluation of the location of the bromide front. The second source of error is choosing the point of downward inflection of the isotope profile. Of all variables used in equation 37, this point (z_{ef}) is the most critical, since most other values are averaged with data within the

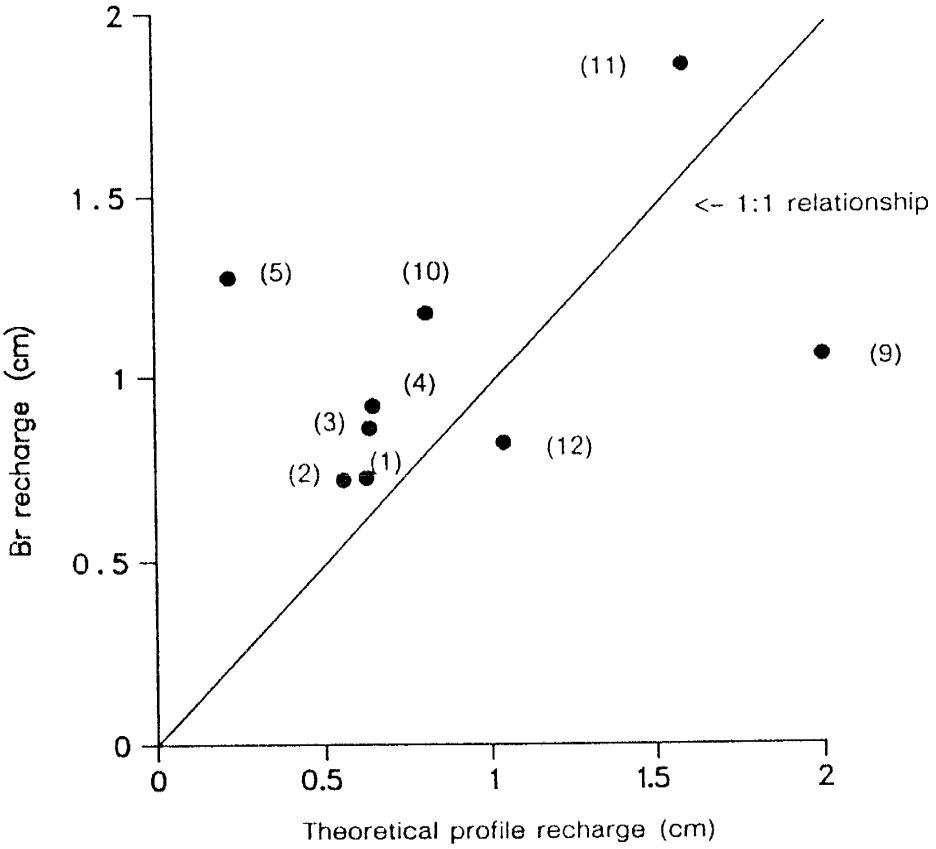

FIGURE 47. Br recharge versus theoretical profile recharge. Columns are represented as numbers in parenthesis. Diagonal line represents the 1:1 relationship between Br and theoretical recharge.

profile, reflecting overall zone characteristics. Changes in z_{ef} by as little as 1/2 cm can result in large variation in recharge estimates. However, the major problem experienced with z_{ef} was in the poorly developed profiles. In natural settings this may not be as severe a problem if the profile is developed in equilibrium with the recharge water and if the evaporation front has reached its "status-quo" at the time of sampling. The third source of error is the soil distillations and sample preparation. As was noted from the mass spectrometer analysis, several samples displayed enrichment believed to be a result of sample evaporation or leakage within the distillation apparatus. The magnitude of enrichment depends

upon the amount of water vapor lost with respect to the amount of water present in the sample. Therefore, a portion of the variation observed in the column profiles could be a result of errors during the distillation process or water loss from the sample containers.

Equation 37 appears to be able to potentially provide reasonable estimates of recharge for developed isotopic profiles which exist in equilibrium with recharge. The results show that for a clean sand, under isothermal conditions, recharge could be estimated close to that of the actual recharge, if the profile is sufficiently developed such that equilibrium conditions exist and if z_{ef} is reasonably defined using a computed profile derived from actual profile data. This would only apply for the conditions presented here. In field situations, where the δD_r is not constant, but fluctuates from site to site, a relationship would need to be developed between Q_p and δD_r instead of q_r, since q_r would not be known, as was the case here.

In natural settings, where the evaporation front exists much deeper than 2 cm and where precipitation varies seasonally in amount and isotopic composition, the development of the profile to equilibrium conditions could conceivably take tens of years or longer to achieve. The presence of vegetation will also influence the profile development. It was demonstrated by Zimmerman et al. (1967) and Allison et al. (1983) that no fractionation of the remaining water occurs as a result of transpiration. Allison et al. (1983) stated that for a site where transpiration is occurring, lower water contents and a reduced evaporation rate will be observed, but there will be an overall greater total loss of water compared with a bare soil under identical conditions. Further, the vegetated site in general will be isotopically lighter than the non-vegetated site. This is a result of the vegetative cover insulating

the soil from evaporation. Whether or not vegetation would preclude the use of equation 37 is not known for certain, however it is probable that, if the site displays a profile which is well developed and is in reasonable equilibrium with the recharge water, the net evapotranspiration will be reflected in the recharge and evaporation zones and equation 37 would be applicable. It should be pointed out that for a site which has experienced a change in land-use or management practices, or where vegetation and soil conditions are manipulated, the isotopic profile may never reach equilibrium with the recharge waters.

ACKNOWLEDGMENTS

This project was funded by the New Mexico Bureau of Mines and Mineral Resources, Socorro, New Mexico, under the supervision of Dr. W.J. Stone, senior hydrogeologist. The author wishes to express sincere gratitude to Dr. Stone and the Bureau for use of facilities and extensive counseling and advisement. The author further wishes to acknowledge the following individuals for assistance during the course of this research project. Dr. F.M. Phillips, associate professor, Hydrology Dept. NMIMT, for long hours in deriving the recharge equation and data review; Dr. A.R. Campbell, associate professor, Geology Dept., NMIMT, for use of the Geoscience department's stable isotope laboratory, assistance in mass spectrometer analysis and valuable advisement in laboratory procedures; R.G. Knowlton, Jr., graduate student, Hydrology Dept., NMIMT, for critically evaluating every aspect of the laboratory procedures and providing assistance in mass spectrometer analysis, J. Thedi, student, Geology Dept., NMIMT for assistance in soil water extractions and bromide analyses, and; Dr. C.J. Yapp, associate professor, Geology Dept., UNM, for providing initial isotopic analysis of the vacuum-distillation samples. The vacuum distillation method was developed from cooperative efforts with R.G. Knowlton, Jr. and Dr. A. R. Campbell.

REFERENCES

Allison, G.B., Barnes, C.J. and Hughes, M.W., 1982. The distribution of deuterium and ^{18}O in dry soils, 2. Experimental. J. Hydrol., 64: 377-397.

Allison, G.B., Barnes, C.J., Hughes, M.W., and Leaney, F.W.J., 1983. The effects of climate and vegetation on ^{18}O and deuterium profiles in soils. Proceedings of the international sym posium on isotope hydrology in water resources development, p105-121.

Allison, G.B., Stone, W.J. and Hughes, M.W., 1985. Recharge in karst and dune elements of a semi-arid landscape as indicated by natural isotopes and chloride. J. Hydrol., 75: 1-25.

Barnes, C.J. and Allison, G.B., 1982. The distribution of deuterium and ^{18}O in dry soils, 1. Theory. J. Hydrol., 60: 141-156.

Barnes, C.J., and Allison, G.B., 1984. The distribution of deuterium and ^{18}O in dry soils, 3. Theory for non-isothermal water movement. J. Hydrol., 74, 119-136.

Black, T.A., Gardner, W.R. and Thurtell, G.W., 1969. Prediction of evaporation, drainage and soil water storage for a bare soil. Soil Soc. Amer. Proc., 33: 655-660.

Coleman, M.L., Shepherd, T.J., Durham, J.J., Rouse, J.E. and Moore, G.R., 1982. Reduction of water to hydrogen using zinc. Anal. Chem. 54: 993-995.

Craig, H., 1961. Isotopic variations in meteoric waters. Science, 133: 1702-1703.

Davis, S.N. and DeWiest, R.J.M., 1966. Hydrogeology. John Wiley & Sons, Inc., NY p. 463.

Hayes, J.M. and Baker, K.L., 1986. Reagent and procedures for preparation of H_2 for hydrogen-isotopic analysis of water, (unpublished memorandum). Indiana State University, Bloomington, IN p. 3.

Hillel, D.I., 1971. Soil and water: Physical principles and processes. Academic Press, Inc., NY p. 288.

Hoy, R.N. and Gross, G.W., 1982. A baseline study of oxygen 18 and deuterium in the Roswell, New Mexico, groundwater basin. Report No. 144: NM Water Resource Research Institute, Las Cruses, NM 94p.

Kirkman, B.J., 1987. A field study on the water use of a Palea Scoparia plant in the northern Chihauhaun desert. Independant study project, NM Institute of Mining and Technology, Socorro, NM, 114p.

Majoube, M.,1971. Fractionnement en oxygene-18 et en deuterium entre l'eau et sa vapeur. J. Chem. Phys., 68: 1423-1436.

Merlivat, L., 1978. Molecular diffusivities of $H_2{}^{16}O$,$HD^{16}O$ and $H_2{}^{18}O$ in gases. J. Chem. Phys., 69(6): 2864-2871.

Merlivat, L and Jouzel, C., 1979. Global climatic interpretation of D-^{18}O relationships for precipitation. J. Geophys. Res., 84: 5029-5033,

Penman, H.L., 1940. Gas and vapour movement in soil, I.J. Agric. Sci., 30: 437-462.

Phillips, F.M., Peeters, L.A., Tansey, M.K. and Davis, S.N., 1986. Paleoclimatic inferences from and isotopic investigations of groundwater in central San Juan basin, New Mexico. Quat. Res., 26: 179-193.

Phillip, J.R., 1967. The second stage of drying. J. Appl. Meteor., 6: 581-581,

Vuataz, F.D., and Goff, F., 1986. Isotope geochemistry of thermal and non-thermal waters in the Valles Caldera, Jemez mountains. J. Geophys. Res., 91: 1835-1854.

Walker, G.R., Hughes, M.W., Allison, G.B. and Barnes, C.J., 1988. The movement of isotopes of water during evaporation from a bare soil. J. Hydrol., 97: 181-197.

Yapp, C.J., 1985. D/H variations of meteoric waters in Albuquerque, New Mexico, U.S.A.. J. Hydrol. 76: 63-84.

Zimmerman, U., Erhalt, P. and Munnich, K.O., 1967. Soil water movement and evapotranspiration: changes in the isotopic composition of water. Proceedings of the international symposium on isotope hydrology, 1966. IAEA, Vienna. p 567-585.

Appendix A

Temperature and Relative Humidity Data

(measured using an Abbeon Cal, Inc. temperature and humidity meter)

Date	RH%	Temp C
1/17/88	35	20.0
1/18/88	35	25.0
1/19/88	35	21.0
1/20/88	34	20.2
1/21/88	34	20.0
1/22/88	35	20.0
1/23/88	33	21.0
1/24/88	35	21.0
1/25/88	33	21.0
1/26/88	33	21.0
1/27/88	33	22.0
1/28/88	33	22.0
1/29/88	32	24.0
1/30/88	32	25.0
1/31/88	30	27.0
2/01/88	30	26.5
2/03/88	38	23.0
2/04/88	35	22.0
2/05/88	36	21.0
2/06/88	37	21.5
2/07/88	37	22.0
2/08/88	35	22.5
2/09/88	33	23.0
2/10/88	33	23.0
2/11/88	33	23.0
2/12/88	32	22.0
2/13/88	32	23.0
2/14/88	32	23.0
2/15/88	30	25.0
2/16/88	29	27.0
2/17/88	30	27.0
2/18/88	30	27.5
2/19/88	27	27.0
2/20/88	27	27.0
2/21/88	26	27.0
2/22/88	24	28.0
2/23/88	23	28.0
2/24/88	23	28.0
2/25/88	22	32.0
2/26/88	25	32.0
2/27/88	28	31.5
2/28/88	30	30.0
2/29/88	30	27.0
3/01/88	27	27.0
3/02/88	25	28.0
3/03/88	29	27.0
3/04/88	26	29.0
3/05/88	25	28.0
3/06/88	25	29.0
3/07/88	23	30.0
3/08/88	24	28.0
3/09/88	23	26.0
3/10/88	22	26.0
3/11/88	20	29.0
3/12/88	20	27.0

Date	RH%	Temp C
3/13/88	20	30.0
3/14/88	20	29.0
3/15/88	19	30.0
3/16/88	20	28.0
3/17/88	19	30.0
3/18/88	23	27.0
3/19/88	23	27.0
3/20/88	21	25.0
3/21/88	22	25.0
3/22/88	21	25.0
3/23/88	23	25.0
3/24/88	23	25.0
3/25/88	23	26.0
3/26/88	24	26.0
3/27/88	23	26.0
3/28/88	23	27.0
3/29/88	22	26.0
3/30/88	22	26.0
3/31/88	24	26.0
4/01/88	28	24.0
4/02/88	28	23.0
4/03/88	27	24.0
4/04/88	26	24.0
4/05/88	25	25.0
4/06/88	24	25.0
4/07/88	28	26.0
4/08/88	28	26.0
4/09/88	28	25.0
4/10/88	28	24.0
4/11/88	28	24.0
4/12/88	27	25.0
4/13/88	21	26.0
4/14/88	21	25.0
4/15/88	34	25.0
4/16/88	35	25.0
4/17/88	34	25.0
4/18/88	32	25.0
4/19/88	36	24.0
4/20/88	34	25.0
4/21/88	30	27.0
4/22/88	32	25.0
4/23/88	31	25.0
4/24/88	31	25.0
4/25/88	30	25.0
4/26/88	30	25.0
4/27/88	30	25.0
4/28/88	31	25.0
4/29/88	31	25.0
4/30/88	32	26.0
5/01/88	31	26.0
5/02/88	31	25.0
5/03/88	30	25.0
5/04/88	30	25.0
5/05/88	28	25.0

Date	RH%	Temp C
5/06/88	27	25.0
5/07/88	27	25.0
5/08/88	27	25.0
5/09/88	28	25.0
5/10/88	28	25.0
5/11/88	28	25.0
5/12/88	29	26.0
5/13/88	31	26.0
5/14/88	33	26.0
5/15/88	38	25.0
5/16/88	43	27.0
5/17/88	38	27.0
5/18/88	41	27.0
5/19/88	39	26.0
5/20/88	40	25.0
5/21/88	44	22.0
5/22/88	45	21.0
5/23/88	46	22.0
5/24/88	47	21.0
5/25/88	45	25.0
5/26/88	48	24.0
5/27/88	50	25.0
5/28/88	49	25.0
5/29/88	45	24.0
5/30/88	43	24.0
5/31/88	39	23.0
6/01/88	40	24.0
6/02/88	42	25.0
6/03/88	44	25.0
6/04/88	43	26.0
6/05/88	47	26.0
6/06/88	44	25.0
6/07/88	42	26.0
6/08/88	41	25.0
6/09/88	41	25.0
6/10/88	45	26.0
6/11/88	46	26.0
6/12/88	47	26.0
6/13/88	46	26.0
6/14/88	46	26.0
6/15/88	47	26.0
6/16/88	47	26.0
6/17/88	50	26.0
6/18/88	49	26.0
6/19/88	47	26.0
6/20/88	50	26.0
6/21/88	50	26.0
6/22/88	51	27.0
6/23/88	53	26.0
6/24/88	58	25.0
6/25/88	60	25.0
6/26/88	65	25.0
6/27/88	65	25.0
6/28/88	67	25.0

Date	RH %	Temp C
6/29/88	70	25.0
6/30/88	65	25.0
7/01/88	68	25.0
7/02/88	70	25.0
7/03/88	69	25.0
7/04/88	73	25.0
7/05/88	72	25.0
7/06/88	72	25.0
7/07/88	67	25.0
7/08/88	67	26.0
7/09/88	72	26.0
7/10/88	72	26.0
7/11/88	70	26.0

Appendix B

Column Data

Table B-1
Column 1 Data

Depth Interval	Sample Mass Wet	Dry	Water Content Grav.	Volum.	Br mol/kg	Del D 0/00
00-02	219.7	218.2	0.7	1.1	13.6	- -
02-04	140.7	136.2	3.3	5.2	0.6	-60
04-06	82.5	79.3	4.0	6.4	1.0	-72
06-08	129.1	124.1	4.5	7.2	0.4	-88
08-10	80.1	76.3	4.9	7.8	0.5	-89
10-12	80.4	76.3	5.4	8.6	0.4	-94
12-14	73.1	69.1	5.9	9.4	0.5	-98
14-16	84.0	79.1	6.5	10.3	0.5	-61 *
16-18	88.9	82.8	7.3	11.1	0.3	-97
18-20	77.3	71.5	8.3	13.2	0.5	-99
20-22	105.7	97.3	8.6	13.6	0.5	-103
22-24	91.3	82.1	11.2	17.8	0.5	-97

- - not analyzed
* probable fractionation during distillation

Table B-2
Column 2 Data

Depth Interval	Sample Mass Wet	Dry	Water Content Grav.	Volum.	Br mol/kg	Del D 0/00
00-02	165.0	163.5	0.9	1.4	11.8	-23 *
02-04	117.6	113.3	3.7	5.9	1.2	-63
04-06	153.4	147.3	3.9	6.2	0.9	-43 *
06-08	132.2	126.7	4.1	6.5	0.9	-74
08-10	119.1	113.9	4.3	6.8	0.7	-84
10-12	145.7	138.9	4.6	7.3	0.4	-52 *
12-14	118.1	112.6	4.7	7.5	0.1	-88
14-16	116.9	111.2	4.9	7.8	0.1	-93
16-18	113.1	107.1	5.3	8.4	0.1	-91
18-20	134.0	126.3	5.7	9.1	0.0	-99
20-22	145.0	135.4	6.6	10.5	0.0	-97
22-24	123.2	114.3	7.2	11.4	0.0	-99

- - not analyzed
* probable fractionation during distillation

Table B-3
Column 3 Data

Depth Interval	Sample Mass Wet	Sample Mass Dry	Water Content Grav.	Water Content Volum.	Br mol/kg	Del D 0/00
00-02	160.4	158.8	0.9	1.4	18.7	-44
02-04	124.7	120.4	3.6	5.7	1.7	-56
04-06	129.0	124.0	4.0	6.4	1.4	-77
06-08	138.1	132.6	4.2	6.7	1.2	-81
08-10	152.8	144.9	5.4	8.6	0.9	-88
10-12	115.7	109.6	5.5	8.7	0.7	-91
12-14	114.1	108.1	5.6	8.9	0.3	-86
14-16	111.2	105.1	5.9	9.4	0.1	-92
16-18	130.8	122.6	6.6	10.5	0.1	-88
18-20	126.7	117.0	8.3	13.2	0.0	-94
20-22	153.1	140.1	9.3	14.8	0.0	-96
22-24	152.5	138.9	9.8	15.6	0.0	-98

- - not analyzed
* probable fractionation during distillation

Table B-4
Column 4 Data

Depth Interval	Sample Mass Wet	Dry	Water Content Grav.	Volum.	Br mol/kg	Del D 0/00
00-02	202.0	198.7	1.6	2.5	14.6	-50
02-04	120.4	115.9	3.9	6.2	1.4	-68
04-06	112.7	108.1	4.3	6.8	1.4	-83
06-08	110.4	105.5	4.6	7.3	1.3	-87
08-10	106.8	101.9	4.8	7.6	1.1	-90
10-12	99.3	94.4	5.2	8.3	0.8	-90
12-14	105.4	100.3	5.1	8.1	0.4	-91
14-16	115.7	109.4	5.7	9.0	0.3	-97
16-18	122.7	114.7	6.9	10.9	0.1	-99
18-20	114.7	105.9	8.3	13.1	0.0	-100
20-22	154.5	143.5	7.7	12.2	0.0	-98
22-24	84.3	78.3	7.6	12.0	0.0	-100
26-28	165.1	149.8	10.2	16.2	0.0	- -

- - not analyzed
* probable fractionation during distillation

Table B-5
Column 5 Data

Depth Interval	Sample Mass Wet	Dry	Water Content Grav.	Volum.	Br mol/kg	Del D 0/00
00-02	157.5	156.0	0.9	1.4	14.2	-41
02-04	151.1	146.0	3.5	5.6	2.1	-57
04-06	107.0	102.8	4.1	6.5	2.0	-76
06-08	115.2	109.7	5.0	7.9	1.8	-78
08-10	124.3	118.3	5.1	8.1	1.3	-79
10-12	84.7	80.0	5.9	9.4	1.3	-89
12-14	83.8	78.5	6.8	10.8	1.2	-85
14-16	99.1	91.8	8.0	12.7	1.0	-94
16-18	131.0	120.4	8.9	14.2	0.6	-88
18-20	99.1	90.7	9.3	14.8	0.5	-89
20-22	112.4	102.3	10.0	15.9	0.3	-94
22-24	180.8	156.7	15.4	24.5	0.3	-97
26-28	136.1	116.8	16.5	26.2	0.1	- -

- - not analyzed
* probable fractionation during distillation

Table B-6
Column 6 Data

Depth Interval	Sample Mass Wet	Dry	Water Content Grav.	Volum.	Br mol/kg	Del D 0/00
00-02	123.9	123.2	0.6	1.0	13.9	-20
02-04	87.5	84.5	3.5	5.6	1.9	-22
04-06	80.2	77.1	3.9	6.2	1.9	-50
06-08	93.8	89.7	4.5	7.2	1.5	-55
08-10	77.3	73.7	4.8	7.6	1.3	-64
10-12	91.6	87.2	5.1	8.1	1.0	-62
12-14	102.6	96.4	6.4	10.1	1.0	-48
14-16	102.7	95.5	7.5	11.9	0.6	- -
16-18	79.4	74.2	7.0	11.1	0.4	-68
18-20	81.2	75.3	7.8	12.4	0.3	- -
20-22	108.8	98.1	10.8	17.2	0.3	- -
22-24	109.8	98.1	11.9	18.9	0.2	- -
26-28	154.9	128.2	20.8	33.1	0.1	- -

- - not analyzed
* probable fractionation during distillation

note: column 6 samples enriched due to probable sample evaporation

Table B-7
Column 7 Data

Depth Interval	Sample Mass Wet	Dry	Water Content Grav.	Volum.	Br mol/kg	Del D 0/00
00-02	63.4	62.0	2.1	3.3	13.6	- -
02-04	76.6	73.9	6.4	10.2	2.1	- -
04-06	77.1	74.1	4.1	6.5	1.9	- -
06-08	56.7	54.3	4.4	7.0	1.9	- -
08-10	63.2	60.5	4.4	7.0	1.7	- -
10-12	53.0	50.8	4.4	7.0	1.4	- -
12-14	57.5	54.5	5.5	8.7	1.3	- -
14-16	56.8	54.1	5.0	8.0	1.0	- -
16-18	54.3	51.2	6.0	8.5	0.6	- -
18-20	64.2	60.7	5.7	9.1	0.5	- -
20-22	57.9	54.5	6.3	10.0	0.4	- -
22-24	58.0	54.4	6.7	10.6	0.3	- -
24-26	94.8	88.2	7.4	11.8	0.1	- -
26-28	117.9	108.8	8.4	13.3	0.0	- -
28-30	93.7	85.6	9.4	14.9	0.0	- -

- - not analyzed
* probable fractionation during distillation
note: column 7 experienced redistribution

Table B-8
Column 8 Data

Depth Interval	Sample Mass Wet	Dry	Water Content Grav.	Volum.	Br mol/kg	Del D 0/00
00-02	117.0	116.1	0.8	1.3	17.9	-17.0
02-04	57.7	55.7	4.0	6.4	1.8	-35.0
04-06	64.0	61.4	4.2	6.7	1.8	-39.0
06-08	88.2	84.5	4.4	6.7	1.6	-65.0
08-10	76.2	64.4	4.4	7.0	1.3	-66.0
10-12	75.9	72.3	5.1	8.1	1.0	-76.0
12-14	55.6	52.8	5.4	8.6	1.0	-65.0
14-16	83.4	78.5	6.2	9.9	0.6	-66.0
16-18	75.6	70.2	7.7	12.2	0.5	-79.0
18-20	85.5	78.3	9.2	14.6	0.3	-79.0
20-22	64.4	59.6	8.1	12.9	0.2	-83.0
22-24	67.5	61.4	10.0	15.9	0.1	-90.0
24-26	64.3	57.4	12.0	19.0	0.0	- -
26-28	91.5	81.7	12.0	19.0	0.0	- -
28-30	93.7	80.7	16.1	25.6	0.0	- -

- - not analyzed
* probable fractionation during distillation
note: column 8 samples enriched due to probable sample evaporation

Table B-9
Column 9 Data

Depth Interval	Sample Mass Wet	Dry	Water Content Grav.	Volum.	Br mol/kg	Del D 0/00
00-02	107.0	104.7	2.1	3.3	4.8	-39
02-04	60.5	58.2	3.9	6.2	1.5	-60
04-06	69.2	66.5	4.1	6.5	1.4	-72
06-08	43.4	41.6	4.2	6.7	1.2	-71
08-10	60.5	58.0	4.4	7.0	1.4	-76
10-12	51.4	49.2	4.5	7.2	1.1	-80
12-14	50.4	48.0	4.8	7.6	0.8	-83
14-16	45.2	43.0	5.1	8.1	0.8	-83
16-18	55.0	52.2	5.4	8.6	0.4	-74
18-20	57.2	53.7	6.5	10.3	0.3	-84
20-22	54.4	50.8	7.1	11.2	0.1	-88
22-24	46.3	43.1	7.5	11.9	0.0	-85
24-26	96.5	88.6	8.9	14.2	0.0	- -
26-28	67.7	62.0	9.2	14.6	0.0	- -
28-30	66.9	59.4	12.6	20.2	0.0	- -

- - not analyzed
* probable fractionation during distillation

Table B-10
Column 10 Data

Depth Interval	Sample Mass Wet	Dry	Water Content Grav.	Volum.	Br mol/kg	Del D 0/00
00-02	93.3	92.0	1.4	2.2	13.6	-45
02-04	39.7	38.4	3.4	5.4	1.9	-57
04-06	60.2	57.9	4.0	6.4	1.2	-55*
06-08	46.1	44.2	4.4	7.0	1.4	-68
08-10	53.6	51.1	4.9	7.8	1.3	-79
10-12	55.2	52.4	5.3	8.4	1.1	-81
12-14	45.3	42.9	5.7	9.1	1.0	-84
14-16	51.0	47.7	6.8	10.8	1.0	-86
16-18	48.9	45.7	7.0	11.1	0.6	-86
18-20	72.7	66.8	8.7	13.8	0.5	-91
20-22	59.7	54.7	9.2	14.6	0.4	-92
22-24	85.9	78.7	9.2	14.6	0.2	- -
24-26	86.1	75.4	10.7	17.0	0.2	- -

- - not analyzed
* probable fractionation during distillation

Table B-11
Column 11 Data

Depth Interval	Sample Mass Wet	Dry	Water Content Grav.	Volum.	Br mol/kg	Del D 0/00	Del 18-O 0/00
00-02	41.5	41.1	1.1	1.7	13.9	-39	-0.7
02-04	52.3	50.6	3.3	5.2	1.3	-54	-0.4
04-06	44.8	43.0	4.2	6.7	1.5	-64	-1.3
06-08	32.4	31.0	4.2	6.7	1.3	-74	-4.7
08-10	37.9	36.3	4.4	7.0	1.3	-78	-10.1
10-12	42.8	40.9	4.9	7.8	1.2	-80	-5.9
12-14	41.2	39.1	5.3	8.4	1.1	-81	-5.8
14-16	51.4	48.9	5.2	8.3	1.0	-84	-8.2
16-18	49.9	47.1	5.9	9.4	0.9	-89	-9.3
18-20	44.1	41.4	6.5	10.3	0.8	-88	-7.9
20-22	40.4	37.8	7.1	11.3	0.7	-88	-10.2
22-24	39.1	36.2	7.9	12.6	0.7	-91	-10.4
24-26	44.0	40.8	8.0	12.7	0.5	- -	- -
26-28	49.5	45.6	8.5	13.5	0.5	- -	- -
28-30	41.5	38.0	9.4	14.9	0.2	- -	- -

- - not analyzed
* probable fractionation during distillation

Table B-12

Depth Interval	Sample Mass Wet	Dry	Water Content Grav.	Volum.	Br mol/kg	Del D 0/00
00-02	60.9	60.4	0.8	1.9	22.0	-51
02-04	33.3	32.4	2.4	3.8	2.0	-53
04-06	44.9	43.4	3.6	5.7	1.3	-55*
06-08	38.5	37.1	3.9	6.2	1.5	-71
08-10	49.2	47.3	4.0	6.4	1.1	-76
10-12	42.6	40.8	4.4	7.0	1.1	-86
12-14	49.3	47.2	4.5	7.2	0.9	-86
14-16	44.7	42.7	4.9	7.8	1.1	-87
16-18	56.0	53.3	5.0	8.0	0.4	-86
18-20	48.7	46.1	5.7	9.1	0.3	-90
20-22	46.5	43.8	6.3	10.0	0.3	-93
22-24	40.0	37.4	7.1	11.3	0.3	-91
24-26	51.9	48.1	7.9	12.6	0.2	-90
26-28	64.0	58.3	9.7	15.4	0.0	-98
28-30	60.6	55.0	10.0	15.9	0.0	-96

- - not analyzed
* probable fractionation during distillation

Appendix C

C/Co Curves for Bromide Analysis

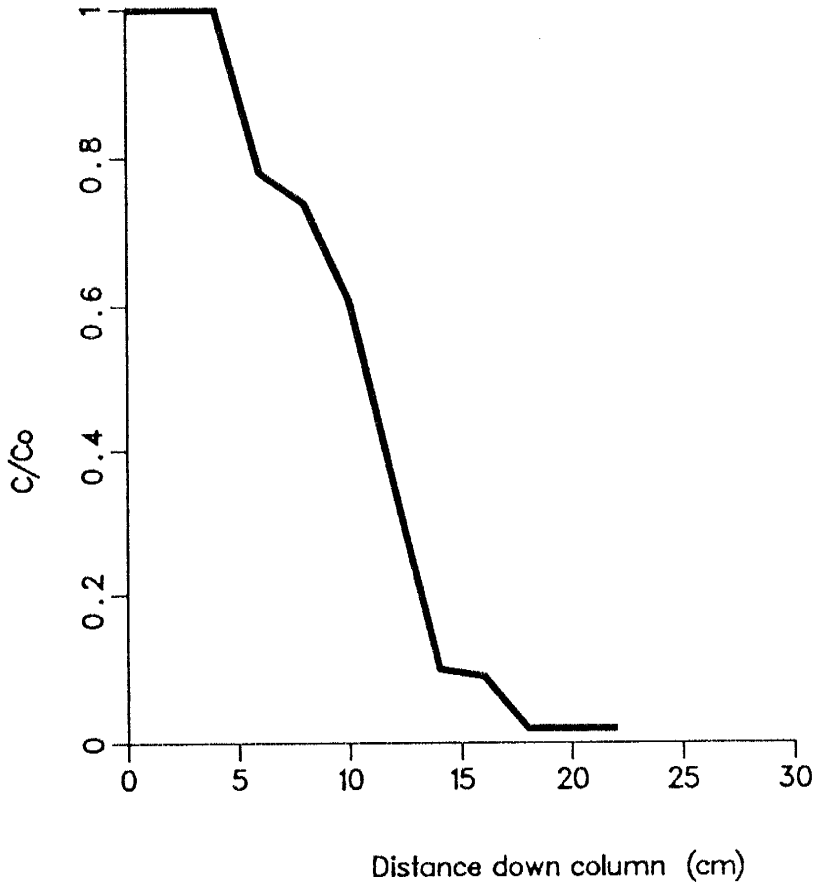

FIGURE C-1. C/Co curve for column 2 .

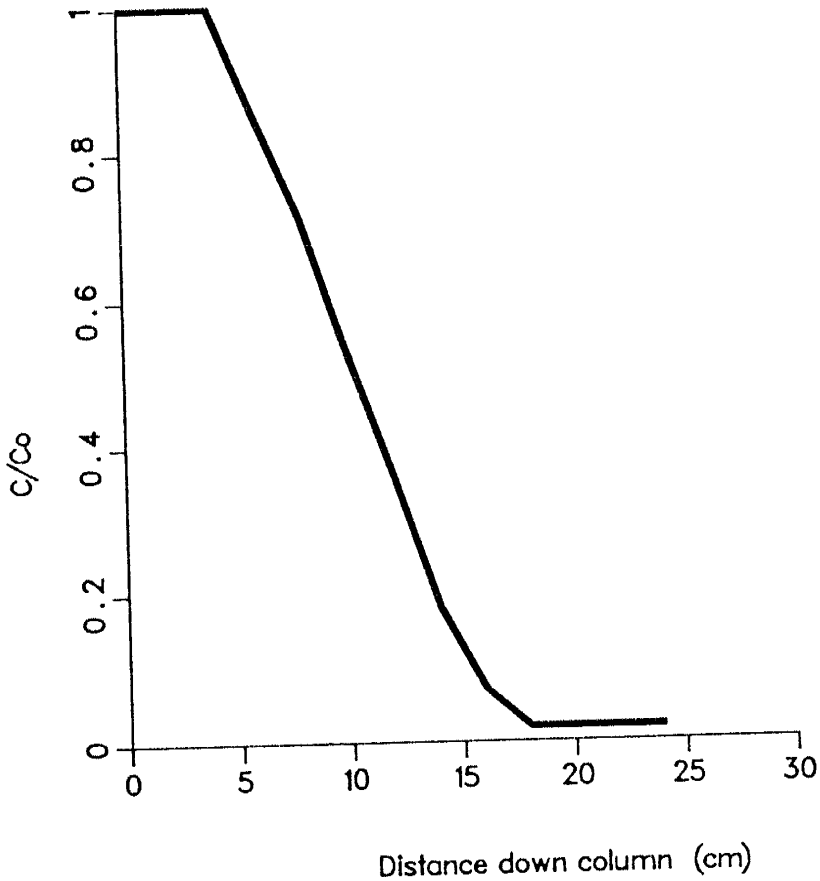

FIGURE C-2. C/Co curve for column 3 .

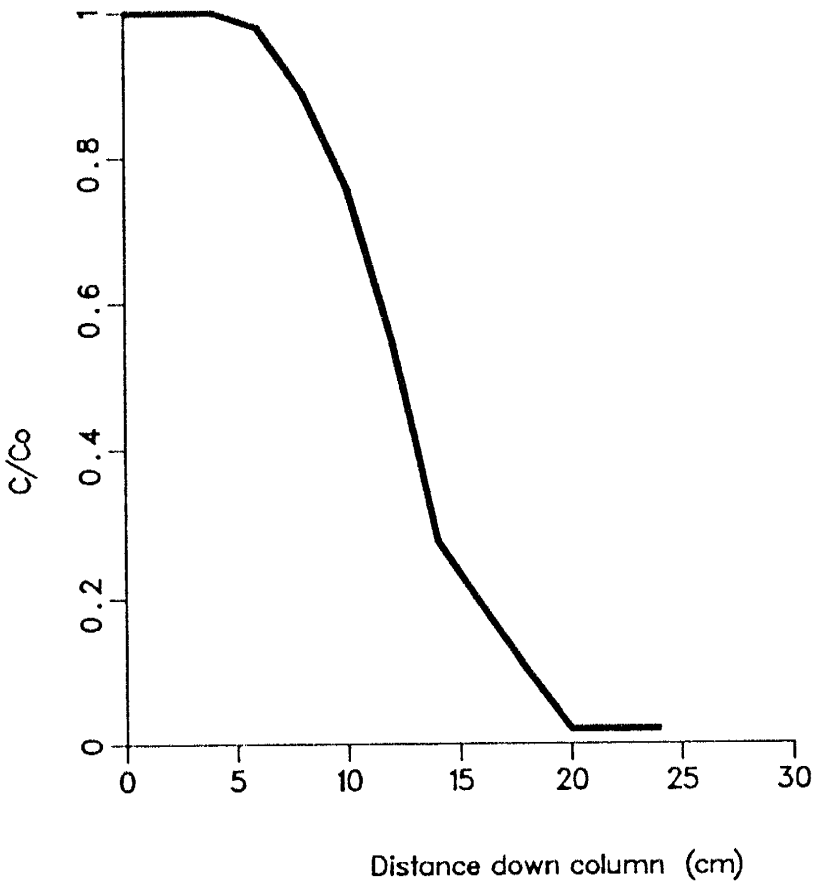

FIGURE C-3. C/Co curve for column 4.

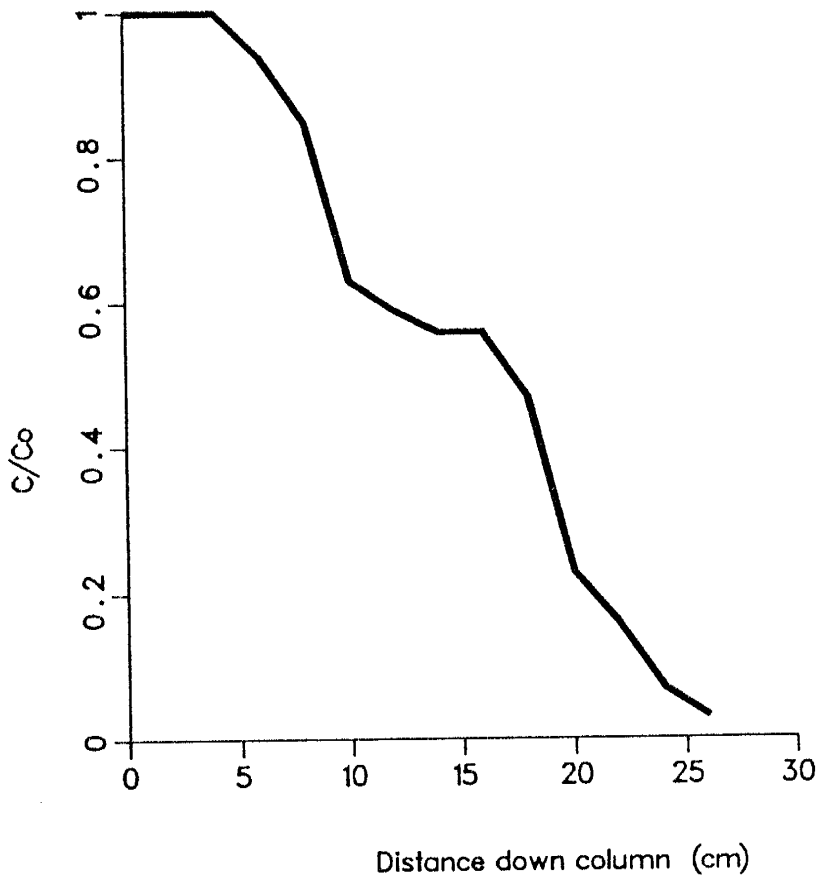

FIGURE C-4. C/Co curve for column 5.

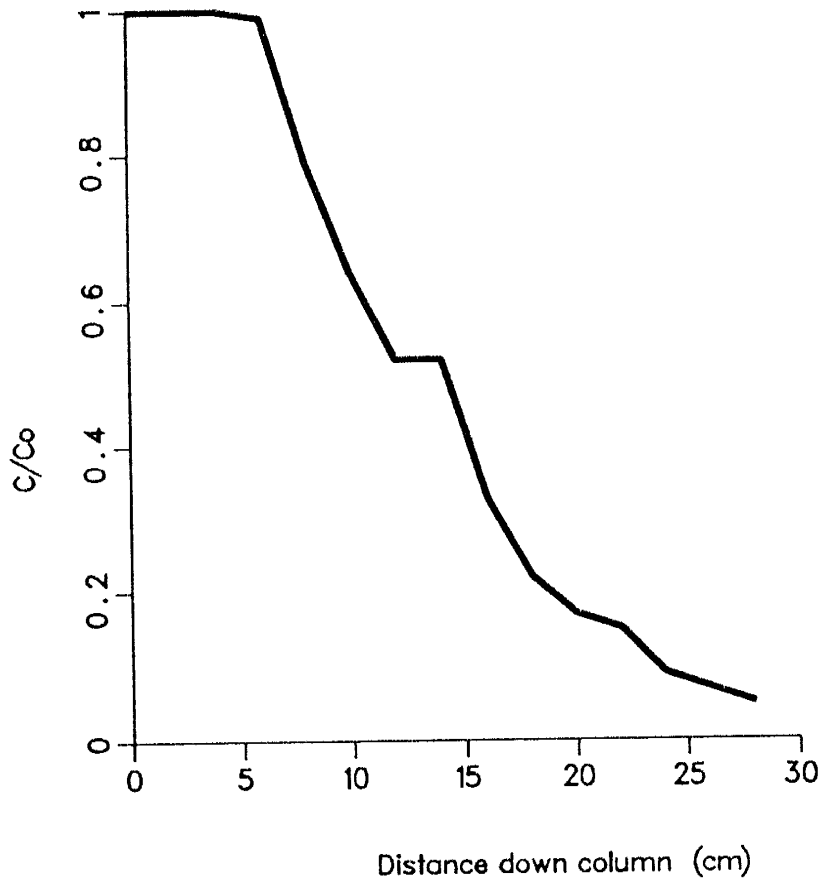

FIGURE C-5. C/Co curve for column 6.

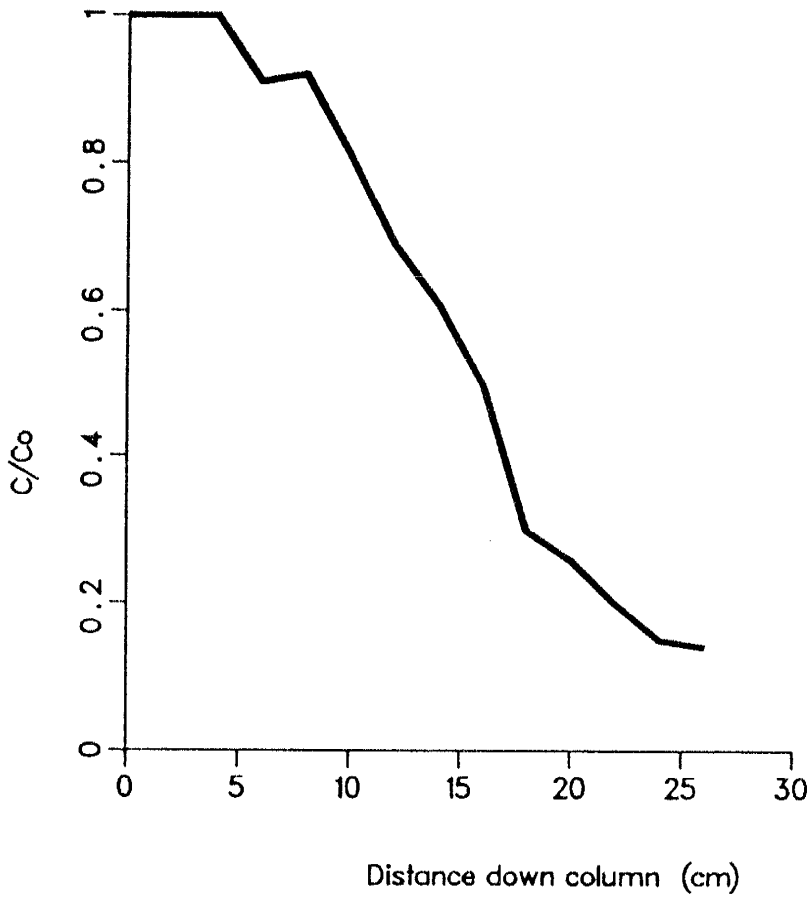

FIGURE C-6. C/Co curve for column 7.

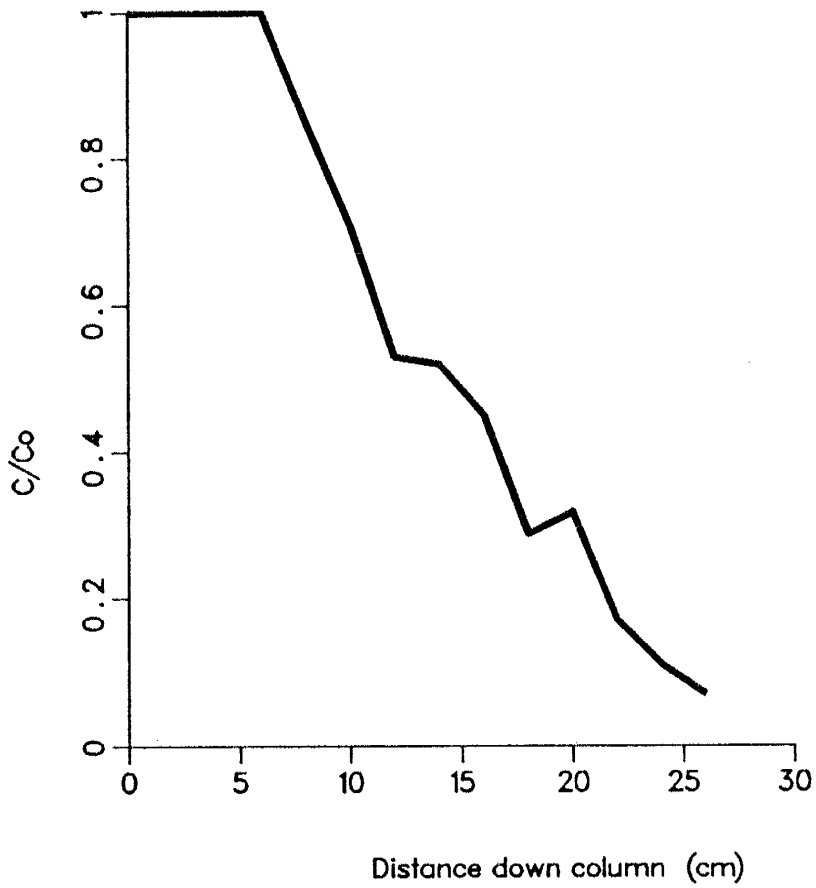

FIGURE C-7. C/Co curve for column 8.

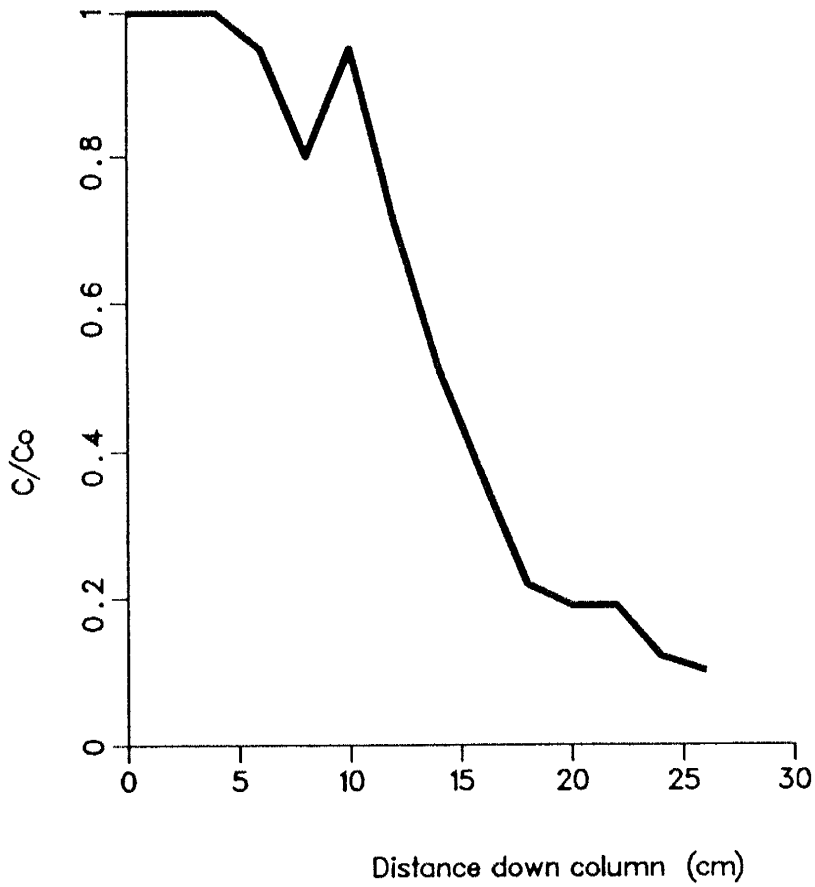

FIGURE C-8. C/Co curve for column 9.

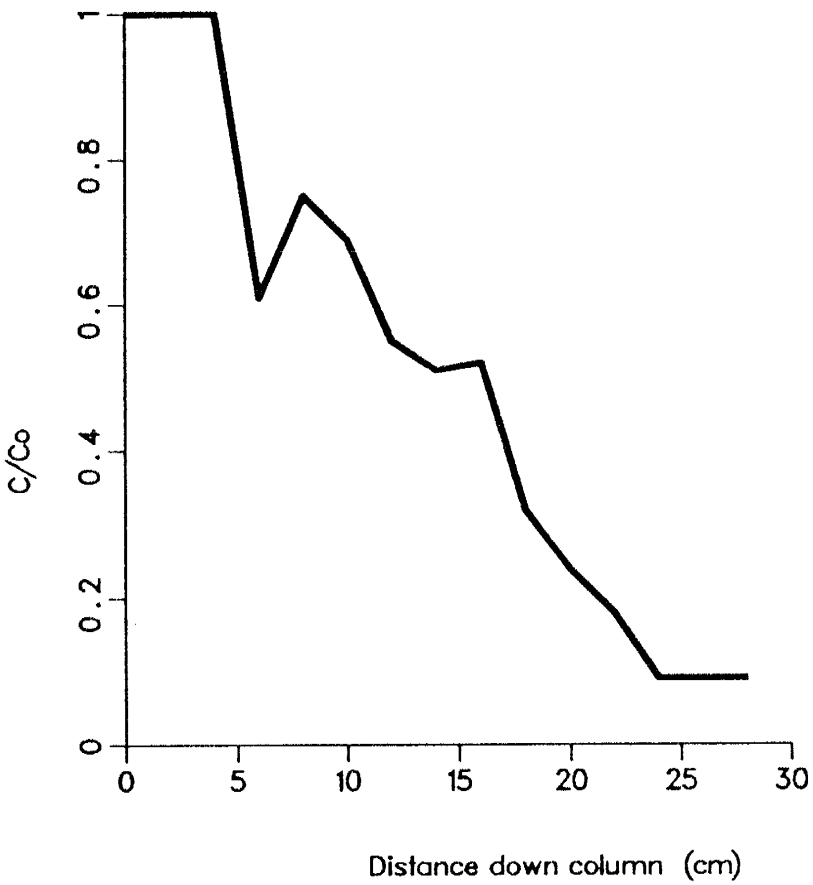

FIGURE C-9. C/Co curve for column 10.

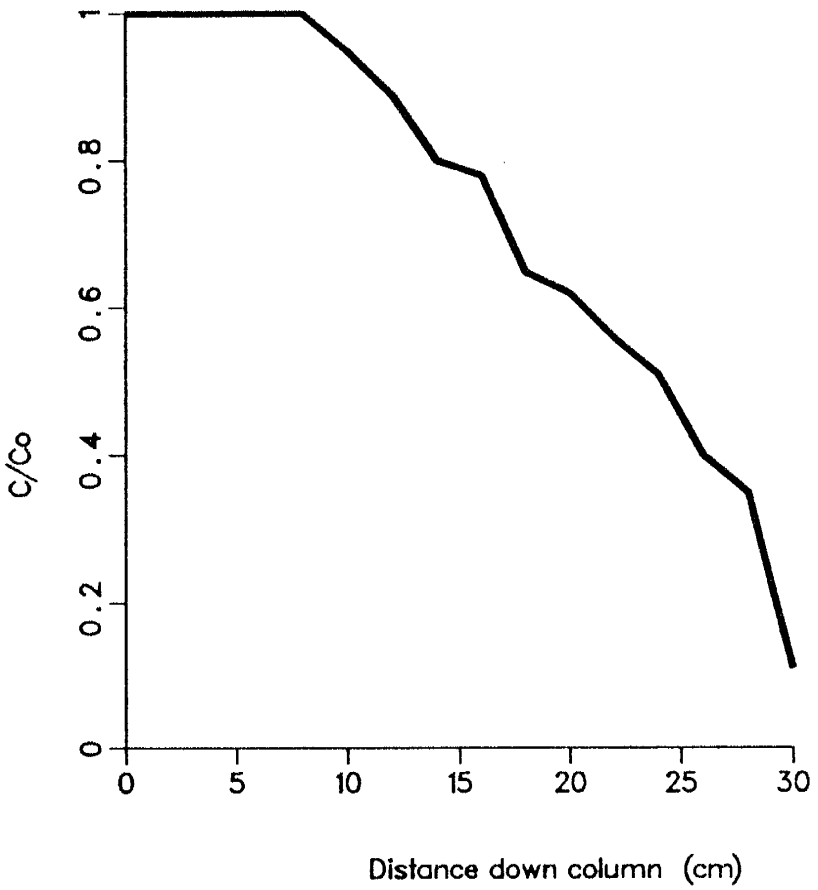

FIGURE C-10. C/Co curve for column 11.

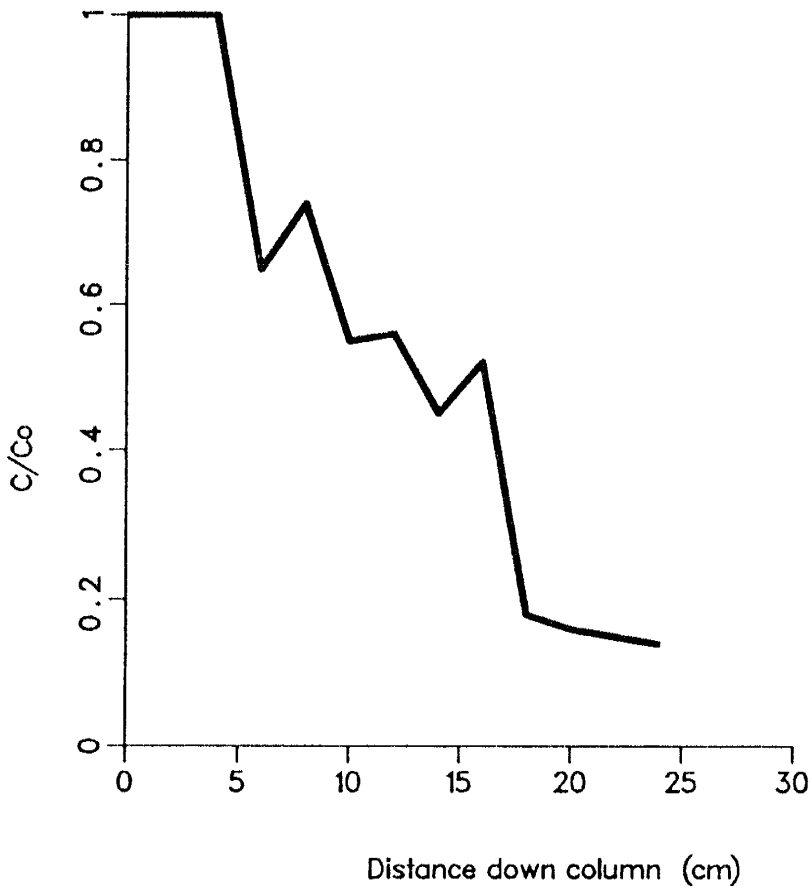

FIGURE C-11. C/Co curve for column 12.

Appendix D

Cost Information

The following information is based upon current supply costs and laboratory/mass spectormeter fees at the time of this study. It is only presented as a basis for planning similar studies.

Item	Unit cost	Total cost
Columns		
Clear Sch.-40 PVC 10.2 cm OD	$ 8.74/ft	$ 174.80
Misc. coupling, cement, tubing etc..	N/A	$ 200.00
Holding rack (wood)	N/A	$ 10.00
Column extruder (wood)	N/A	$ 5.00
	Sub total	$ 389.80
Laboratory anaylses (based upon 132 samples)		
Bromide concentration		*
Vacuum distillations	10.50 ea	$ 1386.00 1
Zinc reduction	8.50 ea	$ 1122.00
H_2O-CO_2 equilibration (18 samples)	13.50 ea	$ 243.00
Mass spectrometer analysis for D	10.00 ea	$ 1320.00
Mass spectrometer analysis for ^{18}O	10.00 ea	$ 180.00
	Sub total	$ 4251.00
	Total Cost	$ 4640.80
	Total cost per sample	$ 35.16

* - Bromide analysis performed in-house, commercial fees would be approximately $5.00/sample.

1 - Cost based without burden, for cost with burden add $20.00 per sample.

This thesis is accepted on behalf of the faculty of the

Institute by the following committee:

W. J. Stone

Fred M. Phillips

Andrew R Campbell

Date 15 Dec 1988